

**Consistent thermosphere density and wind data from satellite observations**  
**A study of satellite aerodynamics and thermospheric products**

March, G.

**DOI**

[10.4233/uuid:862e11b6-4018-4f63-8332-8f88066b0c5c](https://doi.org/10.4233/uuid:862e11b6-4018-4f63-8332-8f88066b0c5c)

**Publication date**

2020

**Document Version**

Final published version

**Citation (APA)**

March, G. (2020). *Consistent thermosphere density and wind data from satellite observations: A study of satellite aerodynamics and thermospheric products*. [Dissertation (TU Delft), Delft University of Technology]. <https://doi.org/10.4233/uuid:862e11b6-4018-4f63-8332-8f88066b0c5c>

**Important note**

To cite this publication, please use the final published version (if applicable).  
Please check the document version above.

**Copyright**

Other than for strictly personal use, it is not permitted to download, forward or distribute the text or part of it, without the consent of the author(s) and/or copyright holder(s), unless the work is under an open content license such as Creative Commons.

**Takedown policy**

Please contact us and provide details if you believe this document breaches copyrights.  
We will remove access to the work immediately and investigate your claim.

# **CONSISTENT THERMOSPHERE DENSITY AND WIND DATA FROM SATELLITE OBSERVATIONS**

A STUDY OF SATELLITE AERODYNAMICS AND THERMOSPHERIC  
PRODUCTS



# **CONSISTENT THERMOSPHERE DENSITY AND WIND DATA FROM SATELLITE OBSERVATIONS**

**A STUDY OF SATELLITE AERODYNAMICS AND THERMOSPHERIC  
PRODUCTS**

## **Proefschrift**

ter verkrijging van de graad van doctor  
aan de Technische Universiteit Delft,  
op gezag van de Rector Magnificus Prof. dr. ir. T.H.J.J. van der Hagen,  
voorzitter van het College voor Promoties,  
in het openbaar te verdedigen op woensdag 11 november 2020 om 12:30 uur

door

**Günther MARCH**

Ingenieur in de Luchtvaart en Ruimtevaarttechniek,  
Technische Universiteit Delft, Delft, Nederland, geboren te Florence, Italië.

Dit proefschrift is goedgekeurd door de

Promotor: Prof. dr. ir. P.N.A.M. Visser

Copromotor: Dr. ir. J.A.A. van den IJssel

Samenstelling promotiecommissie:

Rector Magnificus,	voorzitter
Prof. dr. ir. P.N.A.M. Visser,	Technische Universiteit Delft
Dr. ir. J.A.A. van den IJssel,	Technische Universiteit Delft

*Onafhankelijke leden:*

Prof. dr. S. Hickel,	Technische Universiteit Delft
Prof. dr. A.P. Siebesma,	Technische Universiteit Delft
Prof. dr. C. Stolle,	GFZ, Helmholtz Zentrum, Duitsland
Prof. dr. D.J. Knipp,	Colorado Boulder Universiteit, Verenigde Staten

*Overige leden:*

Dr. ir. E.N. Doornbos,	Koninklijk Nederlands Meteorologisch Instituut
------------------------	--

*Reservelid:*

Prof. dr. L.L.A. Vermeersen,	Technische Universiteit Delft
------------------------------	-------------------------------

*Keywords:* Thermosphere, Satellite drag, Thermospheric density, Thermospheric wind, Gas-surface interactions

*Printed by:* Ipskamp Printing

*Front & Back:* Southern tip of Italy image taken by the Expedition 49 crew aboard the International Space Station on Sept. 17, 2016. A Russian Soyuz spacecraft can be seen in the foreground. Artistic representations of the CHAMP, GRACE, GOCE and Swarm satellites are added using the geometry models designed by the author of the dissertation. Background Image Credit: NASA.

Copyright © 2020 by G. March

ISBN 978-94-6421-079-8

An electronic version of this dissertation is available at  
<http://repository.tudelft.nl/>.

*It takes something more than intelligence  
to act intelligently.*

Fyodor Dostoevsky

# CONTENTS

<b>Preface</b>	<b>ix</b>
<b>Summary</b>	<b>xi</b>
<b>Samenvatting</b>	<b>xiii</b>
<b>1 Introduction</b>	<b>1</b>
1.1 The importance of the thermosphere . . . . .	1
1.2 Satellite observations . . . . .	3
1.2.1 Acceleration observations . . . . .	4
1.2.2 Analyzed missions . . . . .	4
1.3 How do we model the thermosphere? . . . . .	7
1.4 Aerodynamic modelling. . . . .	8
1.5 Research objectives, motivation and scope . . . . .	9
<b>2 Geometry models for improving satellite density products</b>	<b>13</b>
2.1 Introduction . . . . .	14
2.2 Methodology . . . . .	16
2.3 Geometry modelling . . . . .	17
2.4 Aerodynamic modelling. . . . .	18
2.4.1 Validation . . . . .	21
2.4.2 Satellite aerodynamics . . . . .	23
2.5 Density processing . . . . .	29
2.5.1 Comparison with semi-empirical models . . . . .	35
2.5.2 Attitude manoeuvres analysis . . . . .	38
2.6 Conclusions and recommendations . . . . .	44
2.7 Appendix-A: Comparison between SPARTA and technical drawing geometries . . . . .	46
<b>3 Influence of gas-surface interactions on thermospheric wind</b>	<b>49</b>
3.1 Introduction . . . . .	50
3.2 Gas-surface interaction modeling. . . . .	52
3.3 Methodology . . . . .	54
3.4 Thermospheric wind data. . . . .	56
3.5 GOCE analysis . . . . .	60
3.6 CHAMP manoeuvre analysis . . . . .	64
3.7 Sensitivity analysis . . . . .	67
3.8 Conclusions. . . . .	68
3.9 Appendix-A: Zonal wind comparison with HWM-14 . . . . .	70
3.10 Appendix-B: Newly derived wind data sets . . . . .	72

<b>4</b>	<b>Influence of gas-surface interactions on aerodynamics and density</b>	<b>75</b>
4.1	Introduction . . . . .	76
4.2	Methodology . . . . .	78
4.3	Gas-surface interactions influence on satellite aerodynamics. . . . .	80
4.4	Gas-surface interactions influence on neutral density . . . . .	85
4.5	Density consistency for Swarm-A and -C . . . . .	89
4.6	Comparisons with atmospheric models. . . . .	92
4.7	Conclusions. . . . .	97
4.8	Appendix-A: New aerodynamics data sets. . . . .	99
4.9	Appendix-B: Speed ratio influence over satellite aerodynamics . . . . .	103
4.10	Appendix-C: Newly generated density data sets. . . . .	106
<b>5</b>	<b>Conclusion</b>	<b>109</b>
5.1	Research questions and goal . . . . .	109
5.1.1	Question 1 . . . . .	109
5.1.2	Question 2 . . . . .	110
5.1.3	Goal . . . . .	111
5.2	The newly derived thermospheric data sets. . . . .	111
5.3	Outlook for future research . . . . .	112
	<b>References</b>	<b>117</b>
	<b>Curriculum Vitae</b>	<b>127</b>
	<b>List of Journal Publications</b>	<b>129</b>
	<b>Selected Presentations</b>	<b>131</b>

# PREFACE

This is the end of a path that made me grow in several aspects. The last four years have been full of exciting experiences, but especially amazing people who helped me with my PhD project.

First of all, I would like to thank my family. This is not the common "thanks", because especially my mother was fundamental during these years. Even if sometimes I did not look very open to her, her help in happy and more difficult periods was crucial and highly appreciated. She raised me all by herself and I am happy that today she can be more and more proud of me, as I am proud of her. Great thanks go also to my brother Riccardo, my sister Hilde and their families for their love and support. They were always there for me, warmly welcoming me when I was in Italy and calling me when I was abroad.

When more than four years ago I decided to move to the Netherlands, I was living in Belgium. Brussels was my first home 2.0, where I had a position at the Von Karman Institute (VKI). It made me discover many friends. Between my "Belgian" mates I cannot stop thanking Federico, Bogdan, Elissavet, Valeria, Fabio, Jan, Davide and many others. The VKI beer meetings, the pool nights in Waterloo, Leuven, Flagey... how can I forget all the good time spent together? Thank you! Beyond the VKI gang, I am grateful to all the "Viola Club Bruxelles" brothers. Max, Enrichino, Forgnigni, Salimba, Davidone and many others made me feel a bit more home supporting our beloved purple team, and giving me many joys with the craziest fantasy football leagues!

Home was distant, however, some friends made the distance shorter because of their constant presence. David, Marchino and Porro were amazing in these years and always, after holidays, made the return to work a bit more difficult to deal with.

Being Italian, football is a great part of weekend life. However, Delft made me think about it also on Monday thanks to our A.C. Brancaloneo team and our super sponsor "Il Peperoncino"! It was great to play the football games between one injury and... another injury! Many thanks for the good time spent together on the pitch and the nice dinners after the matches. Among all, I will always remember my striker partners Seb and Imco together with captain Thomas. Thank you, guys!

Delft is a lovely city and despite I could not be a 100% "Delftian" for most of the past years, I succeeded to create very good friendships. Marc, Bas and Teresa were special, particularly in the last months. I highly appreciated to have them always ready to spend some time together. They were great listeners. Thank you Marc for being there whenever I would need you, even if you were just back from US and super tired. Thank you Bas for being a friend ready to share suggestions in "your way", which always includes a friendly (or less friendly) pat on your head. Your Dutch lessons are going to be super useful. Get ready... I will impress you! Teresa made me become the Italian version of Michael Phelps. However, after a few times, the swimming pool was not enough and I decided to focus again on my lovely thermosphere. It was very nice going to swim and share time together. Elisabetta was a solid reference point that made me feel good many times

with our "Italian" talks. It will be very nice to continue these talks in the near future! Yuxin made me become a professional ice skater in just one evening in Scheveningen. Great thanks go to all the people from room 9.18. Tim-oteo, Jacco-po, Svenjia, Marcel, Dora, Thomas were great office mates in the last years and months of my period in Delft. With Tim, I spent a lot of time brainstorming and working together meeting atmospheric and FORTRAN challenges... and we always won (somehow)! Jacco saved me several times when the fights with my computer were too nasty and when small rocks decided to visit my computer fan. Svenjia made me fatter and fatter with her cakes! Also all other colleagues were special in these years and I will always be grateful to them. Eelco was my supervisor for most of my PhD journey. He was a brilliant supervisor who made me discover a new world and fall in love with the art of presenting science. Pieter, my promoter, was always there. His door was always open and his supervision and feedback were constructive and efficient. I will always remember our ski day in Canada just before my first big conference abroad. I almost fainted on those slopes due to the jet-lag on the first day! Jose, Christian and Elisabetta formed an amazing team for the ESA Swarm density data processing, but especially I will be deeply thankful for their suggestions and friendship. Jose replaced Eelco as supervisor in the last months and gave me many tips to reach the PhD defense. We traveled a lot together and, despite our constant stress in arranging business trips, we always had a lot of fun (especially when a lot of Mexican food was involved)! Christian was our ESA-guy, but in the end, we were so nice that he decided to join us in Delft. It was a pleasure to work together especially in the last months on Daedalus. He was extremely helpful in the dissertation review phase and especially with all the suggestions for my next career step at ESA. Christian always had a solution ready for each possible doubt or problem. Among the colleagues, gratitude goes also to Relly for the nice talks and her availability in these 4 years. She welcomed me as a family member and she was always ready to help me in good and bad times.

A special acknowledgement goes to Sean, the French-Delft connection, for his support and interest in my work. We met in many different countries like Belgium, Unites States, Italy and it was always a pleasure to discuss work and many other topics with him. The ESA Swarm mission made me meet great people. Roger, Rune, Leda, Filomena, Lorenzo, Jan, Claudia, Guram, Juan, Serenella and Ignacio are just a few of them. Thank you all!

Representing Delft, it was great to be a visiting scientist in Boulder in Colorado! It was an amazing experience! Thanks again for everything to Federico, Hanli, Marcin, Delores and many other colleagues at HAO, CU Boulder and LASP. Working with you was extremely inspiring.

In the last period, moving to Leiden created the opportunity to meet very nice people too. Among them, a great "grazie" goes to Matteo and his amazing Padovan accent. Special gratitude goes to my "doc-doc". Thank you for the wonderful time during my last dissertation "fights". It was extremely good to get some calm moments with you, counting also the agitated ones full of spicy food at your favourite Asiatic restaurants!

Summing up, it was a real pleasure to work and spend time with all of you. I hope this is just the beginning...  
The best has to come! Thank you!

# SUMMARY

The German CHAMP, US/German GRACE, and European Space Agency (ESA) GOCE and Swarm Earth Explorer satellites have provided a data set of accelerometer observations allowing the derivation of thermospheric density and wind products for a period spanning more than 15 years. With the advent of highly accurate satellite accelerometer measurements, the neutral density and wind characterization has been significantly improved. These observations provided detailed information on the thermospheric forcing by Solar Extreme Ultraviolet radiation and charged particles, and revealed for the first time the extent of forcing by processes in lower layers of the atmosphere.

Because the focus of most of previous research was on relative changes in density, the scale differences between the CHAMP, GRACE, GOCE and Swarm data sets, so far, have been largely ignored. These scale differences originate from errors in the aerodynamic modelling, specifically in the modelling of the gas-surface interactions (GSI) of the satellite. Once detailed 3D geometry models of these satellites are available, the key parameters to describe the satellite aerodynamics can be estimated by cleverly making use of variations in satellite orientation and simultaneous observations by multiple satellites.

The first step for obtaining more consistent density and wind data sets consisted of meticulously modelling the satellite outer surface. For this dissertation work, this was done by collecting information from technical drawings and pre-launch pictures, and generating a CAD model of the selected satellites. In the following phase, these geometries were given as input to a rarefied gas-dynamics simulator. The Direct Simulation Monte Carlo approach was used with the SPARTA software to compute the force coefficients under different conditions of satellite speed, atmospheric temperature and local chemical composition. Once all the mission scenarios had been simulated, an aerodynamic data set was generated and applied in the processing of satellite accelerations into thermospheric density and wind data products. To this aim, the Near Real-Time Density Model (NRTDM) software, developed at TU Delft, was used. The data were generated from accelerometer observations and, when necessary, with the help of GPS-based accelerations estimated by a Precise Orbit Determination (POD) technique. Multiple comparisons were performed with empirical and physics-based models. This helped in determining for which conditions the models are performing better, and also which models' features would need further development.

In the second step, the interaction between atmospheric particles and satellite surfaces was investigated. The way in which atmospheric particles collide with the satellite surfaces have a large influence on the satellite aerodynamic forces and, if proper assumptions are not implemented, can produce large discrepancies in the final thermospheric products. Initially, the GSI assumptions were selected in agreement with the fully diffusive reflection mode. This assumption was adopted to exclusively investigate the geometry modelling influence on thermospheric products. Later, to cover also this research area, multiple simulations described different reflection modes. A wide range

of GSI parameters was investigated, and more optimal values were found allowing the derivation of new consistent thermospheric products. Within this study, the energy accommodation coefficient, which describes the energy exchange between particles and satellite surfaces, played a crucial role. Although the value of 0.93 is used commonly in the literature, in this study lower values were identified as optimal. Indeed, a value of 0.82 for the GOCE satellite, and a value of 0.85 for the Swarm and CHAMP satellites have been found to provide more consistent thermospheric data. This resulted in new improved thermospheric density and wind data sets, which have been made available to the scientific community. Among the possible applications, these data can be used for data assimilation for improving current atmospheric models. Resolving the problem of deriving the true absolute thermosphere density scale from satellite dynamics measurements improves orbit predictions for the space debris population and its long-term evolution. Moreover, the new capabilities for computing more consistent drag, density and wind, can also be exploited for future missions that are currently in the design phase.

# SAMENVATTING

De Duitse CHAMP, Amerikaanse/Duitse GRACE, en GOCE en Swarm ESA Earth Explorer satellieten hebben gezorgd voor een dataset van versnellingsmetingen die het mogelijk maakt de dichtheid en windsnelheden in de thermosfeer over de laatste 15 jaar in kaart te brengen. Door de opkomst van uitermate precieze versnellingsmetingen, is onze kennis over de neutrale dichtheid en de windeigenschappen significant verbeterd. Deze metingen hebben gedetailleerde informatie verschaft over de thermosferische invloeden als gevolg van Extreme Ultraviolette Zonnestraling en geladen deeltjes, en hebben voor het eerst in de geschiedenis de oorzaak van verstoringen in de thermosfeer als gevolg van processen in de onderlagen van de atmosfeer getoond.

Omdat het grootste gedeelte van voorgaand onderzoek zich normaliter richtte op relatieve veranderingen in de dichtheid, zijn de verschillen als gevolg van een mogelijk incorrecte absolute schaling tussen de CHAMP, GRACE, GOCE en Swarm datasets voor een belangrijk deel buiten beschouwing gelaten. Deze verschillen als gevolg van een incorrecte schaling komen voort uit onnauwkeurigheden in de aerodynamische modellen, in het bijzonder in de modellen betreffende interacties tussen de thermosfeer en de buitenkant van de satelliet. Wanneer gedetailleerde 3D geometrische modellen van de desbetreffende satellieten beschikbaar zijn, kunnen de sleutelparameters, die de aerodynamica van de satelliet beschrijven, geschat worden door slim gebruik te maken van de variaties in satellietoriëntatie en gelijktijdige waarnemingen van meerdere satellieten.

De eerste stap voor het verkrijgen van meer consistente dichtheid en wind datasets bestond uit het nauwkeurig modeleren van het uitwendige van de satelliet. In deze dissertatie was dit gedaan door middel van het vergaren van informatie uit technische tekeningen en foto's van voor de lancering. Vervolgens werd een CAD model gegenereerd voor ieder van de geselecteerde satellieten. In de volgende fase waren deze modellen als input gebruikt voor een lage druk gasdynamica simulator. De Directe Monte Carlo methode was gebruikt in combinatie met de SPARTA software om krachtcoëfficiënten te berekenen voor verscheidene condities betreffende de snelheid van de satelliet, de atmosferische temperatuur en de lokale chemische samenstelling. Toen alle missie-scenario's gesimuleerd waren, kon een aerodynamische dataset gegenereerd worden en toegepast bij het verwerken van de satellietversnellingen tot thermosferische dichtheid en wind dataproducten. Om dit te kunnen bewerkstelligen was de "Near Real-Time Density Model" (NRTDM) software, ontwikkeld door de TU Delft, gebruikt. De data waren gegenereerd op basis van accelerometrie waarnemingen en, waar nodig, met behulp van op GPS gebaseerde schattingen van de satellietversnellingen door middel van precieze baanbepaling. Er zijn meerdere vergelijkingen uitgevoerd met empirische en fysische modellen. Dit heeft geholpen bij het bepalen voor welke condities de kenmerken van deze beter presteren, alsmede welke modellen nog verder ontwikkeld moeten worden.

In de tweede stap zijn de interacties tussen atmosferische deeltjes en de oppervlaktes aan de buitenkant van de satelliet onderzocht. De manier waarop atmosferische

deeltjes in botsing komen met het satellietoppervlak heeft een grote invloed op de aerodynamische krachten die op de satelliet werken en, wanneer geen correcte aannames worden gemaakt, kunnen grote discrepanties ontstaan in het uiteindelijke thermosferische product. In eerste instantie was aangenomen dat de interactie tussen de thermosferische deeltjes en de buitenkant van de satelliet gebaseerd is op volledig diffuse reflectie. Deze aanname was gedaan om enkel de invloed van de geometrische modellen te onderzoeken op de thermosferische producten. Later, om ook dit onderzoeksgebied te dekken, zijn verschillende modi van oppervlakte-reflectiviteit beschreven op basis van meerdere simulaties. Een grote verscheidenheid aan gas-oppervlakte interactie parameters, beter bekend als *GSI parameters* in het Engels, zijn onderzocht en verder geoptimaliseerde waardes werden gevonden. Hierdoor was de afleiding van nieuwe consistente thermosferische producten mogelijk. Binnen dit onderzoek is de energie-accommodatiecoëfficiënt, die de energie-uitwisseling beschrijft tussen een deeltje en satellietoppervlakken, een cruciaal onderdeel. Ondanks dat normaliter de waarde van 0.93 in literatuur wordt gehanteerd, zijn binnen dit onderzoek lagere waardes geïdentificeerd die optimaal bleken. De waardes van 0.82 voor de GOCE satelliet en 0.85 voor de Swarm en CHAMP satellieten bleken consistentere thermosferische data op te leveren. Dit resulteerde in vernieuwde en verbeterde thermosferische dichtheid en wind datasets, die heden beschikbaar zijn voor de wetenschappelijke gemeenschap. Een voorbeeld van de mogelijke toepassingen is het gebruik van deze data voor het verbeteren van huidige atmosferische modellen. Wanneer het probleem van het bepalen van de juiste schaalfactor van versnellingsmetingen kan worden opgelost, kunnen betere voorspellingen worden gedaan van de banen en evolutie van ruimteafval. Verder kunnen de nieuwe mogelijkheden voor het berekenen van consistentere luchtweerstand, dichtheid en wind ook gebruikt worden voor toekomstige missies die zich nu nog in de ontwerp-fase bevinden.

# 1

## INTRODUCTION

The atmosphere blocks most of Sun's dangerous radiation, traps heat allowing for comfortable temperatures on Earth's surface, and contains oxygen, which is essential for life. Therefore, the atmosphere is what makes our planet livable. Beyond protecting us, the atmosphere, in particular the thermosphere, hosts most of our satellite missions and often highly influences their successfulness. One of the first scientific uses of artificial Earth satellites has been the estimation of thermospheric neutral density. This is a fundamental quantity of interest, which has an impact on several factors during mission design and lifetime. Using optical and radio-tracking observations, and applying a basic theory on satellite drag, a first estimate of density was already determined from the rate of change of Sputnik's orbital period (*Hele and Massey, 1959; Hele and Walker, 1958*). The same techniques, applied to several satellites during the early years of the space age, revealed the correlation of density with solar and geomagnetic activity (*Newton and Pelz, 1973*). These early findings paved the way for creating the first generation of empirical density models. With time, these models became essential tools in space industry, because of their applications in orbit determination and predictions during space mission design and operations.

The research presented in this dissertation aims at improving current models by increasing the accuracy of atmospheric density and wind observations. In particular, deep attention is dedicated on a better description of satellite aerodynamics for precise modelling of drag and other driving forces within the thermosphere region. The target is to provide a better understanding of the upper atmosphere dynamics by studying the neutral component, which is crucial for several applications that will be introduced later in this chapter.

### 1.1. THE IMPORTANCE OF THE THERMOSPHERE

The atmosphere has four primary layers: the troposphere that we live in near the Earth's surface, the stratosphere that houses the Ozone layer, the mesosphere, where the temperature decreases, and the thermosphere, the top layer, where the temperature rises

again. The thermosphere layer ranges between approximately 100 and 600 km altitude and provides a unique opportunity to investigate space physics. Within this region, density and winds are strongly influenced by external drivers, including solar flux and wind, geomagnetic activity, and tidal and gravity waves propagating through the atmosphere (Rees, 1989). For these reasons, this area of the Earth's atmosphere is fundamental for understanding the solar-terrestrial environment, space physics and practical applications of satellite missions.

A detailed description of this region is needed for reliable estimations of the acting forces on satellites with a direct influence on mission analysis and operations. Re-entry estimations are heavily affected by thermospheric characteristics. Numerous catalogues keep track of as many objects as possible that are orbiting our planet (Sridharan and Pensa, 1998). However, information in these catalogues, such as orbital elements and decay rates, lack reliability because of a combination of uncertainty in neutral density, and debris size, shape and attitude motion. Two recent examples are the uncontrolled re-entries of the Gravity Field and Steady-State Ocean Circulation Explorer (GOCE) satellite in 2013 (Gini et al., 2015) and the Tiangong-1 Chinese station in 2018 (Szücs-Csillik, 2017).

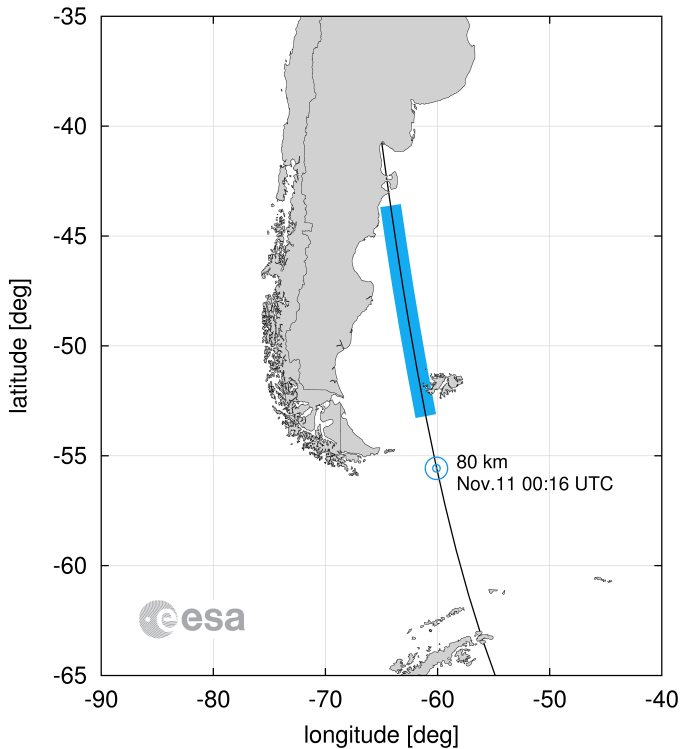


Figure 1.1: ESA's GOCE satellite re-entered Earth's atmosphere on 11 November 2013 at 01:16 CET over the South Atlantic Ocean near the Falkland Islands, at an approximate altitude of 80 km (Credits: ESA).

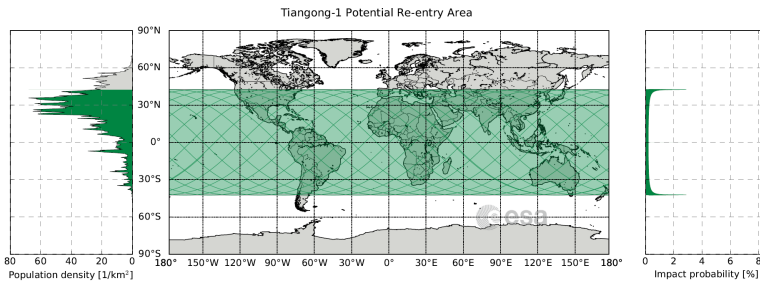


Figure 1.2: Tiangong-1 potential re-entry area estimated on March 26th (slightly more than one week before the actual re-entry). The map shows the area between 42.8 degrees north and 42.8 degrees south latitude (in green), over which Tiangong-1 was predicted to re-enter. (Credits: ESA).

Both re-entries created alarm through media. However, in these cases, the probability to cause damage and have an impact on highly populated areas were relatively small. As illustrated in Fig. 1.1, which shows the GOCE re-entry corridor, sometimes populated areas are at risk for impact, especially if the re-entering satellite contains high-temperature resistant systems (e.g. propellant tanks, or in case of GOCE the well-insulated gravity gradiometer). Uncertainties of the impact location are unluckily still large and, mostly, reliable estimations can generally only be done in the very last hours. In March–April 2018, media and research institutes followed the decay evolution of the Tiangong-1 station. Current density models were not able to predicting reliably the specific impact location a few days before the collision (Fig. 1.2). Also in this case, the generated debris had a favourable re-entry location in the sea without creating damages, injuries or casualties. However, to raise the current precision of re-entry estimations, the understanding of drag and atmospheric density needs to be enhanced.

Similar applications of upper atmosphere models can be found in collision avoidance procedures and in other operations involving ground segments. Indeed, the capability to accurately predict contact windows is crucial and can be a critical requirement during mission design. Reducing current uncertainties would mitigate costs and enhance efficiency and performances.

A detailed characterization of the thermosphere also helps in the estimation of mission lifetime. This estimation is based on many inputs, including predicted solar and geomagnetic activity. Studying the interaction in the solar-terrestrial environment helps to achieve more accurate estimations. This can be further expanded to orbit determination and manoeuvre planning. In the future, with the improvement of on-board instrumentation and modelling capabilities, current density and wind computations will be further improved. This dissertation aims at providing an enhanced input for current and future atmospheric models and the next generation of thermospheric products.

## 1.2. SATELLITE OBSERVATIONS

In order to further understand the atmospheric dynamics and tune current models, satellite observations are fundamental because they provide in situ observations with high spatial and temporal resolutions. Most of the time, ground observations cannot provide the same level of accuracy due to the several corrections that are needed in

the data processing and, moreover, they offer very limited coverage in space and time. Ground observations of temperature and winds can be provided by incoherent scatter radars, scanning doppler imaging and Fabry-Perrot interferometers. However, uncertainties can be large and sometimes results can be difficult to interpret (*Harding et al., 2017*). Therefore, having in-situ observations in the upper atmosphere from multiple satellites provides a unique opportunity to have a great number of data points during a long time. If data have high consistency, it is possible to merge multiple missions' data to investigate a specific quantity of interest over a long time period and at different altitudes.

### 1.2.1. ACCELERATION OBSERVATIONS

The investigation of the neutral density and winds is facilitated by on-board accelerometers. These instruments can measure non-gravitational accelerations with exceptional high precision. Since the start of the millennium, accelerometer measurements have provided detailed information on the forcing by solar EUV radiation and charged particles (*Bruinsma et al., 2006*) and for the first time the extent of thermospheric forcing by processes in lower layers of the atmosphere (*Forbes et al., 2009*). The working principle of the used accelerometers is based on the accurate electrostatic levitation of a proof-mass, which is ideally located at the center of mass of the satellite (*Touboul et al., 1999*). The perturbations on the proof-mass position and the electrostatic forces which are needed to keep the mass in its nominal position can be converted into non-gravitational accelerations measurements. This information can be analyzed to retrieve information about density, winds and solar radiation pressure.

Additional methods to derive non-gravitational satellite accelerations are based on precise orbit determination. Thanks to these techniques the highly accurate information of orbits, which is at the centimeter level, can help to determine satellite accelerations and density scaling parameters, and also to calibrate accelerometers. These measurements are typically based on Global Positioning System (GPS) (*Dow et al., 2005*), Satellite Laser Ranging (SLR) (*Pearlman et al., 2002*) or Doppler radio tracking (*Tavernier et al., 2006*). An additional method based on the Two-Line Elements (TLE) approach has been widely used in the past, especially for the first thermosphere models (*Harris and Priester, 1962; Jacchia, 1965*), but also in the past decade for space debris applications (*Picone et al., 2005*). Although temporal resolutions are much lower than accelerometer-based observations, these data are available since the 1960s and provide a great opportunity to investigate long-term thermospheric neutral density change (*Emmert et al., 2008*).

### 1.2.2. ANALYZED MISSIONS

A new era in space research began in 2000 with the launch of CHAMP (CHALLENGING Mini Satellite Payload), which for the first time carried a very precise accelerometer in combination with a high-quality, dual-frequency GPS receiver in a circular polar orbit (*Reigber et al., 2006*). This enabled the production of a global coverage of high-resolution thermosphere density data (*Bruinsma et al., 2004*). The Challenging Minisatellite Payload (CHAMP) is one of the selected satellites within this work. The other missions are the Gravity Recovery and Climate Experiment (GRACE) (*Bettadpur, 2007*), GOCE (*Floberghagen et al., 2011*) and Swarm (*Olsen et al., 2013*).

The German CHAMP satellite (Fig. 1.3) was operated by the German Research Centre for Geosciences (GFZ). The main objective consisted of observing and measuring the Earth's magnetic field together with the gravity field and observing atmospheric characteristics through radio occultation. The on-board accelerometer provided high-resolution non-gravitational acceleration data. The mission operated from July 2000 to September 2010, providing a large volume of data with exceptional quality. These data covered 300–500 km altitude and almost a full solar cycle, providing fundamental data on Earth's magnetic and gravity fields, and Earth's atmosphere.

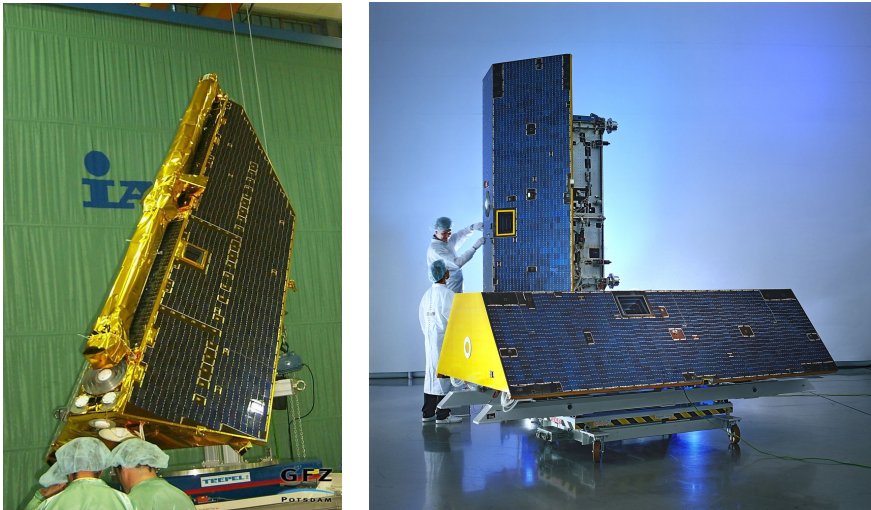


Figure 1.3: The CHAMP (left) and GRACE (right) satellites during pre-launch preparations (Credits: GFZ, Astrium).

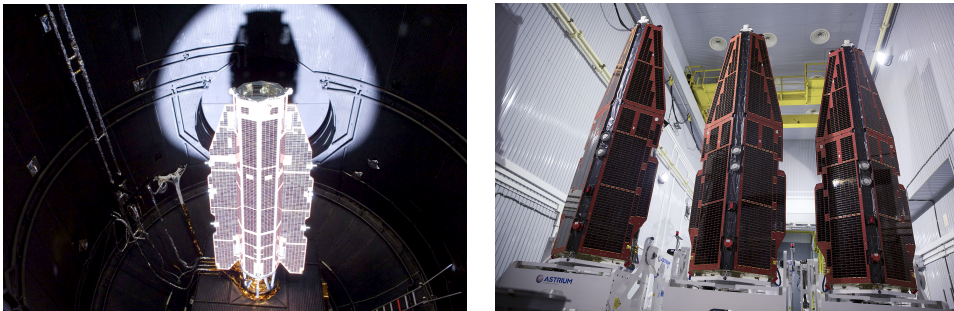


Figure 1.4: On the left, the GOCE satellite ready for testing in the Large Solar Simulator at ESA-ESTEC at the end of 2007 (Credits: ESA-Anneke Le Floc'h). On the right, the three Swarm satellites in vertical positions, ready to join the launch adapter (Credits: ESA/M. Shafiq).

The GRACE twin satellites (Fig. 1.3) measured the tiny changes in Earth's gravity field caused by mass change on and near Earth's surface through microwave ranging between

the two spacecraft. It was a joint mission of NASA and the German Aerospace Center (DLR). This mission operated for a long time from March 2002 to October 2017, and performed similar accelerometer measurements as CHAMP, but at higher altitudes and for all 3 directions (the CHAMP accelerometer data suffered from a electrode problem affecting the observations along the instrument Z-axis, which was predominantly aligned with the height direction *Perosanz et al.* (2003)). Within this long period also another gravity mission was operated by the European Space Agency (ESA). Between March 2009 and November 2013 the ESA GOCE mission (Fig. 1.4) provided exceptional observations of the gravity gradients at very low altitude around 260 km. This extremely low altitude made necessary the use of a drag-free system utilizing electric propulsion to counteract drag forces and maintain the altitude (*Floberghagen et al.*, 2011). The ESA Swarm mission (Fig. 1.4) is the most recent among the selected missions and is still operational (status May 2020). It is composed of three identical satellites: Swarm-A, Swarm-B and Swarm-C (also known as Alpha, Bravo and Charlie). These are the first ESA satellites carrying accelerometers dedicated to thermosphere density retrieval. The main objective of Swarm is to investigate the magnetic field and its evolution in time (*Olsen et al.*, 2013). Swarm-A and -C fly together with an initial orbit at 460 km separated in longitude by 1 degree, while the third satellite is around 60–70 km higher. Overlapping in time with GRACE and the recently launched successor GRACE Follow-On (*Kornfeld et al.*, 2019), this mission provides an exceptional opportunity to build a continuous multi-decadal record of thermosphere density data.

All these spacecraft are equipped with one or more accelerometers and can provide quantitative information on satellite aerodynamics. Solar radiation pressure, wind and density are the main contributions that can be measured with this instrumentation. Without accelerometers, the atmospheric drag experienced by satellites can be determined with different approaches. Other observation techniques, such as Precise Orbit Determination (POD), also provide observations of density albeit at lower temporal resolution, i.e. minutes instead of seconds (*van den IJssel*, 2014).

The use of accelerometer data is therefore highly preferred. However, if data quality is affected by accelerometer malfunctions, it is necessary to utilize alternative observation techniques. This happened for the Swarm mission, where GPS-derived accelerations have been created as an alternative to the accelerometer data, which suffer from numerous discontinuities or steps, spikes and other artifacts (*Siemes et al.*, 2016). In Fig. 1.5, the step corrections for Swarm-C accelerations along the longitudinal satellite axis are shown in the period from June 1, 2014, to May 31, 2015. The magnitude and the number of these steps in combination with temperature-induced bias fluctuations made the interpretation of accelerometer-derived density data very difficult. GPS-derived accelerations are computed in an orbit determination processing using a Kalman filter approach (*van den IJssel et al.*, 2020; *Wermuth et al.*, 2010) and used for the calibration of the accelerometer data. This also allows to calculate GPS-derived densities. The new data sets are produced at TU Delft and are provided to the public as an official ESA data product (<https://swarm-diss.eo.esa.int/>). In recent years (2015–2020), the research from this dissertation provided significant improvements to these data sets. In fact, for Swarm it was found that the originally specified and used geometry model caused an error of about 32% in the magnitude of the thermospheric density values. These find-

ings culminated in a completely novel approach for the current Low Earth Orbit (LEO) satellites density data processing (*van den IJssel et al., 2020*).

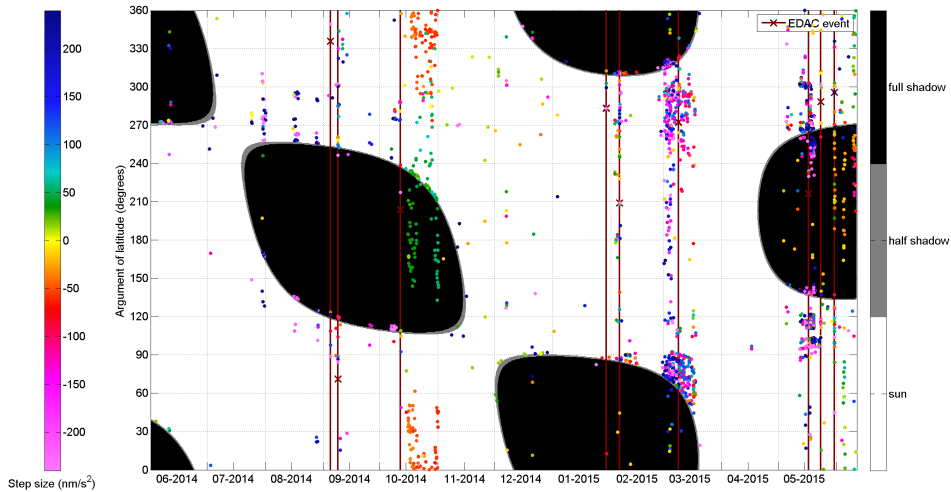


Figure 1.5: Step corrections in along-track accelerations of Swarm C in the period from June 1, 2014, to May 31, 2015. White/grey/black areas indicate that the satellite is in Sun/half-shadow/full shadow of the Earth. Colored dots mark modified steps with respect to time and argument of latitude, where the color indicates the step size (*Siemes et al., 2016*).

### 1.3. HOW DO WE MODEL THE THERMOSPHERE?

The ground- and space-based observations of the last decades provided inputs for creating the first atmospheric models. Currently, there are two classes of models. The ones that are based on collected data through an empirical approach, and the ones which describe the atmospheric physics with equations. These are the empirical and physics-based models, respectively.

Empirical models use relatively simple parameterized equations as a function of time, location and a set of space weather proxies. They are generated with a fit against a database of past observations. Through an interpolation and extrapolation, they provide information on atmospheric characteristics. They provide information on density for the major atmospheric constituents, which can be summed to retrieve the total neutral density. These models lack reliability for describing short spatial or temporal scales. Beyond satellite locations and altitudes, the model inputs rely on solar and geomagnetic proxies. Among the most used models, we can find the MSIS (*Picone et al., 2001*), the DTM (*Bruinsma, 2015*) and the Jacchia (*Jacchia, 1965*) series. The output of these models depends on space weather conditions and, therefore, does not allow for highly consistent analyses during different activity conditions (*Emmert, 2015*). In this research, one of the most used models is the NRLMSISE-00 model from the MSIS family (*Picone et al., 2001*).

Together with these models, the studies on thermospheric horizontal winds paved the way for the Horizontal Wind Model (HWM) series. These models have similar inputs as density models and provide zonal and meridional winds. Inputs are based on rocket, incoherent scatter radar, Fabry-Perot interferometer and satellite measurements. The HWM model series is under constant development at the Naval Research Lab (United States). The latest edition is HWM-14 (*Drob et al., 2015*), which benefited from much extra high-quality observational data as compared to the previous HWM-07 version (*Drob et al., 2008*).

Physics-based models, on the other hand, compute the variations in the thermosphere based on first principles, by solving the energy, momentum and continuity equations. These models try to fully describe with fundamental physics-driven equations the atmospheric behaviour and dynamics. This is a complex task and many models are constantly under development and validation. These are high-resolution models which can provide more refined and suitable outputs for scientific studies for both densities and winds. However, a disadvantage is that they are computationally very demanding. Among the most common and used models are the TGCM (*Peymirat et al., 1998*), GITM (*Ridley et al., 2006*), and WACCM (*Liu et al., 2010*) models. Also in these models, the solar and geomagnetic activity play a role and careful tuning is often required in the model development phase (*Masutti et al., 2016*). In this dissertation some comparisons are performed with the WACCM-X model, which is an extension of the WACCM series (Chapter 4).

#### 1.4. AERODYNAMIC MODELLING

Nearly all of the research using accelerometer- and TLE-derived thermosphere densities over the past decades has focused on the analysis of relative changes in density. Therefore, scale differences between the CHAMP, GRACE, GOCE and Swarm data sets have so far been largely ignored, or quickly fixed by applying a scale factor to each density data set. When comparing the satellite data with models, the average ratios show systematic discrepancies between data and models up to 50% for current solar minimum and NRLMSISE-00 atmospheric model. In past studies by *Doornbos (2011)* and *Pardini et al. (2012)*, these inconsistencies have been investigated. However, the problem was not fully addressed.

Thermosphere density and winds are determined from observations of the satellite non-gravitational accelerations by making use of the proportionality with the aerodynamic acceleration. Therefore, precisely determining the scale of the thermosphere densities from satellite dynamics observations requires a very careful modelling of satellite aerodynamics. The scale differences between the various data sets originate from errors in the aerodynamic modelling, specifically in the modelling of the satellite outer surface geometry and the gas-surface interactions (GSI).

The proposed research, in its first phase, focused on collecting detailed information on the outer surface geometry of all selected missions, on implementing this geometry information into a 3D satellite surface model, and on meticulously checking this model against the original information and against other existing models. Only then the research could move to the next phase, in which the geometry models were applied in the data processing to convert the measured satellite accelerations to thermosphere density

and crosswind information. Within this approach, the SPARTA Direct Simulation Monte Carlo (DSMC) simulator (*Gallis et al., 2014*) was used to bombard the final geometries with particles and compute the resulting force coefficients. Finally, the thermospheric products were obtained with the use of the Near Real-Time Density Model (NRTDM) software developed at TU Delft (*Doornbos, 2006*) based on previous work by *Doornbos (2011)*. This new approach highly improved the previous generation of density and winds data, which were mostly based on analytic solutions by (*Sentman, 1961a,b*). The intermediate version of density and aerodynamics data have been described in *March et al. (2019a)*. The complete discussion of the results and further details are available in Chapter 2.

During a second phase, the gas-surface interaction parameters that determine the satellite aerodynamic forces needed to be estimated and adjusted by making use of variations in satellite orientation and simultaneous observations by multiple satellites. During the nominal forward-flying mode, the satellite usually presents only a small frontal area to the flow, while the large solar panels and bottom panel are close to parallel to the flow. The satellite is usually an elongated aerodynamic shape in this configuration. During sideways flight, this situation is reversed, and the satellite is not in an aerodynamically favourable orientation. Due to the different sensitivity to the aerodynamic gas-surface interactions of surfaces oriented parallel and perpendicular to the flow, this allows for an estimation of the mode of reflection of gas particles and of the energy accommodation coefficient parameter, assuming a stationary atmosphere. In particular, the value of the energy accommodation coefficient describes the energy exchange between particles and satellite surfaces and plays a crucial role in the aerodynamics. Further details and analyses about the influence on thermospheric products of this parameter will be provided in the following chapters. Beyond the GSI study, manoeuvres have been also used in the geometry modelling to validate the accuracy of the newly designed satellite geometries. Comparing two different satellite orientations within a short time, it was indeed possible to get very consistent densities. This was not the case for previous works based on simple geometries and macro model surfaces. Many investigations performed on such manoeuvres showed very interesting scenarios for further scientific studies (*Doornbos, 2011; Pilinski et al., 2013*). For Swarm an additional advantage is that there are three identical satellites, making simultaneous measurements, while only one satellite at a time will make such a manoeuvre. In Chapter 3, these studies on manoeuvres are mainly focused on winds and the CHAMP and GOCE satellites; while in Chapter 4 the GSI influence is studied for aerodynamics and density products for all the selected missions. Due to the lack of large attitude manoeuvres for some missions like GOCE, further analyses on seasonal and solar activity variations could be performed as well. The results from these studies led to conclusions about gas-surface interactions assumptions which will be further discussed in Chapters 3 and 4.

## 1.5. RESEARCH OBJECTIVES, MOTIVATION AND SCOPE

The previous sections included examples of applications of atmospheric models. Practical mission design and space science studies can be enhanced with improved atmospheric models. The research presented in this dissertation started as an extension of the previous work by Dr. Eelco Doornbos at TU Delft, who already analyzed neutral den-

sity and winds (*Doornbos, 2011*). From this study, the presence of systematic errors was highlighted. The source of these discrepancies was associated with errors in the geometry and aerodynamic modelling. In this dissertation, this modelling has been improved in order to reduce errors and obtain more consistent thermospheric density and wind data sets. To accomplish such a task, the introduction of high-fidelity geometries was crucial for the new data processing. The overall research objective for this dissertation is indeed to improve the understanding of geometry and aerodynamic modelling and its influence on atmospheric products. Afterwards, additional goals focused on the characterization of the gas-surface interactions, providing a better definition of key parameters. Throughout a detailed analysis, the main outcome is the estimation of more accurate parameters to generate thermospheric products. The final objective can be set as follows.

*The goal of this dissertation is to improve estimates of aerodynamic parameters and assess the quality of accelerations-derived thermospheric density and wind data, by introducing high-fidelity geometry and aerodynamic information with a special focus on the gas-surface interactions.*

This can be achieved by answering two primary questions:

1. *What is the influence of high-fidelity geometry inputs on satellite aerodynamics and the derivation of neutral thermospheric density?*
2. *What are the enhanced gas-surface interactions parameters which allow for more consistent thermospheric data products?*

The first question is addressed in detail in Chapter 2 and *March et al. (2019a)*. The second question is addressed and answered in two papers. The first paper is focused on the GSI modelling influence on thermospheric winds for the CHAMP and GOCE satellites (*March et al., 2019b*). In the second paper (*March et al., 2020*), the attention is focused on the aerodynamic and density data sets for the CHAMP, GRACE, GOCE and Swarm satellites.

As a parallel objective, the improvement of the ESA Swarm density product played a crucial role in this research. Indeed, in the last years, the enhanced information about geometry and satellite aerodynamics was already applied for deriving thermospheric data sets as part of the official ESA data products. Similar improvements could be achieved in the new version of the GOCE density and wind data. For both missions the achieved results from this dissertation were exploited and the newly derived data are now available on the ESA website (<https://earth.esa.int>).

The dissertation is intended to bring an added value to the scientific community and all those interested in the processing of atmospheric products from satellite observations. As the outcome of this research, the density and winds data reached a high consistency level. Direct applications consist in the improvement of current empirical and physics-based models. The newly derived data sets are suitable for data assimilation and follow-on research. The new data can be used for developing a new generation of empirical models. This would introduce a benefit on orbit and propellant requirements for

new space missions, on long-term atmospheric studies and climate change investigations. The use of these improved data sets in empirical modelling will enable an increase of the accuracy for all the mentioned applications. The increased consistency will allow us to characterize the solar-terrestrial activity dependency of total density and the long-term density trends to a higher accuracy. This could significantly affect predictions for the evolution of space debris in the low Earth orbit environment, which will, in turn, affect mitigation procedures required for the long-term sustainability of satellite missions in low Earth orbits. The accurate scale of density data will enable an accurate estimate of the potential energy contribution to the total thermospheric energy density, required to investigate the magnetospheric forcing of the thermosphere (*Burke et al., 2009*). This dissertation will also contribute to knowledge on satellite aerodynamics, specifically on the gas-surface interactions, and will help to establish a much-needed international standard on this topic, creating the basis for higher consistency satellite drag computations for all low orbiting satellites.

As a first step, this dissertation provides an improvement of the geometry and aerodynamic modelling of a selected set of missions (Chapter 2). The studied satellites are CHAMP, GRACE, GOCE and Swarm. All of them are LEO missions and provide fundamental information of the ionosphere-thermosphere region. Then, the effect of the interaction between atmospheric particles and satellite surfaces on aerodynamics and thermosphere products is investigated. In Chapter 3, the analysis is centred on thermospheric winds, while in Chapter 4 the attention is focused on the aerodynamics and neutral density. Finally, the work described in this dissertation provides recommendations for further works and missions. Conclusions and suggestions for future missions and thermospheric product processing and improvement are made in the final Chapter 5.



# 2

## HIGH-FIDELITY GEOMETRY MODELS FOR IMPROVING THE CONSISTENCY OF CHAMP, GRACE, GOCE AND SWARM THERMOSPHERIC DENSITY DATA SETS

**G. MARCH, E.N. DOORNBOS and P.N.A.M. VISSER**

*During the last two decades, accelerometers on board of the CHAMP, GRACE, GOCE and Swarm satellites have provided high-resolution thermosphere density data to improve our knowledge on atmospheric dynamics and coupling processes in the thermosphere-ionosphere region. Most users of the data have focused on relative density variations. Scale differences between datasets and models have been largely neglected or removed using ad hoc scale factors. The origin of these scale differences arises from errors in the aerodynamic modelling, specifically in the modelling of the satellite outer surface geometry and of the gas-surface interactions. Therefore, the first step to remove the scale differences is to enhance the geometry modelling. This chapter forms the foundation for the improvement of characterization of satellite aerodynamics and gas-surface interactions models,*

---

Parts of this chapter have been published in *Advances in Space Research* **63**(1), 213–238, 2019 [March et al. \(2019a\)](#).

as well as for extending the use of sideways and angular accelerations in the aerodynamic analysis of accelerations and derivation of thermosphere datasets. Although work to improve geometry and aerodynamic force models by other authors has focused on CHAMP and GRACE, this chapter includes the GOCE and Swarm satellites as well. In addition, it uses a density determination algorithm that is valid for arbitrary attitude orientations, enabling a validation making use of attitude manoeuvres. The results show an improvement in the consistency of density data between these four missions, and of data obtained before, during and after attitude manoeuvres of CHAMP and Swarm. The new models result in larger densities, compared to the previously used panel method. The largest average rescaling of density, by switching to the new geometry models is reached for Swarm at 32%, the smallest for GRACE at 5%. For CHAMP and GOCE, mean differences of 11% and 9% are obtained respectively. In this chapter, an overview of the improvements and comparisons of data sets is provided together with an introduction to the next research phase on the gas-surface interactions.

## 2.1. INTRODUCTION

The accuracy of tracking- and accelerometer-derived thermospheric density data sets is closely connected to satellite drag modelling. The previous generation of thermospheric density data sets used simplified satellite geometries (Doornbos, 2011; Sutton, 2008). These geometries are commonly characterized by a limited number of flat panels, which aim to describe the full satellite outer surface geometry. Weaknesses in these models turned out to adversely affect the accuracy and consistency of the derived densities. Large scale differences between data sets and atmospheric models have been detected. Until now, these discrepancies have been neglected or removed using specific scale factors (Bowman et al., 2008; Weimer et al., 2016). However, more accurate thermospheric densities require improved satellite geometry models and rarefied flow analysis on these models. Once the geometry and aerodynamic models are enhanced, high fidelity drag coefficients can be computed to provide new density estimations.

In general, aerodynamic coefficients or ballistic coefficients can be obtained either by estimating them from tracking data during orbit determination, or by analytically or computationally modelling the aerodynamics for defined satellite geometries. When estimating drag coefficients from orbit tracking data, errors in the thermosphere density model that was used will affect the estimate. In many cases, this is desirable, for example when using the estimate for subsequent orbit predictions, based on e.g., GPS, S-Band or satellite laser ranging tracking. If the drag coefficient is used to generate independent density data sets however, it should be free of such model dependencies. Emmert (2009) applied the relations between Two-Line Element (TLE data) and thermosphere density of Picone et al. (2005), and resolved constant per-object ballistic coefficients for approximately 5000 objects in the process, based on the physical drag coefficient of one spherical reference object. For non-spherical objects, a higher fidelity modelling solution is required. If the satellite shape can be approximated by a combination of elementary shapes, this can be obtained with a closed-form analytical approach (Sentman, 1961a). Otherwise, a simulation of aerodynamic effects on detailed satellite geometries with physics-based rarefied gas dynamics solvers (e.g. Bird (1994)) is required. The analytical approach is accurate only for simple geometries (i.e. flat panel, sphere, cylinder,

cube), which usually do not fully describe an operational satellite. Whereas, the computational methods can analyse complex shapes and provide more accurate information. Throughout this work, physical drag coefficients have been determined for different scenarios, in order to improve current density datasets. The technique presented in this chapter provides the opportunity to enhance the estimation of force coefficients and, consequently, satellite aerodynamics. The obtained improvement over the selected missions increases the understanding of the thermospheric region and new density data sets are provided as an outcome of this research.

The implemented methodology is summarized in Section 2.2. The adoption of a high fidelity geometry model is crucial for estimating aerodynamic coefficients. Therefore, for the introduced set of satellites, new geometries have been designed by making use of available technical drawings and pre-launch photographs. A description of the geometry modelling can be found in Section 2.3. The following aerodynamic investigation uses the output of this first modelling phase.

The satellite aerodynamic forces are computed by a rarefied gas dynamics simulator based on the Direct Simulation Monte Carlo (DSMC) technique (*Bird, 1994*). Section 2.4 presents validations and comparisons. In order to simulate rarefied atmospheric flows, it is also possible to use additional approaches. One of those is the Test Particle Monte Carlo (TPMC) method (*Davis, 1960*). Together with the DSMC, it is one of the most common techniques used for rarefied flow simulators. Both methods can treat multiple reflections and shadowing, but have the main limitation of being computationally expensive. The TPMC model interacts with the surface elements but does not implement intermolecular collisions. This makes simulations faster than common DSMC computations. However, for both methods, atmospheric particles impinge on surfaces with velocities that are computed using a Maxwellian velocity distribution. The energy exchange between molecules and surface elements is computed and resulting forces can be processed.

Within the last years, numerous works have been performed on satellite aerodynamics by Monte Carlo techniques and there is an increasing interest in processing satellite data with high fidelity geometries. In *Pilinski et al. (2016)*, a similar approach to the method presented in this thesis is applied to the DANDE satellite. The SPARCS software (*Pilinski, 2011*), based on the test particle technique, analyses a triangulated mesh to provide aerodynamic coefficients. The numerical test-particle technique has been used also by *Mehra et al. (2017)* for the CHAMP and GRACE satellites. In this work, data have been processed with new improved geometries. Results show average differences with respect to the panellized models previously in use in Delft (*Doornbos, 2011*) of 14-18% for CHAMP and 10-24% for GRACE.

In this work, different assumptions have been made and in addition to CHAMP and GRACE, also the GOCE and Swarm satellites have been investigated. The main mission details are listed in Table 2.1, whereas an overview of the altitudes evolution within the satellite lifetimes is provided in Figure 2.1. Section 2.5 describes all the differences between these approaches and the resulting densities in detail. Multiple comparisons with existing data sets and atmospheric models are available. Section 2.6 provides conclusions and an outlook on future work.

Table 2.1: List of the mission characteristics for the CHAMP, GRACE, GOCE and Swarm satellites.

Satellite	CHAMP	GRACE-A, -B	GOCE	Swarm-A, -C	Swarm-B
Operator	GFZ	NASA/DLR	ESA	ESA	ESA
Launch date	Jul. 2000	Mar. 2002	Mar. 2009	Nov. 2013	Nov. 2013
End of the mission	Sept. 2010	Oct. 2017	Oct. 2013	-	-
Initial altitude	460 km	505 km	270 km	470 km	530 km
Inclination	87.3 deg	89.0 deg	96.7 deg	87.4 deg	87.8 deg

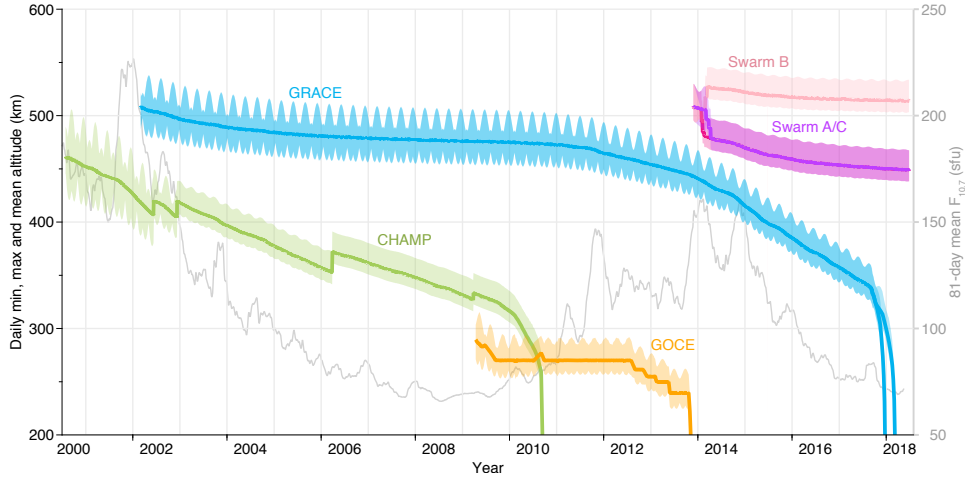


Figure 2.1: CHAMP, GRACE, GOCE and Swarm altitudes evolution.

## 2.2. METHODOLOGY

Satellite aerodynamic forces and torques can be estimated as a function of many inputs. The atmospheric density is a crucial contribution among them. In this chapter, the reverse process is used to provide an improved density data set starting from a detailed aerodynamic modelling. Starting from the expression of the aerodynamic drag acceleration ([Bruinsma et al., 2004](#)), the following equation allows to calculate the atmospheric density.

$$\rho = \frac{2 m a_{drag}}{C_D A_{ref} V_{rel}^2} \quad (2.1)$$

In equation 2.1,  $\rho$  is the neutral mass density,  $m$  the satellite mass,  $a_{drag}$  the drag acceleration,  $C_D$  the drag coefficient,  $A_{ref}$  a reference area and  $V_{rel}$  the velocity relative to the atmosphere. This equation highlights the direct influence of drag coefficients on the density estimation accuracy.

Previous estimations of the neutral mass density have been processed with force coefficients generated from panellized satellite geometries. However, the inability to model multiple reflections and shadowing effects introduced systematic errors at the level of 5-15% ([Doornbos, 2011](#)). In general, the panel method consists of the application of Sentman's equations for flat panels to simplified geometries constructed from multiple panels with different orientations ([Sentman, 1961b](#)). A limited number of flat panels

describe the entire structure of the satellite. Normal vectors and areas of each panel provide the fundamental information needed to retrieve aerodynamic coefficients.

Within this thesis, the aerodynamic modelling is enhanced using the DSMC approach in combination with high fidelity geometries. Satellite accelerations are reprocessed leading to higher fidelity densities in better agreement with atmospheric models. Panel model geometry and aerodynamic modelling turned out to reduce the reliability of derived densities, especially for satellites with complex shape.

The use of DSMC introduces flexibility for analysing not only free-molecular regimes, but also transition to continuum flow in re-entry conditions for additional research scenarios. In particular, the Stochastic Parallel Rarefied-Gas Time-Accurate Analyzer (SPARTA) simulator from SANDIA Laboratories ([Gallis et al., 2014](#)) is used in this work for the aerodynamic modelling. The collisions between atmospheric particles and satellite outer surfaces are simulated within a fixed domain. Pressures and shear stresses associated to each surface element are computed and processed to retrieve overall satellite force coefficients. Aerodynamic data sets from this processing are obtained as a preliminary output. For each analysed configuration, the computed coefficients in the aerodynamic and body fixed frames are listed together with the characteristic simulation inputs (i.e. speed ratio, Euler angles). These data sets are successively processed to obtain atmospheric densities. Further details about the process of extracting densities from accelerometer data can be found in Section 2.5 and in [Doornbos \(2011\)](#). For the Swarm satellites, GPS-derived accelerations have been used instead of accelerometer data due to the presence of numerous spikes and anomalies ([Siemes et al., 2016](#)). These alternative accelerations are estimated within the orbit determination processing using a Kalman-filter approach ([Wermuth et al., 2010](#)). In particular, Swarm densities resulting from this procedure were already analysed during the June 2015 geomagnetic storm in [Astafyeva et al. \(2017\)](#).

In this chapter, for the complete set of satellites, accelerations have been processed with panel and SPARTA-DSMC methods in order to analyse discrepancies between the two approaches. Further comparisons have been performed with a set of semi-empirical atmospheric models. The achieved results are provided in Section 2.5.

## 2.3. GEOMETRY MODELLING

The low level of information about existing panel model surfaces is a significant problem for properly modelling satellite aerodynamics. Within this chapter, the CHAMP-TU Delft ([Doornbos, 2011](#)), GRACE-Bettadpur ([Bettadpur, 2007](#)), GOCE-Alenia ([Cometto, 2007](#)) and Swarm-Astrium ([Siemes, 2018](#)) have been used for the panel model geometries. These macro model surfaces are respectively characterized by 16 panels for CHAMP, 12 for GRACE, 44 for GOCE and 15 for Swarm. Further details about these models and others can be found in Tables 2.2 and 2.3. In general, for each panel, information about normal vector components, area, reflectivity, diffusivity and emissivity indexes are listed in the macro models. Information about panels relative locations are not provided. For this reason, multiple reflections and shadowing effects are not easy to implement within this method. Moreover, for this model, complex instruments like protruding antenna or beams turned out to be difficult to model with a satisfactory accuracy.

As input for SPARTA-DSMC, new high fidelity geometry models were designed. These

geometries are the inputs for the SPARTA-DSMC simulations, which will be discussed in the next Section 2.4. In order to reproduce satellite geometries with high fidelity, technical drawings (e.g. [Schulz \(1999\)](#), [Lühr \(2000\)](#), [Hess \(2001\)](#), [Bettadpur \(2012\)](#), [Severino \(2004a\)](#), [Severino \(2004b\)](#), [Hammond \(2006\)](#)) have been used and compared with the generated surfaces. An overview of the new geometry models is available in Figure 2.2. Qualitative and quantitative comparisons with technical drawings and the previous panel models are available in Section 2.7 and in Table 2.3. In order to raise the reliability, all the possible outer surface elements have been implemented in the geometry modelling. For this reason, technical drawings from satellite manufacturing companies and pre-launch pictures have been exploited in order to correctly model structures, coatings, thermal blankets and further details, which were not implemented in previous models. Table 2.3 shows small differences in the projected areas along the spacecraft body-fixed axes for GRACE and GOCE. These discrepancies reach a maximum value of 6% with respect to the newly designed geometries. Larger differences are highlighted for CHAMP. This is especially verified comparing the projected areas along X-axis for [Lühr \(2002\)](#) and [Bruinsma and Biancale \(2003\)](#), which register differences of 40.3% and 19.1% respectively. These higher percentages are consistent with similar comparisons in [Doornbos \(2011\)](#). The Swarm satellites show the largest differences with respect to the new model. The highest contribution in the discrepancy is associated to the X-axis projection which has a much smaller area with respect to the Astrium geometry model.

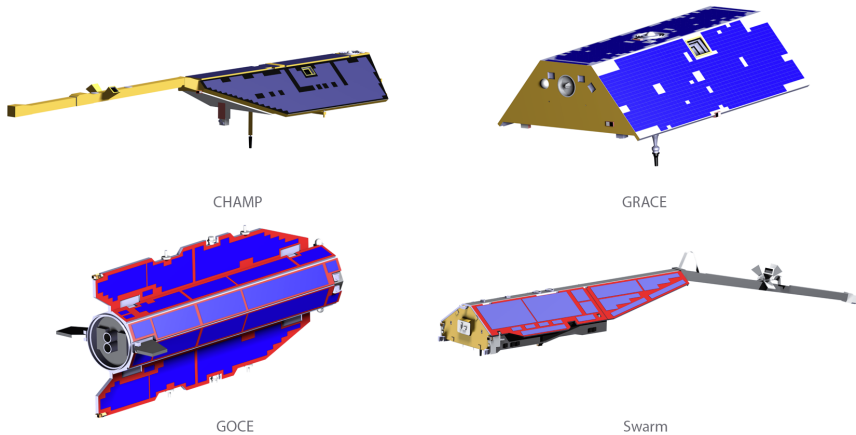


Figure 2.2: Rendering of satellite geometry models designed with CATIA V5 R21.

## 2.4. AERODYNAMIC MODELLING

The accelerometers on board of the CHAMP, GRACE, GOCE and Swarm satellites provide measurements of non-gravitational accelerations. The measured accelerations contain several contributions, which are not exclusively related to atmospheric drag. In order to process satellite aerodynamics from accelerometer data, a correct modelling of additional contributions needs to be performed. In addition to the aerodynamic, other ac-

Table 2.2: List of the satellite models with reference ID and description.

Satellite	ID	Title	Description	Reference
CHAMP	1	SPARTA-March	3D model	This work
	2	CH-IT-DID-001	Tech. drawings, panel model	<a href="#">Lühr (2000)</a>
	3	ANGARA-CH	3D model	<a href="#">Doornbos et al. (2009)</a>
	4	Luehr	Panel model	<a href="#">Lühr (2002)</a>
	5	Bruinsma	Panel model	<a href="#">Bruinsma and Biancale (2003)</a>
	6	TU Delft	Panel model	<a href="#">Doornbos (2011)</a>
GRACE	7	SPARTA-March	3D model	This work
	8	CSR-GR-03-02	Panel model	<a href="#">Bruinsma and Biancale (2003)</a>
	9	ANGARA-GR	3D model	<a href="#">Doornbos et al. (2009)</a>
	10	Bettadpur	Panel model	<a href="#">Bettadpur (2007)</a>
GOCE	11	SPARTA-March	3D model	This work
	12	Alenia	Tech. drawings, Panel model	<a href="#">Cometto (2007)</a>
Swarm	13	SPARTA-March	3D model	This work
	14	Astrium	Panel model	<a href="#">Siemes (2018)</a>

celerations are associated to solar radiation pressure, Earth infra-red radiation pressure, Earth albedo radiation pressure and propulsive thrust. Once all these accelerations are modelled as in [Doornbos \(2011\)](#), the aerodynamic accelerations can be retrieved. In lack of reliable accelerations from the accelerometers, GPS data processing can also provide the necessary information about non-gravitational forces ([van den IJssel, 2014](#)). This method has been already implemented for deriving Swarm L2 density products ([Doornbos et al., 2017](#)) and is used as well in this research.

At LEO altitudes, the thermospheric gas particles have long enough free path lengths and a free molecular flow regime can be assumed. This allows us to neglect particle-particle collisions, which speeds up DSMC simulations. In this work, the aerodynamic coefficients are provided by the SPARTA simulator. The performed simulations cover several different characterizations of thermospheric flows. Moreover, within a specific domain, several attitude configurations have been simulated in order to describe all possible scenarios encountered throughout the mission lifetime. Specific ranges for both attack and side-slip angles have been introduced depending on each spacecraft operational history. Once that geometry modelling has been improved, the influence of gas-surface interactions between particles and satellite surfaces on the aerodynamic accelerations is crucial to be investigated. One of the most important parameters for this investigation is the energy accommodation coefficient ( $\alpha_E$ ). This parameter provides information about the energy exchange between atmospheric particles and satellite outer surfaces ([Pilinski et al., 2016](#)) and at this point will be an input of the new aerodynamic model. If the particles retain their mean kinetic energy after the collision, this parameter is zero, whereas if particles adjust their temperature to the satellite surface temperature, this coefficient reaches 1. The energy accommodation coefficient is defined as follows:

$$\alpha_E = \frac{T_{inc} - T_{re}}{T_{inc} - T_w} \quad (2.2)$$

Table 2.3: Projected areas (in  $m^2$ ) of the CHAMP, GRACE, GOCE and Swarm satellites as viewed along the spacecraft body-fixed axes for different sources. Percentages provide the difference between the results of the earlier models and those based on the newly designed geometries. The direction of X is along-track, whereas those of Y and Z are along cross-track and nadir orientations, respectively.

Satellite	Ref. ID	X	[%]	Y	[%]	Z	[%]
CHAMP	1	0.787		3.193		6.540	
	2	0.742	-5.7	3.120	-2.3	6.444	-1.5
	3	0.794	0.9	3.245	1.6	6.621	1.2
	4	0.470	-40.3	3.377	5.8	6.295	-3.7
	5	0.637	-19.1	3.377	5.8	6.295	-3.7
	6	0.743	-5.7	3.122	-2.2	6.456	-1.3
GRACE	7	1.008		2.488		6.103	
	8	1.001	-0.6	2.463	-1.0	-	-
	9	1.043	3.5	2.550	2.5	6.153	0.8
	10	1.001	-0.6	2.638	6.0	6.365	4.3
GOCE	11	1.038		10.738		5.759	
	12	1.035	-0.3	11.210	4.4	6.049	5.0
Swarm	13	0.784		3.181		6.517	
	14	1.497	90.9	3.381	6.3	5.081	-22.0

Within this formula,  $T_{inc}$  is the particles temperature before the collision,  $T_{re}$  the re-emitted particles temperature and  $T_w$  the satellite outer surface temperature. The thermosphere is influenced by quasi-diffusive gas-surface interactions. The  $\alpha_E$  value depends on different factors like solar activity, altitude and adsorbed gas composition over satellite surfaces ([Pardini et al., 2010](#); [Pilinski et al., 2013](#)). In order to fix an accommodation coefficient to focus exclusively on geometry and aerodynamic modelling, an ideal fully-diffusive reflection mode ( $\alpha_E=1$ ) has been selected for this study. The implementation of a detailed gas-surface interactions model with the introduction of optimal accommodation coefficients is an important next step, which will be further described in following chapters.

The energy accommodation coefficient has been introduced in Sentman's equation, and consequently in the panel method, by [Moe et al. \(2004\)](#) and [Sutton \(2009\)](#) as well as [Doornbos \(2011\)](#) for accelerometer data processing.

The relative velocity ( $V_r$ ) is defined as the velocity of the satellite with respect to the surrounding atmosphere. Following this implementation, the drag unit vector ( $\hat{u}_D$ ) and the  $\vec{V}_r$  vectors have the same direction, whereas the lift unit vector for each single panel ( $\hat{u}_{L,i}$ ) can be found by equation 2.3, where  $\hat{n}_i$  is the normal vector of the  $i$ -th flat plate element. The negative dot products of drag and lift unit vectors with  $\hat{n}_i$  are defined as  $\gamma_i$  and  $l_i$  respectively.

$$\hat{u}_{L,i} = - \frac{(\hat{u}_D \times \hat{n}_i) \times \hat{u}_D}{\|(\hat{u}_D \times \hat{n}_i) \times \hat{u}_D\|} \quad (2.3)$$

In order to retrieve information about drag and lift, Sentman's formulas for a single-sided flat plate can be modified using equations (2.4) and (2.5),

$$C_{D,i,j} = \left[ \frac{P_{i,j}}{\sqrt{\pi}} + \gamma_i Q_i Z_{i,j} + \frac{\gamma_i}{2} \frac{v_{re}}{v_{inc}} (\gamma_i \sqrt{\pi} Z_{i,j} + P_{i,j}) \right] \frac{A_i}{A_{ref}} \quad (2.4)$$

$$C_{L,i,j} = \left[ l_i G_j Z_{i,j} + \frac{l_i}{2} \frac{v_{re}}{v_{inc}} (\gamma_i \sqrt{\pi} Z_{i,j} + P_{i,j}) \right] \frac{A_i}{A_{ref}} \quad (2.5)$$

where

$$\gamma_i = -\hat{u}_D \cdot \hat{n}_i \quad l_i = -\hat{u}_L \cdot \hat{n}_i \quad (2.6)$$

$$G_j = \frac{1}{2s_j^2} \quad P_{i,j} = \frac{1}{s_j} \exp(-\gamma_i^2 s_j^2) \quad Q_j = 1 + G_j \quad Z_{i,j} = 1 + erf(\gamma_i s_j) \quad (2.7)$$

The  $j$ -index is related to the  $j$ -th constituent. The overall aerodynamic coefficients consist in the weighted sum of major constituents of local atmosphere. Furthermore, in the previous equations, the velocity ratio between re-emitted and incoming particles ( $v_{re}/v_{inc}$ ) is obtained as a function of the energy accommodation coefficient and wall temperature by equation (2.8) from [Koppenwallner \(2009\)](#).

$$\frac{v_{re}}{v_{inc}} = \sqrt{\frac{1}{2} \left[ 1 + \alpha_E \left( \frac{4RT_w}{v_{inc}^2} - 1 \right) \right]} \quad (2.8)$$

Within atmospheric flow investigations, the speed ratio ( $s$ ) has a crucial importance. This parameter is the ratio between satellite speed ( $v_{inc}$ ) and the most probable speed of the atmospheric particles (denominator of equation 2.9). Analytically, the equation 2.9 provides the mentioned parameter.

$$s = \frac{v_{inc}}{\sqrt{\frac{2RT_{inc}}{m}}} \quad (2.9)$$

From the previous formula, it is possible to see that the speed ratio is directly connected with the satellite speed, local atmospheric temperature ( $T_{inc}$ ), molecular mass ( $m$ ) and gas constant ( $R$ ). Analysing a certain range of speed ratios, including attitude variations as well, all encountered mission scenarios can be simulated. For the selected satellites, within the performed simulations, the speed ratio ranges between 1 and 14. This interval guaranteed a complete description of experienced thermospheric conditions. After a validation, provided in next Subsection 2.4.1, results concerning satellite aerodynamics are presented in Section 2.4.2.

### 2.4.1. VALIDATION

In order to validate SPARTA computations, simple geometries have been introduced and compared with panel method results. In this section, two validations for a flat panel and a box are presented. Figure 2.3 gives a first comparison between the panel method result (solid lines) and SPARTA aerodynamic coefficients (markers) for a two-sided flat panel. At 0 degree of attack angle, the normal vector is aligned with the atmospheric flow direction and the drag force reaches its maximum value. Figure 2.4 shows the same analysis for a box with angle of attack (a) and side-slip (b) angle variations. The aerodynamic coefficients have been normalised with a reference area set to 1 m<sup>2</sup>.

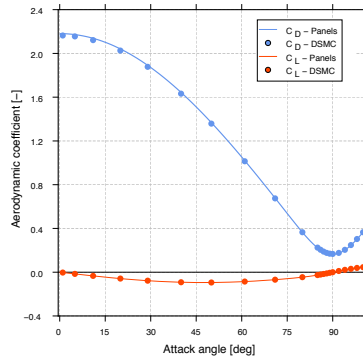
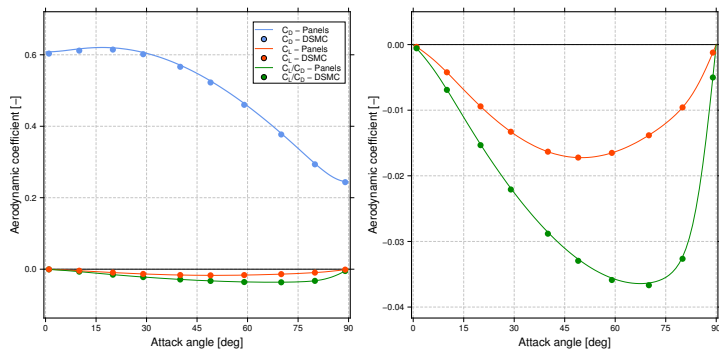
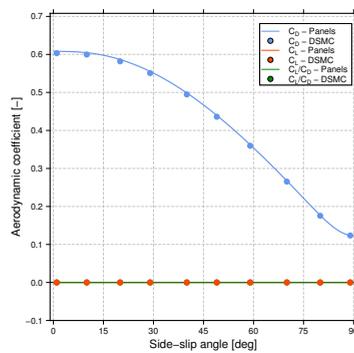


Figure 2.3: SPARTA validation for a two-sided flat plate. Aerodynamic coefficients computed using the panel method (solid lines) are compared with DSMC computations (markers).



(a)



(b)

Figure 2.4: SPARTA validation for a attack angle (a) and side-slip (b) rotations of a box. Aerodynamic coefficients for panel method (solid lines) are compared with DSMC computations (markers).

For both investigations, the two approaches turned out to be in good agreement. The presented simulations in Figures 2.3 and 2.4 have been performed for a fixed speed ratio equal to 7, atmospheric temperature of 1000 K and satellite surface temperature of 400 K. The atmospheric composition is assumed to be 100% atomic oxygen. Changes in selected inputs do not modify the agreement between the two approaches.

In combination with the presented validations, a sensitivity analysis has been performed. This study showed a relevant influence of energy accommodation coefficient and molecular mass on aerodynamic coefficients in agreement with *Doornbos (2011)*. Whereas, for temperatures the influence is smaller, especially for the surface temperature, which is not significantly affecting computed coefficients.

### 2.4.2. SATELLITE AERODYNAMICS

In order to compare the panel and SPARTA methods for realistic satellite aerodynamics, normalised force coefficients as a function of attack and side-slip angle have been investigated. A representation of the analysed angles is available in Figure 2.5.

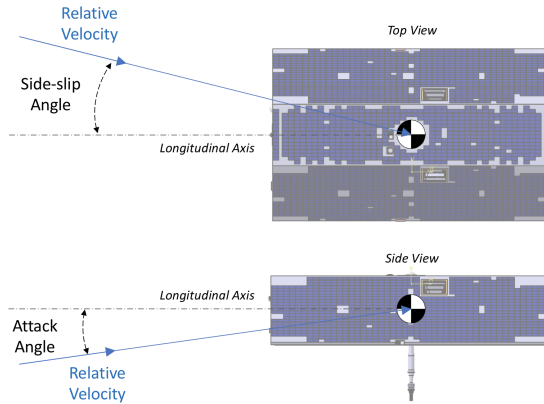


Figure 2.5: Representation of side-slip and attack angles for GRACE.

In the following results, inputs are assumed to be the same as the previously defined validations (Section 2.4.1). However, additional settings are also tested at the end of this section. Figures 2.6 and 2.7 show the drag, lift and lift over drag ratio for CHAMP. Figure 2.6 analyses attack angle influence, whereas Figure 2.7 shows the aerodynamic coefficients for side-slip angle variations. For these figures, the left plot contains all quantities of interest (drag, lift and lift over drag ratio), whereas, the right plots offer a detailed description of exclusively lift and lift over drag ratio, which are characterised by lower values. The selected aerodynamic coefficients have been normalised with a reference area set to 1 m<sup>2</sup> for all missions. This reference area does not depend on the attack and side-slip angles, and therefore variations of the true flow-exposed area of the satellites do not need to be independently calculated. These are already captured in the normalised force coefficients which are a function of these angles. The normalised force coefficients shown in Figures 2.6 – 2.13 were calculated with a speed ratio corresponding to 100%

atomic oxygen and a temperature of 400 K. In order to process the new densities, the drag coefficients need to be computed for all the atmospheric constituents and summed to obtain the on-track values (*Doornbos, 2011*). Temperatures and the relative mass concentrations of atmospheric constituents depend on satellite locations and play a crucial role in the final density estimation.

2

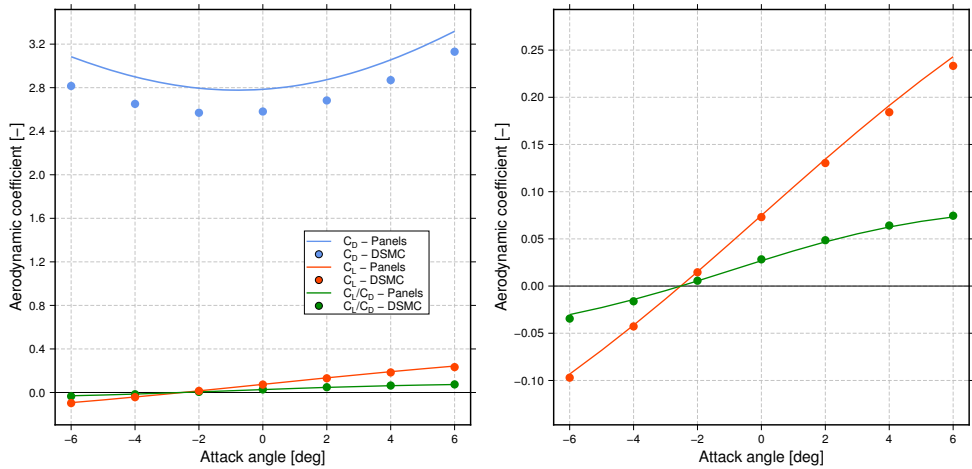


Figure 2.6: Comparison between panel and SPARTA aerodynamic coefficients as a function of attack angles for CHAMP.

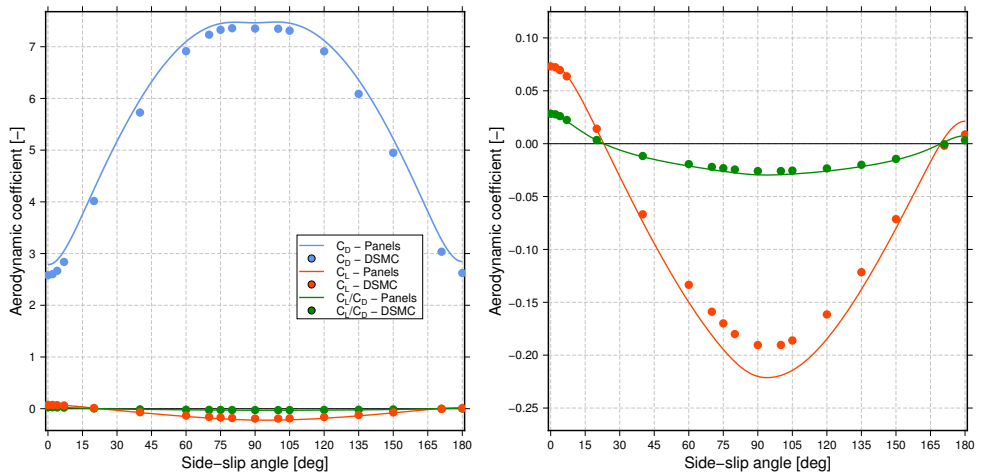


Figure 2.7: Comparison between panel and SPARTA aerodynamic coefficients as a function of side-slip angles for CHAMP.

Introducing the results for the other satellites, Figures 2.8 and 2.9 are for GRACE, Figures 2.10 and 2.11 for GOCE and finally Figures 2.12 and 2.13 for Swarm. Aerodynamic

coefficients are available on the vertical axis, whereas selected attitude angles are on the horizontal axis.

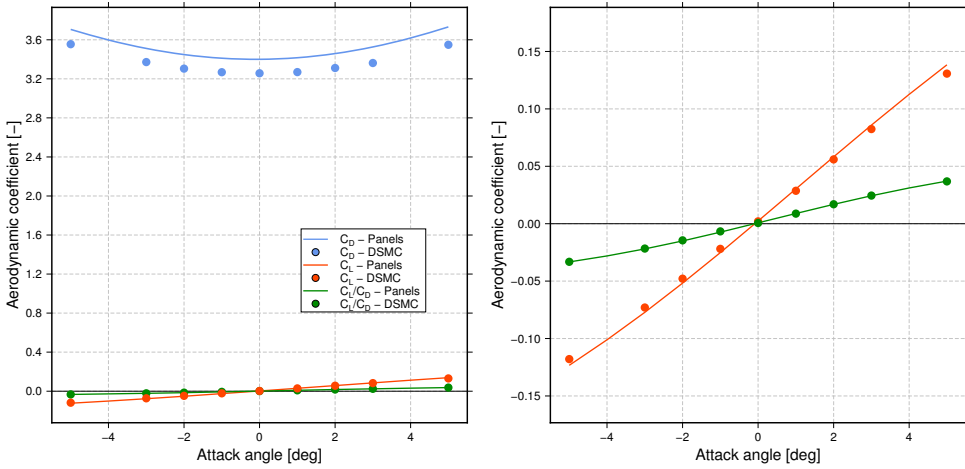


Figure 2.8: Comparison between panel and SPARTA aerodynamic coefficients as a function of attack angles for GRACE.

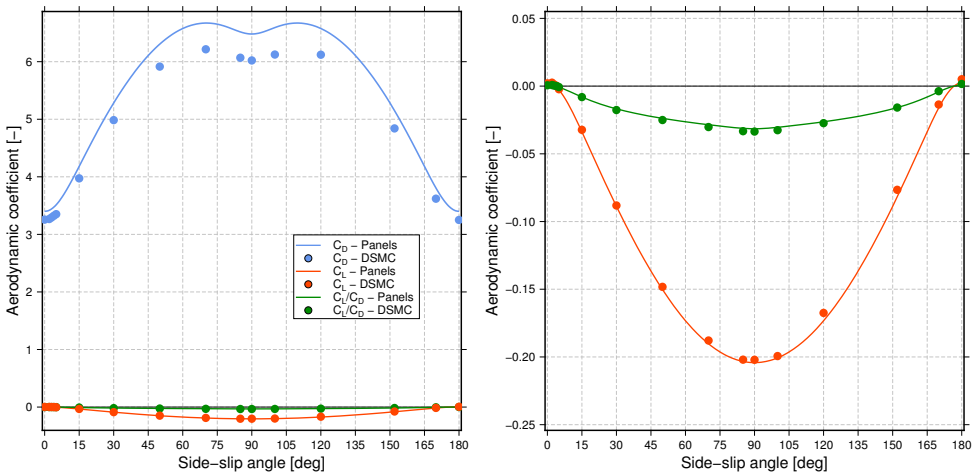


Figure 2.9: Comparison between panel and SPARTA aerodynamic coefficients as a function of side-slip angles for GRACE.

The drag coefficient is the predominant coefficient and analyzing each satellite, it can be observed that coefficient differences are up to 32%. These discrepancies between panel and SPARTA methods are not constant between different satellites and turned out to be strictly related to satellite outer surface complexity. Indeed, the best agreement can be found for GRACE, which in comparison with other satellites is characterized by a

simpler shape. Large differences are obtained for Swarm, while the differences are at a similar intermediate level for CHAMP and GOCE.

2

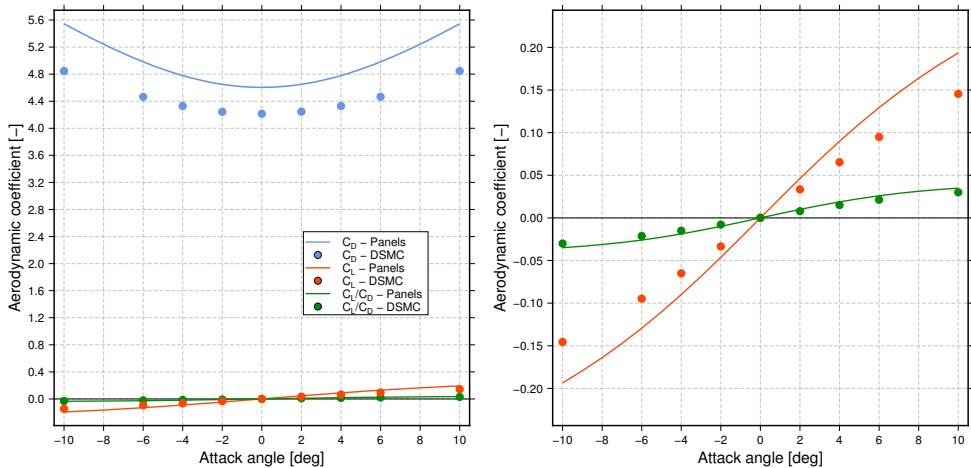


Figure 2.10: Comparison between panel and SPARTA aerodynamic coefficients as a function of attack angles for GOCE.

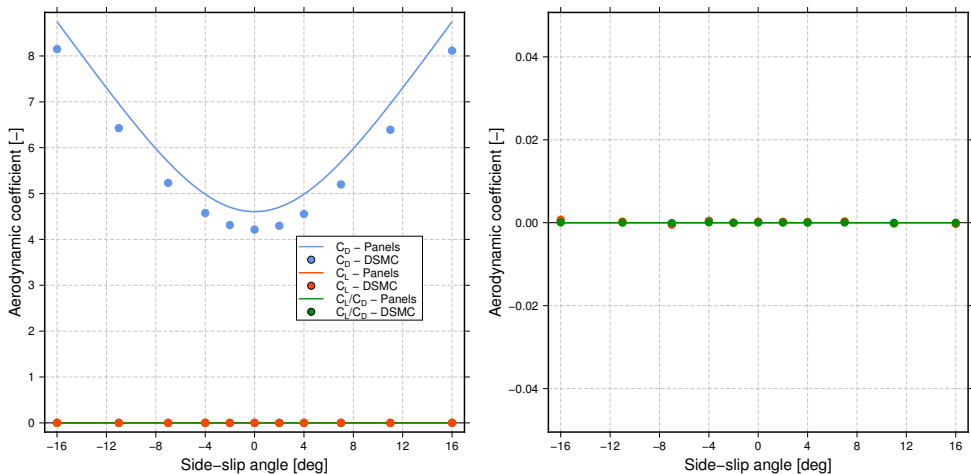


Figure 2.11: Comparison between panel and SPARTA aerodynamic coefficients as a function of side-slip angles for GOCE.

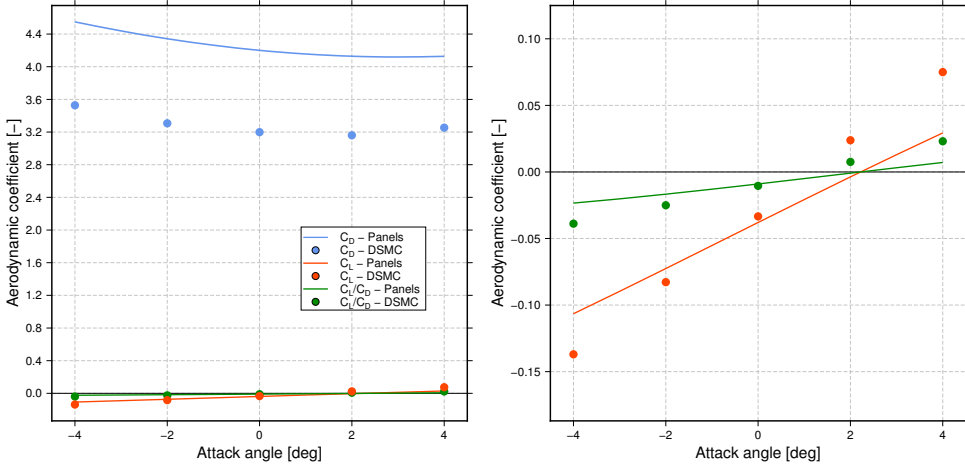


Figure 2.12: Comparison between panel and SPARTA aerodynamic coefficients as a function of attack angles for Swarm.

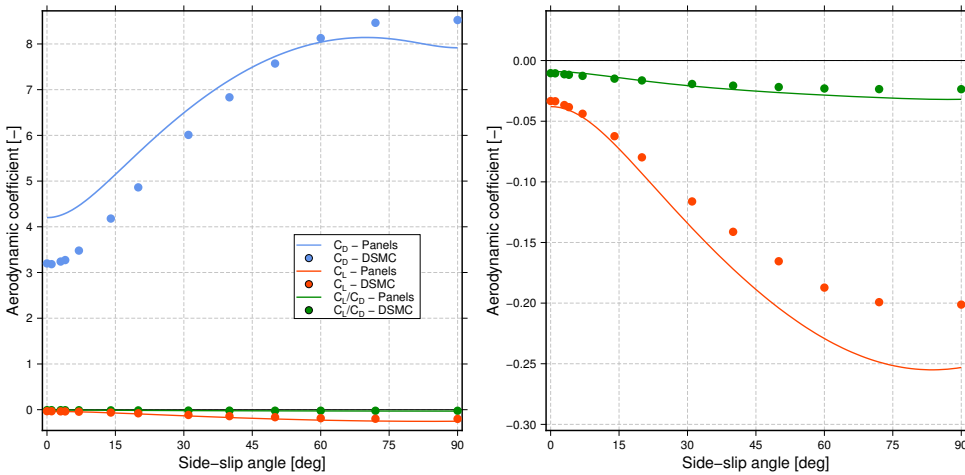


Figure 2.13: Comparison between panel and SPARTA aerodynamic coefficients as a function of side-slip angles for Swarm.

The previous results have been obtained for a fixed speed ratio equal to 7. However a full range of different speed ratios between 1 and 14 has been analysed for each satellite. Low speed ratios occur at low molecular mass of the gas, and at high gas temperature.

Whereas, high speed ratios are characterized by the opposite trends according to Equation (2.9). Figure 2.14 shows the evolution of drag coefficients depending on different speed ratios and selected side-slip angles.

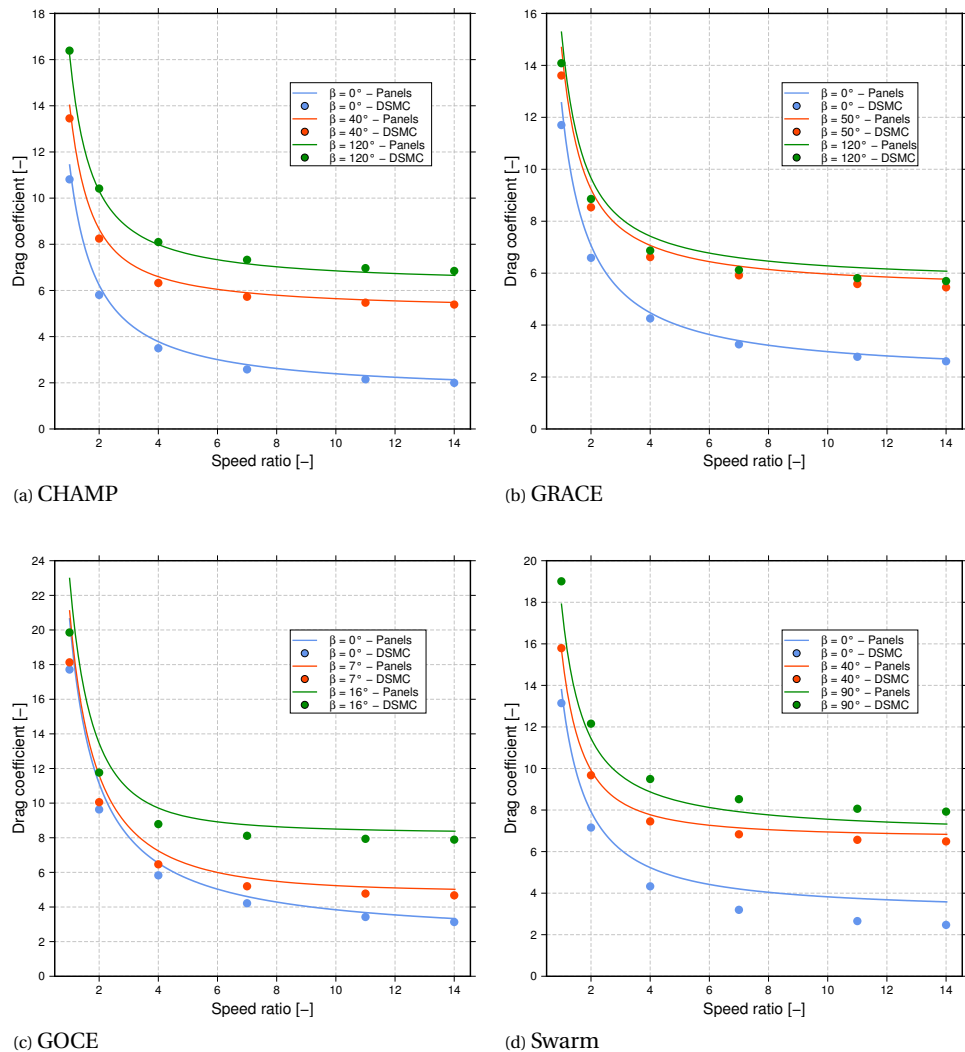


Figure 2.14: Drag coefficients as a function of the speed ratio for selected side-slip angles.

From Figure 2.14, it is possible to have a complete overview of the drag for the selected satellites and different speed ratios. It turns out that nominal flight configuration ( $\beta = 0$ ) always provide overestimated drag coefficients from the panel method with respect to the DSMC approach. As shown before, for the CHAMP, GRACE, and GOCE satellites, the drag difference turns out to be less significant compared to Swarm. How-

ever, from these diagrams, it is clear that there are different behaviours also for different side-slip angles. The panel method is not constantly overestimating or underestimating the drag, but the difference depends on the attitude and speed ratio. For the same satellite and side-slip angle, it is possible to find a better agreement or a larger discrepancy depending on the value of the speed ratio. This makes it necessary to have a complete and detailed description of satellite aerodynamics as a function of each of these inputs encountered during the mission lifetime. An accurate description about the orbit is obtained from the star camera attitude data. Whereas, the information about the atmospheric composition to model the speed ratio along the orbit is provided by the NRLMSISE-00 model (*Picone et al., 2001*). A complete and detailed aerodynamic data set is generated from these outputs and these preliminary results are used as input for the density processing explained in the next section.

## 2.5. DENSITY PROCESSING

Processing accelerations introduces the use of three orthogonal acceleration observations and four unknowns which are the density and the three wind velocity components. The satellite relative velocity is provided by the combination of orbit, co-rotation and wind velocities. The first two are known with higher fidelity with respect to the winds, which can be obtained from specific models. Raw accelerometer data need to be processed to remove various non-aerodynamic accelerations. These are mostly due to radiation pressure, thrusters and mechanical forces from electrical currents (*Flury et al., 2008*). The density is one of the scientific results obtainable from accelerations. As mentioned in the introduction, many studies have been published on this processing. Among recent scientific papers, *Pilinski et al. (2016)* and *Mehta et al. (2017)* provided improved aerodynamic modelling for the DANDE, POPACS (*Pilinski et al., 2016*), CHAMP and GRACE (*Mehta et al., 2017*) satellites. In *Pilinski et al. (2016)*, the main attention is focused on the aerodynamics of two satellites independently of the atmospheric density. Similar computations (as explained in Section 2.4) are used and a comparison with closed-form solutions is also available. Simpler satellite shapes like DANDE allow for a direct comparison with analytical solutions. However, the geometric complexity of the selected satellites of this work does not allow a direct comparison with a single closed-form solution, but only with a sum of multiple contributions from flat panels. As mentioned in the introduction, both papers use the TPMC technique. In particular, *Mehta et al. (2017)* simulations are based on new geometries, which are designed with a CAD software. Unlike this work, *Mehta et al. (2017)* assumes zero atmospheric winds. The absence of atmospheric winds introduces uncertainties between 5% and 20% on estimated densities (*Sutton, 2008*). Large uncertainties are especially detected for high latitudes and geomagnetic active conditions. In this thesis, atmospheric winds are computed with atmospheric models (i.e. HWM07), and where possible, wind components can be derived from the acceleration data. Wind models are based on large amounts of observations, the uncertainties are usually based on the natural variability of the system and the observational uncertainties which can reach values greater than 100 m/s (*Drob et al. (2008)*, *Drob et al. (2015)*).

Both *Pilinski et al. (2016)* and *Mehta et al. (2017)* use variable gas-surface interactions (GSI) models. These models provide different behaviours with respect to fully diffusive

reflections and are applicable to the presented geometries. However, a further development of current GSI models is necessary. Exploiting multiple satellite data sets as well as analysing lift, torques, in addition to drag, would potentially allow an optimization of GSI parameters, which will help to obtain more consistent density data. This is based on a first crucial step that consists of a high-fidelity geometry modelling, which is fully characterized in this work.

The densities from [Sutton \(2008\)](#) and [Mehta et al. \(2017\)](#) have been retrieved from the supplemental data from [Mehta et al. \(2017\)](#). In this section, a comparison for the three representative days selected in [Mehta et al. \(2017\)](#) is performed with the new densities presented in this chapter. An additional comparison with Sutton results is also included. The analysed days are: 2002-10-27, 2005-05-15 and 2009-08-28. The day in 2002 is associated to high solar activity, whereas the 2005 and 2009 days are respectively for moderate and low activities. This comparison covers the data of the CHAMP and GRACE satellites. Full statistical details for the complete days are provided in the [Table 2.4](#). Whereas, [Figures 2.15, 2.17 and 2.18](#) show the comparison between SPARTA, [Mehta et al. \(2017\)](#), [Sutton \(2008\)](#) and [Doornbos \(2011\)](#) estimated densities for the CHAMP satellite within the first three hours of each day. [Figures 2.19, 2.20 and 2.21](#) show the same comparison for the GRACE satellite. In each Figure, a direct comparison between densities is available in the top plot. The second plot presents the ratio between external and SPARTA densities. Only for the CHAMP satellite, a full day plot is available in [Figure 2.16](#) to highlight a lack of data among the data sets. The flagged area in grey associated to a lack of accelerations is due to missing star camera attitude data. This interval ranges between 18:32-19:20 UTC. This gap was linearly interpolated in [Figure 3 of Mehta et al. \(2017\)](#). In [Table 2.4](#) the flagged data are excluded from statistical comparisons. All the other days, including those ones for GRACE, do not have additional flags. In [Table 2.4](#), the mean difference (MD) and mean ratio (MR) are computed as

$$MD = mean\left(\frac{|\rho_{ext} - \rho_{spa}|}{\rho_{spa}} \cdot 100\right) \quad MR = mean\left(\frac{\rho_{ext}}{\rho_{spa}}\right) \quad (2.10)$$

The  $\rho_{ext}$  is the density estimated by one of the external sources, whereas  $\rho_{spa}$  is the density obtained from SPARTA simulations. The comparison for CHAMP shows a higher agreement with the results from Mehta and Doornbos. However, for Sutton's data set, the differences are larger. The new results match well with Doornbos' previous data for both missions. The density ratios based on Doornbos' data in [Figures 2.15–2.21](#) have a smoother behaviour compared to the other two data sets, especially for GRACE. Indeed, a nearly constant density ratio can be found in the [Figures 2.19–2.21](#). Analogous trends are obtained comparing independently Sutton and Mehta results. This might be related to a similar accelerometer calibration processing between Sutton-Mehta results from one side and Doornbos-SPARTA results from the other. For example, for the GRACE satellite, the presence of spikes in the SPARTA-Doornbos results are associated to attitude thruster effects. These disturbances in the accelerations have been differently filtered out in the other two sets. This creates a double similarity and discrepancy respectively within and between the two couples of sets. Differences in dealing with additional acceleration contributions, such as solar radiation pressure, can create further variations

between the analysed sets.

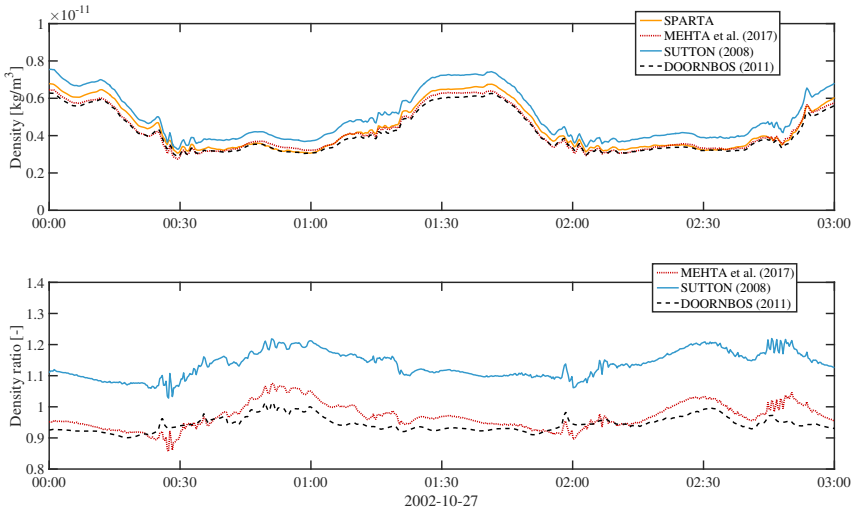


Figure 2.15: Comparison of SPARTA results with *Sutton (2008)*, *Mehta et al. (2017)* and *Doornbos (2011)* CHAMP density data sets on the first 3 hours of 2002-10-27.

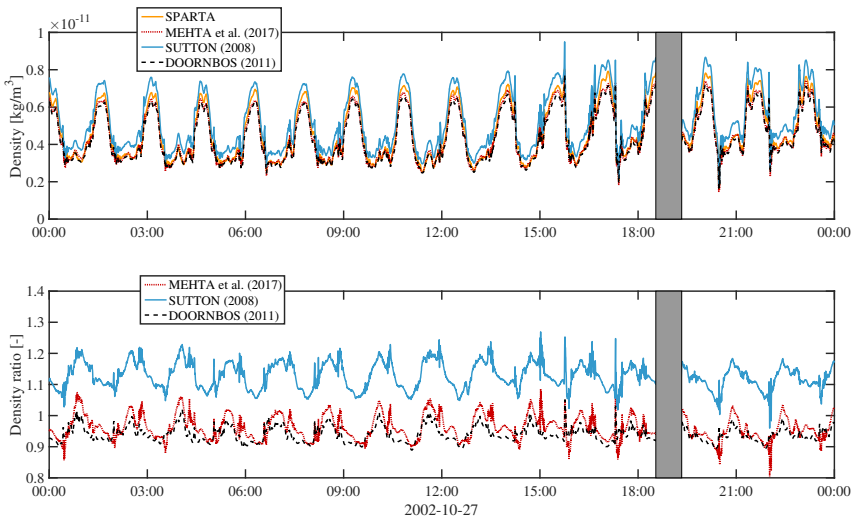


Figure 2.16: Comparison of SPARTA results with *Sutton (2008)*, *Mehta et al. (2017)* and *Doornbos (2011)* CHAMP density data sets on 2002-10-27. The grey area is associated to a lack of star camera attitude data (18:32-19:20 UTC).

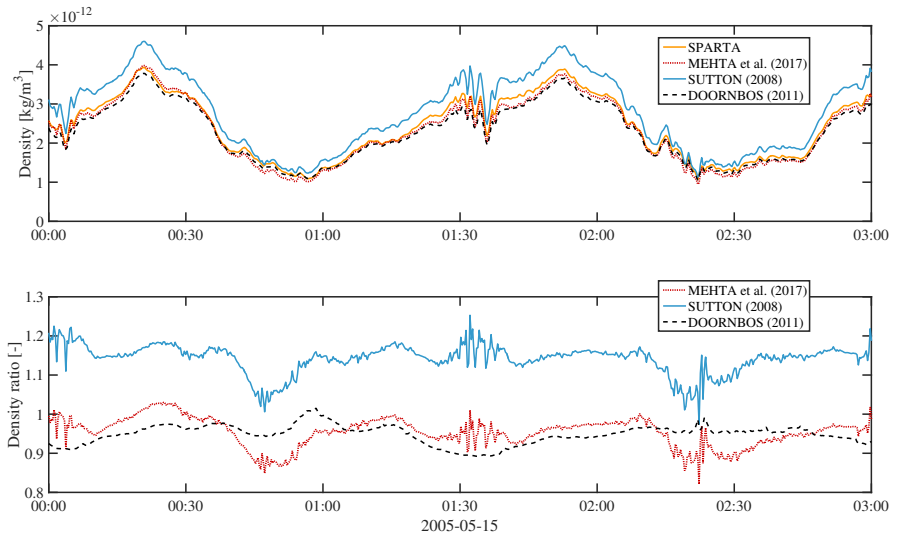


Figure 2.17: Comparison of SPARTA results *Sutton (2008)*, *Mehta et al. (2017)* and *Doornbos (2011)* CHAMP density data sets on the first 3 hours of 2005-05-15.

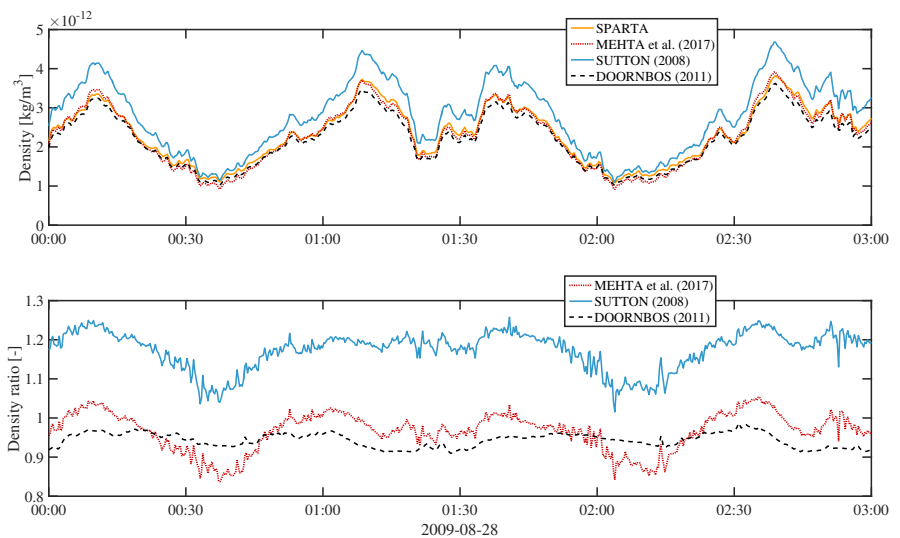


Figure 2.18: Comparison of SPARTA results *Sutton (2008)*, *Mehta et al. (2017)* and *Doornbos (2011)* CHAMP density data sets on the first 3 hours of 2009-08-28.

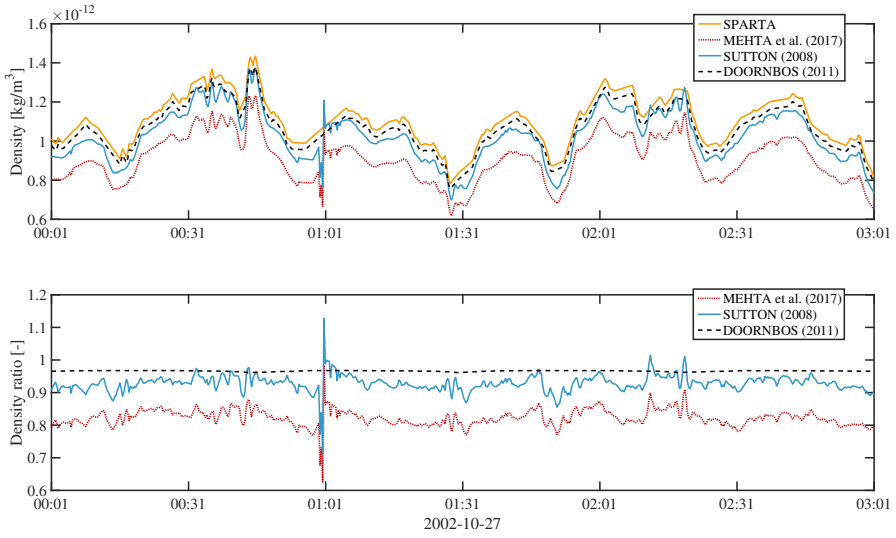


Figure 2.19: Comparison of SPARTA results with *Sutton (2008)*, *Mehta et al. (2017)* and *Doornbos (2011)* GRACE density data sets on the first 3 hours of 2002-10-27.

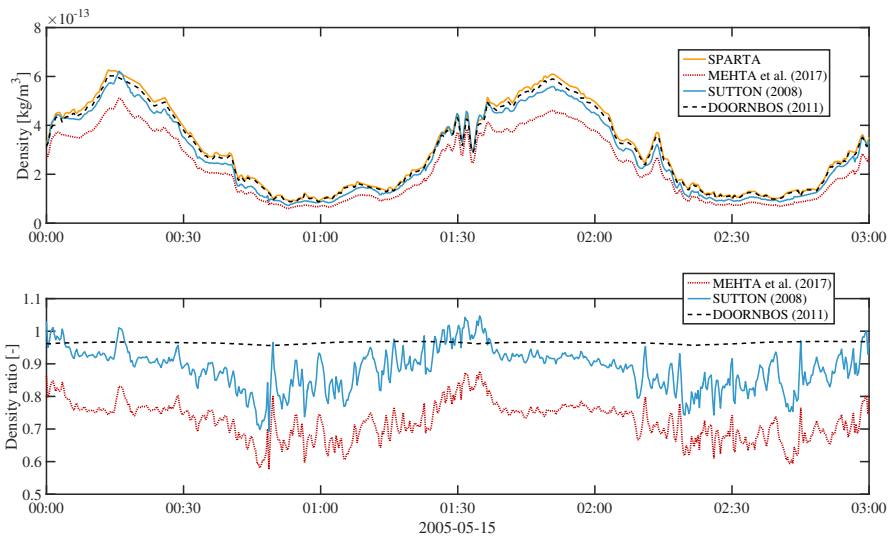


Figure 2.20: Comparison of SPARTA results *Sutton (2008)*, *Mehta et al. (2017)* and *Doornbos (2011)* GRACE density data sets on the first 3 hours of 2005-05-15.

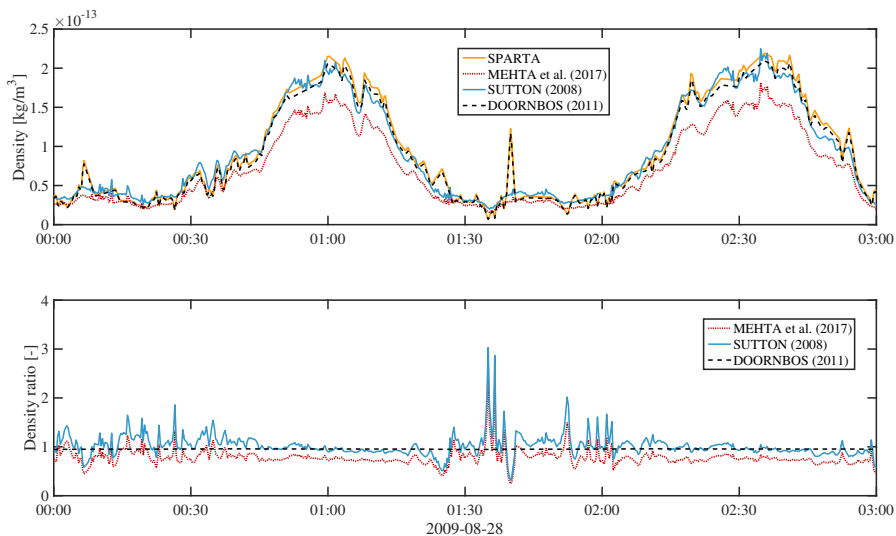


Figure 2.21: Comparison of SPARTA results *Sutton* (2008), *Mehta et al.* (2017) and *Doornbos* (2011) GRACE density data sets on the first 3 hours of 2009-08-28.

Table 2.4: Comparison of SPARTA results with *Mehta et al.* (2017) [M] *Sutton* (2008) [S] and *Doornbos* (2011) [D] estimated densities

Satellite		Source	27-10-2002	15-05-2005	28-08-2009
CHAMP	Mean Diff. [%]	M	5.27	3.92	5.41
		S	12.92	15.84	16.15
		D	6.03	5.84	6.09
	Mean Ratio [-]	M	0.96	0.97	0.95
		S	1.12	1.16	1.16
		D	0.94	0.94	0.94
GRACE	Mean Diff. [%]	M	17.38	22.84	23.93
		S	7.05	8.67	17.65
		D	3.39	3.44	4.67
	Mean Ratio [-]	M	0.83	0.77	0.83
		S	0.93	0.92	1.08
		D	0.97	0.97	0.95

For CHAMP, Table 2.4 shows a higher agreement between SPARTA and *Mehta et al.* (2017) with respect to *Doornbos* (2011) and *Sutton* (2008). Indeed, among the three representative days, there is an average percentage difference of 4.9% with *Mehta et al.* (2017), 6% with *Doornbos* (2011) and 15% with *Sutton* (2008). Whereas, for GRACE, the agreement with *Doornbos* (2011) is better. Calculated average differences are 21.4% with

*Mehta et al. (2017)*, 11.1% with *Sutton (2008)* and 3.8% with *Doornbos (2011)*. Differences within the three representative days are similar. However, densities estimated by Sutton turned out to be highly correlated with SPARTA results for high solar activity. This result can be associated to the different assumptions on the gas-surface interaction. Indeed, *Sutton (2008)* used a constant value of 0.93 for the energy accommodation coefficient, which is in agreement with high solar activities (*Mehta et al., 2013*). From the other side, for *Mehta et al. (2017)*, a Cercignani-Lampis-Lord (CLL) model is used (*Walker et al., 2014*) and the comparison shows a more constant behaviour for differences. The adoption of lower accommodation coefficients leads to higher drag coefficients, which result in lower densities. Therefore, further research on GSI can reduce current discrepancies with *Mehta et al. (2017)*.

In the following subsections 2.5.1 and 2.5.2, the results concerning density processing are provided through two different studies. The first relies on statistical comparisons between panel and SPARTA method for long time periods. The second one is focused on specific yaw-manoeuvres in short time windows.

### 2.5.1. COMPARISON WITH SEMI-EMPIRICAL MODELS

In order to process data, the Direct and the Iterative algorithms from *Doornbos (2011)* have been adapted to SPARTA and applied to the complete set of CHAMP, GRACE, GOCE and Swarm satellites. Using these algorithms, panel method output can be directly compared with new aerodynamic datasets from SPARTA. Taking into account nominal flight conditions for long periods, it is possible to retrieve statistical information about densities in comparison with available atmospheric models. These comparisons have been performed for both panel and SPARTA methods. The reference axis is chosen with X direction along the track, Y along cross-track and Z along radial orientation. For a nominal flight configuration, Euler angles are small and the inertial satellite velocity is mostly aligned with the satellite longitudinal axis. In this case, it is possible to take into consideration only the X-component of the accelerations. This procedure is used within the Direct algorithm for density processing discussed in *Sutton (2008)* and *Doornbos et al. (2010)*. All four selected missions have been investigated. Swarm-A and -C provided the same results because of their similar orbit and for this reason, they are listed together. For GRACE, only new densities from GRACE-A are shown because the twin satellite (GRACE-B) provided the same results. Figure 2.23 presents a comparison of thermospheric densities for Swarm Charlie with the two different geometry modellings. In this figure, SPARTA and panel method results are compared with NRLMSISE-00 atmospheric model (*Picone et al., 2001*). The statistical results are presented in the top left part of each diagram by two parameters. These values are the log-normal mean ratio of estimated densities over atmospheric model densities ( $\mu^*$ ) and the log-normal standard deviation ( $\sigma^*$ ). Densities are estimated in the period between 2014-07-19 and 2016-09-30. For this particular density model, the mean ratio shows a significantly better agreement. The standard deviation is nearly constant. This is associated to the same difficulty in modelling additional contributions like solar radiation pressure. Looking at low densities, the data cloud turns out to be wider. Indeed, lower densities are characterized by lower aerodynamic contribution to the total acceleration which reaches radiation pressure magnitudes. In these areas, solar radiation pressure incorrect modelling have more

impact on densities. Further improvement of radiation pressure modelling would reduce errors in the measured densities. The achieved percentage differences for the set of satellites depends on the reliability of previous panel geometry modellings, which turns out to have been more accurate for simpler satellite geometries. For GRACE, which is characterized by a simpler shape, the improved densities registered a difference of +5%. Whereas, new geometry models for CHAMP and GOCE provided changes of 11% and 9% respectively. In all cases, the changes were towards better agreement with the models (Figure 2.22). This study has been conducted also comparing with different atmospheric models (NRLMSISE-00, JB-2008 (*Bowman et al., 2008*) and DTM-2013 (*Bruinsma, 2015*)).

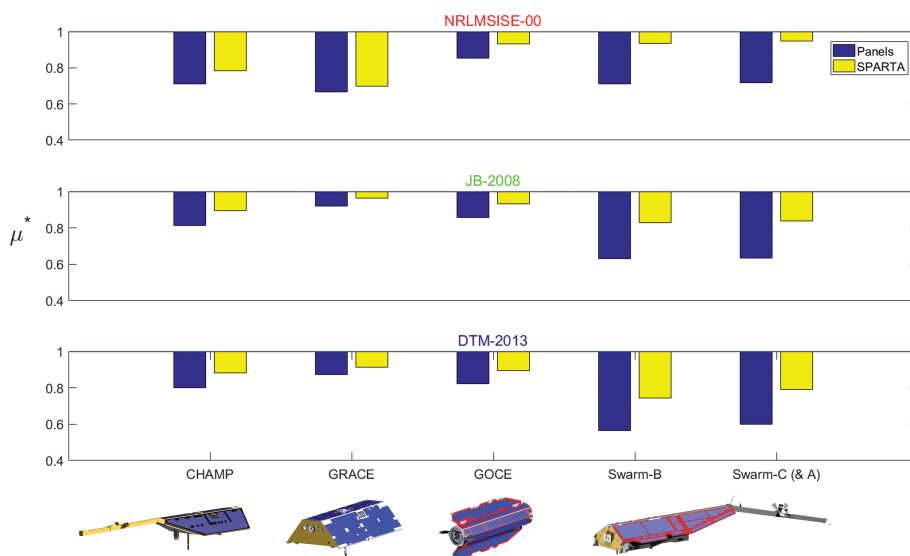


Figure 2.22: Comparison between panel and SPARTA densities for CHAMP, GRACE, GOCE and Swarm.

Investigated periods cover years of data in order to provide satisfactory statistical information. The longest periods between manoeuvres and the quality of satellite data have been analysed in order to provide a reliable statistical information. In particular, the analysed periods range between 2002-11-07 and 2008-12-31 for CHAMP, 2005-12-12 and 2009-03-17 for GRACE, 2009-11-01 and 2013-11-05 for GOCE and, as mentioned before, 2014-07-19 and 2016-09-30 for Swarm satellites. For all the comparisons, an improvement in the agreement with atmospheric models is achieved. An overview of obtained results is available in Table 2.5.

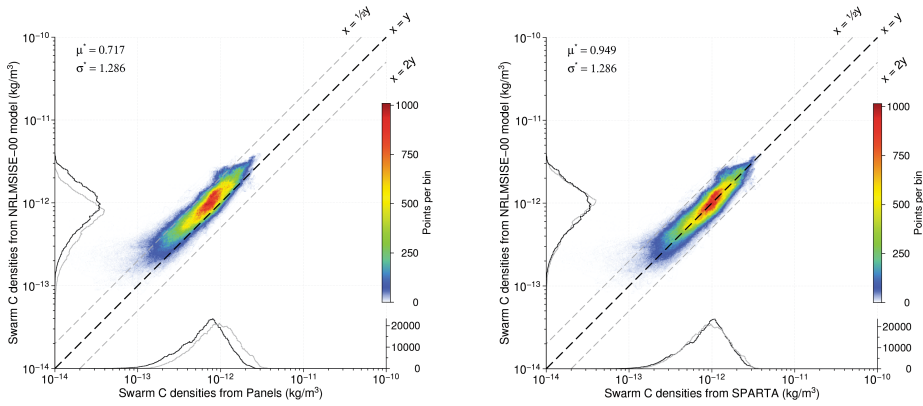


Figure 2.23: Diagrams showing the distribution of Swarm C density data with equivalent NRLMSISE-00 model output. The colour scale indicates the number of points per bin. Panel method densities (left) are compared with SPARTA results (right).

Table 2.5: Comparison of SPARTA results with NRLMSISE-00, JB-2008 and DTM-2013 atmospheric models

Satellite	$\mu^*$ -panel	$\mu^*$ -SPARTA	$\sigma^*$
<b><i>NRLMSISE-00</i></b>			
CHAMP	0.712	0.785	1.27
GRACE	0.668	0.699	1.42
GOCE	0.854	0.931	1.18
Swarm B	0.711	0.935	1.46
Swarm C (& A)	0.717	0.949	1.29
<b><i>JB-2008</i></b>			
CHAMP	0.813	0.896	1.22
GRACE	0.920	0.964	1.44
GOCE	0.856	0.933	1.16
Swarm B	0.630	0.828	1.42
Swarm C (& A)	0.633	0.837	1.24
<b><i>DTM-2013</i></b>			
CHAMP	0.800	0.882	1.22
GRACE	0.874	0.915	1.38
GOCE	0.823	0.896	1.16
Swarm B	0.566	0.745	1.41
Swarm C (& A)	0.598	0.791	1.24

Depending on the mission and atmospheric model, average mean ratios change. New Swarm densities turned out to be better correlated with the NRLMSISE-00 model.

However, CHAMP and GRACE are in better agreement with JB-2008. GOCE satellite densities are performing nearly equally for both NRLMSISE-00 and JB-2008. The results of this analysis provided scale factors which can be applied to previous panel method output to have a fast improvement of current densities. This is a reliable approach in case of nominal flight configurations. However, in the presence of manoeuvres or prolonged attitude changes, the provided factors are not applicable. For what concerns the Swarm mission, the presented results are currently adopted for Swarm L2 data product processing of the DNSxPOD products (Doornbos *et al.*, 2017).

### 2.5.2. ATTITUDE MANOEUVRES ANALYSIS

In this section, the presented geometry models cover additional attitude configurations demonstrating that high fidelity densities can be provided also within manoeuvres. In order to estimate the new densities, it is necessary to use the iterative algorithm from Doornbos *et al.* (2010). Differently from the Direct algorithm, the relative velocity vector is not assumed to be aligned with the X axis of the satellite body frame, but it is adjusted to the realistic direction resulting in a match between directions of observed and modelled accelerations. After the adjustment in direction, it is necessary to match the magnitude of the acceleration to finally retrieve the density. After a few iterations, the density is modified in order to reach the final match and find the best fitting value. If the geometric and aerodynamic modelling would be reliable, the processed density remains nearly constant between the periods inside and outside the attitude manoeuvre. If the geometry is not accurately modelled, alterations in the density trends can be found. A perfect continuous match is not achievable because of the variability of the thermosphere. However, the densities are expected to stay approximately in the same range within a few orbits under stable geomagnetic activity conditions.

In this section, the results about densities within three attitude manoeuvres encountered within the CHAMP and Swarm missions are shown. The first manoeuvre is a 40 deg yaw-manoeuvre for Swarm-A. This change of attitude has been performed on the 5th of May 2015. The variation started at 10:50 UTC and was back to the nominal state at 14:20 UTC. Figure 2.24 includes a wider time domain (6:00 to 18:00 UTC), which shows the differences in accelerations and densities before, during and after the manoeuvre. Figure 2.25 provides a similar plot. In this case, the performed manoeuvre is about 90 degrees. This is a combination of manoeuvres, four times the satellite changed its attitude by 90 degrees. Figure 2.25 presents only a zoom-in within the first rotation. For both plots, panel method densities are characterized by large alterations between outside and inside the manoeuvre. However, for SPARTA a higher level of consistency is detected.

The side area is the predominant part for all these satellites and it is easier to model with respect to the frontal area, which is full of instruments protruding out of the main satellite body. For this reason, when the satellite is out of the nominal state, a better agreement between the two models is reached. The panel method differently describes the two attitudes for both manoeuvres, whereas, a continuous consistency is detected for the SPARTA model. If the attention is focused within two orbits, outside and inside the presented manoeuvres (highlighted in grey areas in Figures 2.24 and 2.25), it is possible to plot the data for the two orbits. The shaded areas are shown in detail in Figures 2.26 and 2.27 for the 40 and 90 degrees yaw manoeuvres respectively. In both plots, there

are the densities predicted with the DTM-2013 atmospheric model, SPARTA and panel methods. The solid lines characterize the densities estimated within the manoeuvre, whereas the dashed lines represent the values estimated outside the manoeuvres. For both the 40 and 90 degree attitude changes, it is possible to appreciate lower differences between the SPARTA densities. This is visible when the satellite changes to a perpendicular orientation with respect to the flow. Figure 2.27, shows high agreement between SPARTA densities and a very large discrepancy for the panel method, which reaches up to 40% of difference.

These findings are also confirmed for CHAMP. For this satellite, a 90 degree yaw manoeuvre has been selected. This sideways-flying attitude period occurred on 6th November 2002, between approximately 9:00 and 20:00 UTC, and it has already been investigated in *Doornbos (2011)*. Similar to Swarm, Figure 2.28 shows the accelerations and estimated densities for this manoeuvre. The solar activity was high and the data provided quite different densities also between short time windows. The results turn out to contain higher frequency information with respect to Swarm. This is mostly related to the smoothed GPS-derived accelerations used for Swarm. However, also in this case, a more stable trend for SPARTA densities is achieved within a few orbits. The panel method continues to have large discrepancies. This is highlighted by Figure 2.29 which shows the densities as a function of the argument of latitude, which is the angle between the ascending node and the satellite along the orbit. For low arguments of latitude, there is a very similar trend between SPARTA densities. However, there is a relevant difference between solid and dashed lines for the panel approach. Discrepancies tend to increase for both methods after the second equator transit, but they get smaller again towards the end of the orbit. Larger differences are reached after crossing the descending equator position and in particular at the south pole. This is explained by the high variability of the thermosphere, especially for high solar activities for regions with complex atmospheric dynamics.

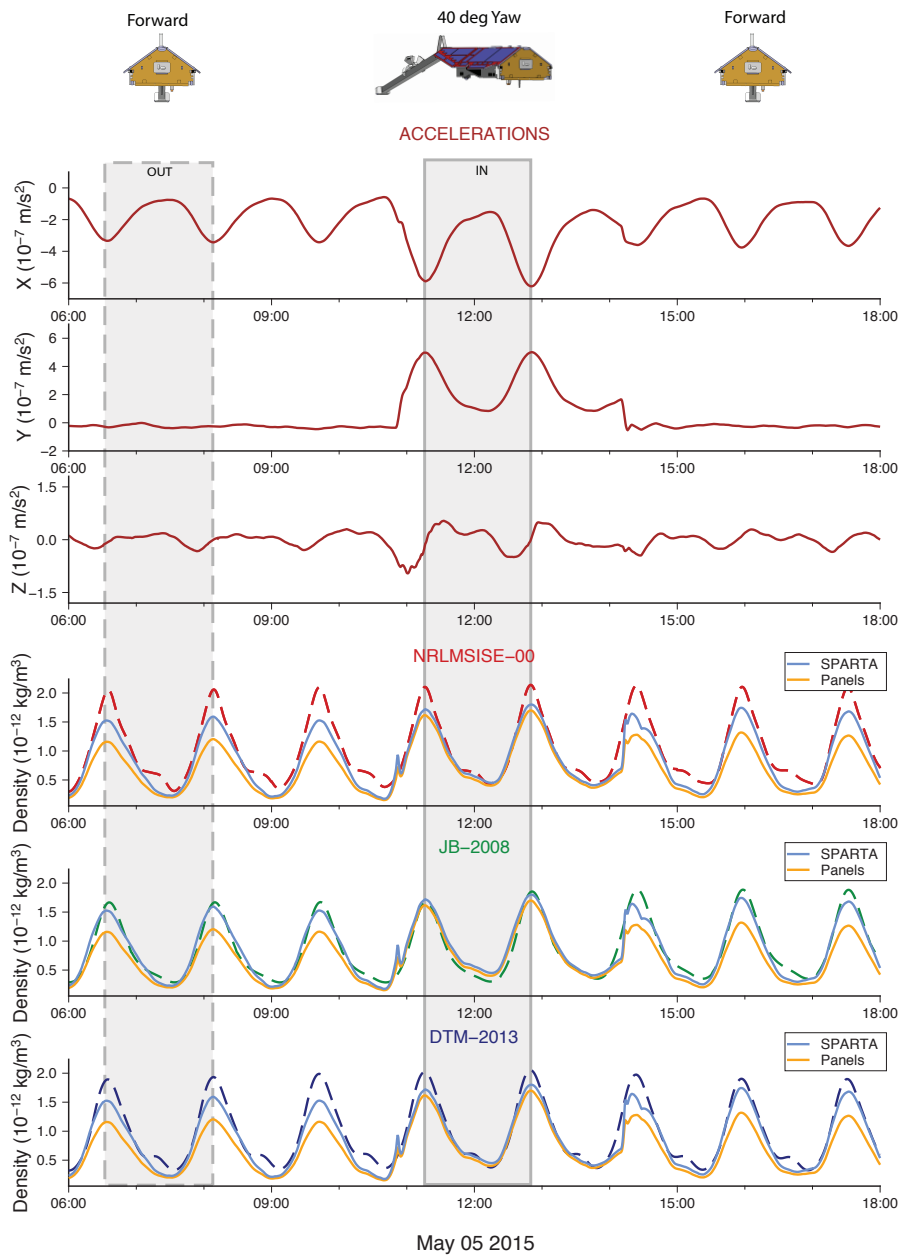


Figure 2.24: Swarm-A densities for panel method and SPARTA during 40 deg yaw manoeuvre on 2015-05-05. Comparison with three atmospheric models: NRLMSISE-00, JB-2008 and DTM-2013.

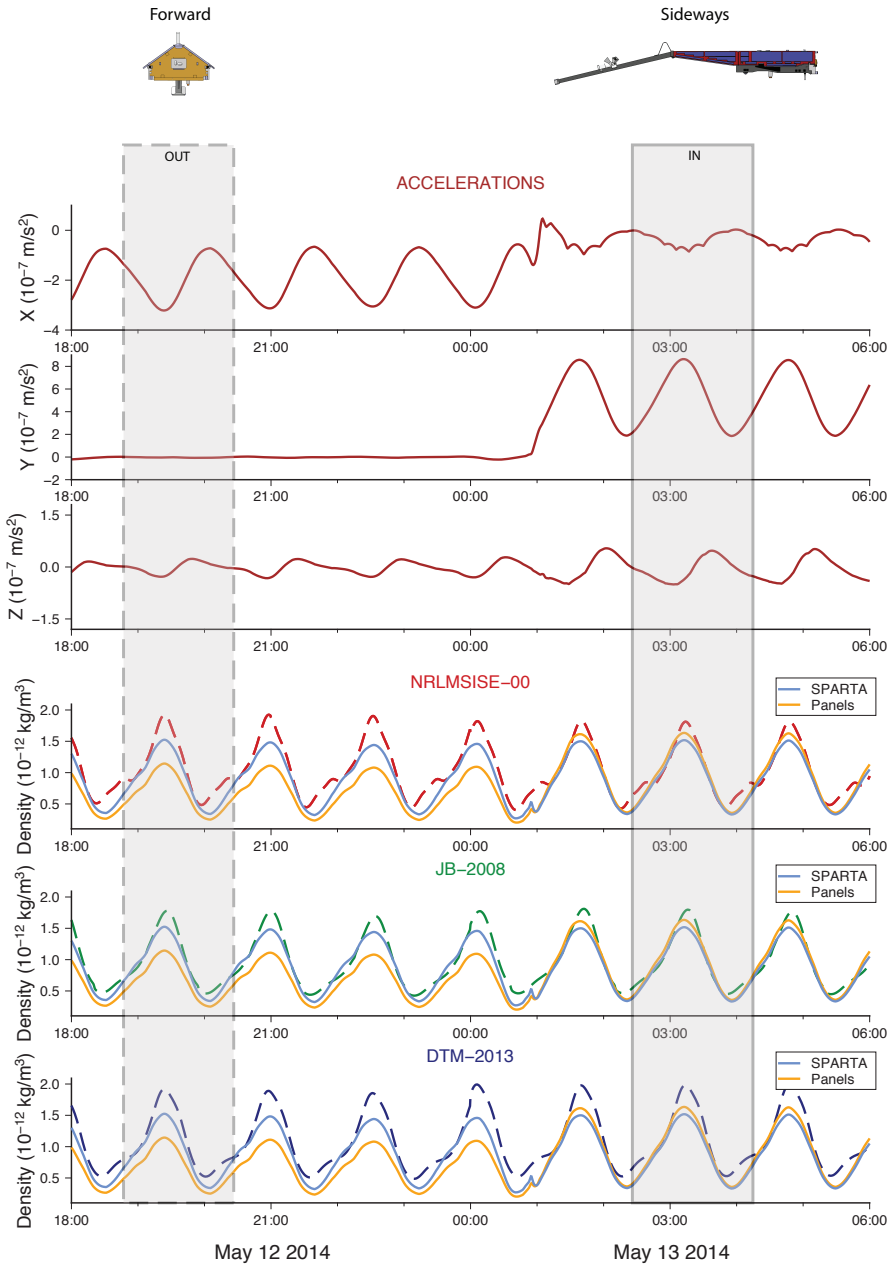


Figure 2.25: Swarm-A densities for panel method and SPARTA during 90 deg yaw manoeuvre on 2014-05-13. Comparison with three atmospheric models: NRLMSISE-00, JB-2008 and DTM-2013.

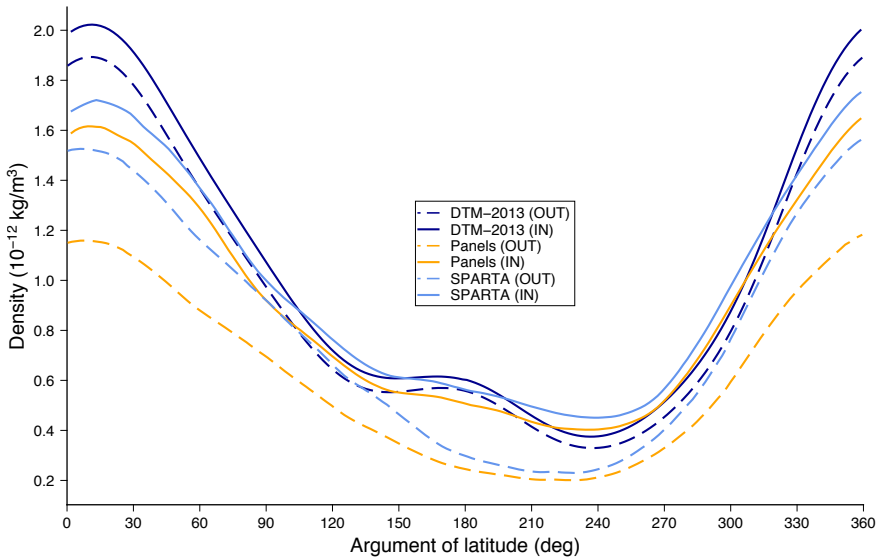


Figure 2.26: Swarm-A densities for panel method and SPARTA during 40 deg yaw manoeuvre on 2015-05-06. Comparison with DTM-2013. The line types correspond to the data equally marked in Figure 2.24 for outside (dashed) and inside (solid) the analysed attitude manoeuvre. Outside: 2015-05-05, 6:32:00 - 8:05:30 UTC. Inside: 2015-05-05, 11:13:30 - 12:46:30 UTC.

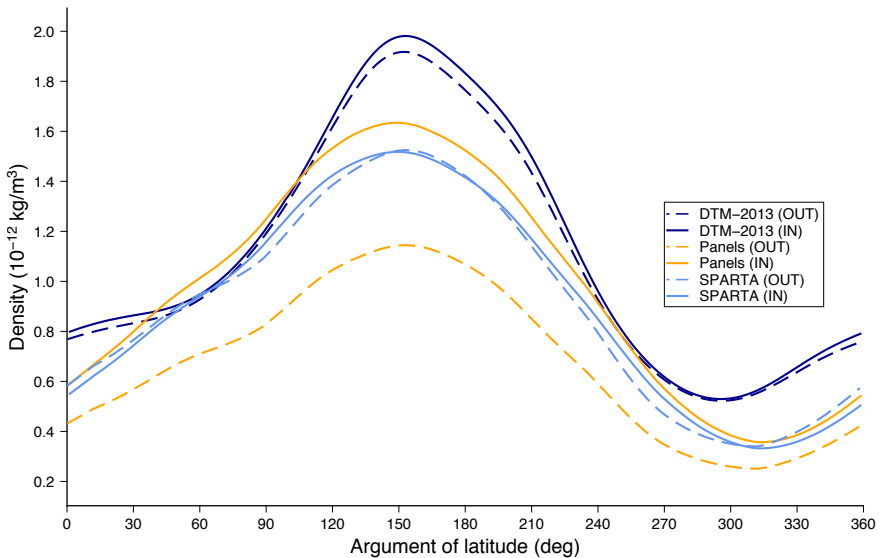


Figure 2.27: Swarm-A densities for panel method and SPARTA during 90 deg yaw manoeuvre on 2014-05-13. Comparison with DTM-2013. The line types correspond to the data equally marked in Figure 2.25 for outside (dashed) and inside (solid) the analysed attitude manoeuvre. Outside: 2014-05-12, 18:44:00 - 20:17:30 UTC. Inside: 2014-05-13, 2:34:00 - 4:07:30 UTC.

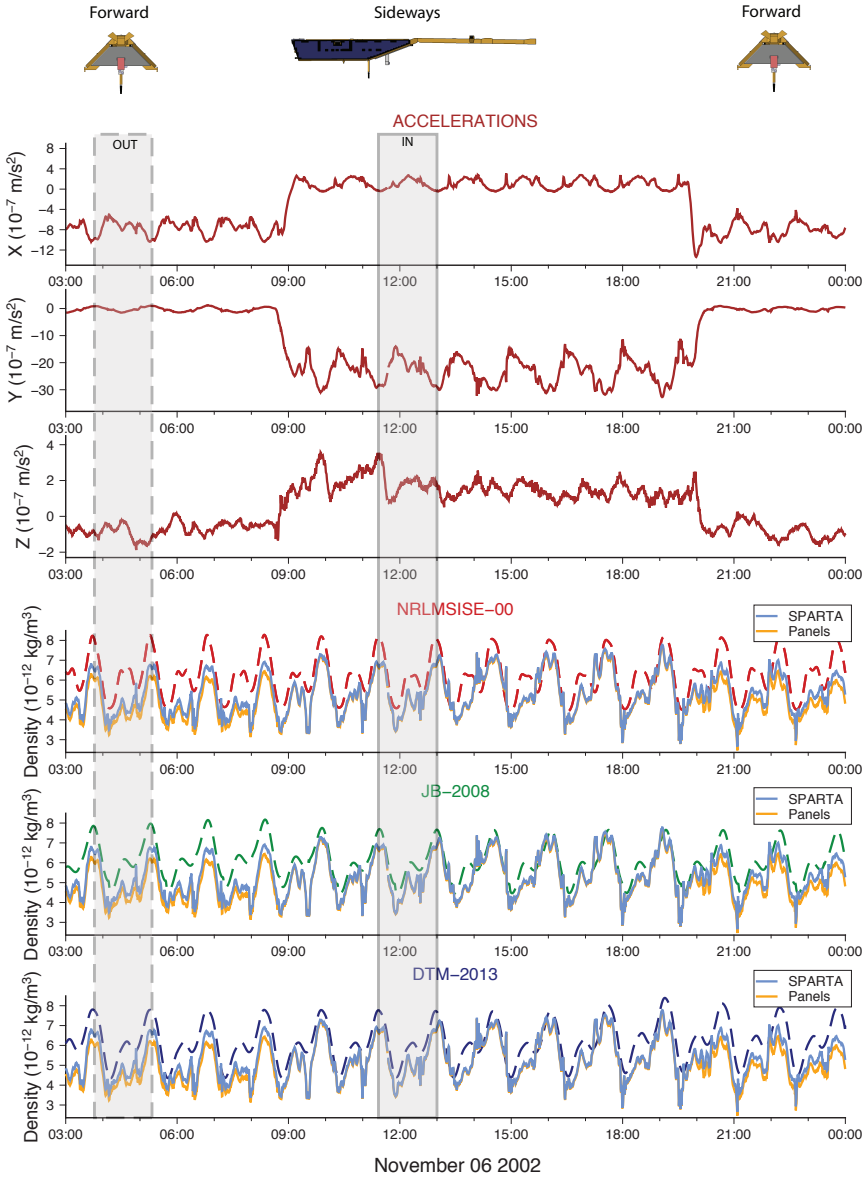


Figure 2.28: CHAMP densities for panel method and SPARTA during 90 deg yaw manoeuvre on 2002-11-06. Comparison with three atmospheric models: NRLMSISE-00, JB-2008 and DTM-2013.

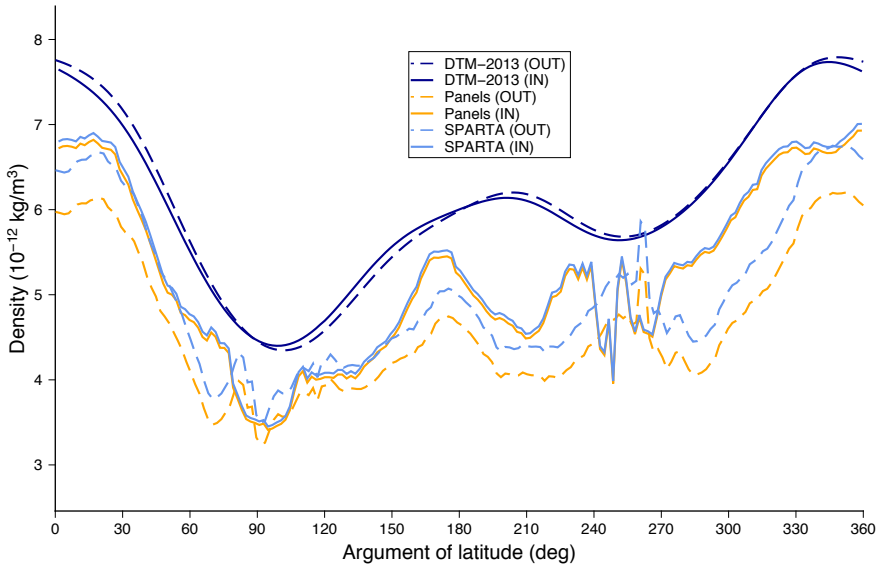


Figure 2.29: CHAMP densities for panel method and SPARTA during 90 deg yaw manoeuvre on 2002-11-06. Comparison with DTM-2013. The line types correspond to the data equally marked in Figure 2.28 for outside (dashed) and inside (solid) the analysed attitude manoeuvre.

## 2.6. CONCLUSIONS AND RECOMMENDATIONS

This first chapter presents new thermospheric density estimations using accelerometer and GPS derived accelerations. High fidelity geometries have been designed using technical drawings and pre-launch photographs in order to raise as much as possible the accuracy level. Physics-based drag coefficients have been obtained as the outcome of a preliminary processing. Further processing of aerodynamic data sets has been applied in order to retrieve improved densities. A general improvement can be found comparing the average mean ratios between panels and SPARTA models with the atmospheric models. The reliability of the new model has been additionally verified with the manoeuvre analyses. This study shows an improvement in the consistency of densities through changes of attitude. New densities turned out to be higher than the panel method results. Indeed, differences of +11% for CHAMP, +5% for GRACE, +9% for GOCE and +32% for Swarm have been detected in this study. The improvement with respect to previous geometry modelling is especially relevant for Swarm and, in general, for satellites with complex shape. For GRACE, the achieved improvements resulted to be lower in magnitude, because of the simpler outer surfaces, which are easier to model also with the panel method approach. The weight of atmospheric models on the final results highlight different behaviours. Further research based on overlap analyses performed between different missions in the same time window will provide additional benefits. Together with a high fidelity gas-surface interactions model, densities and wind will be also improved. Based on the presented results, further research can now investigate and provide tools for gas-surface interactions models optimization and atmospheric models tuning. Different accommodation coefficients and GSI modellings based on the presented model

will provide more consistent thermospheric density data sets, improved atmospheric models and accurate predictions of satellite drag.

## 2.7. APPENDIX-A: COMPARISON BETWEEN SPARTA AND TECHNICAL DRAWING GEOMETRIES

2

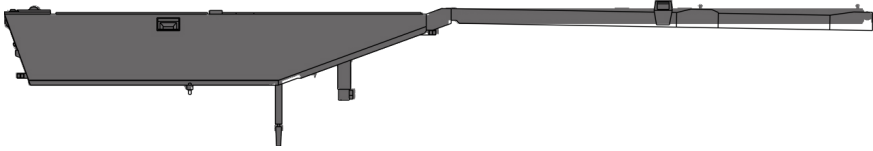


Figure 2.30: Comparison between technical drawing (shaded area) and SPARTA geometry model (black lines) for CHAMP. Inclination of boom has been modified from technical drawings by 1 deg (Lühr, 2000). Side view.

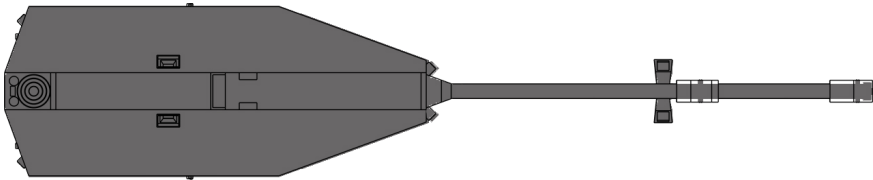


Figure 2.31: Comparison between technical drawing (shaded area) and SPARTA geometry model (black lines) for CHAMP. Larger SPARTA geometry areas are modelled to take into account covering materials, which are not included in the technical drawings. Top view.

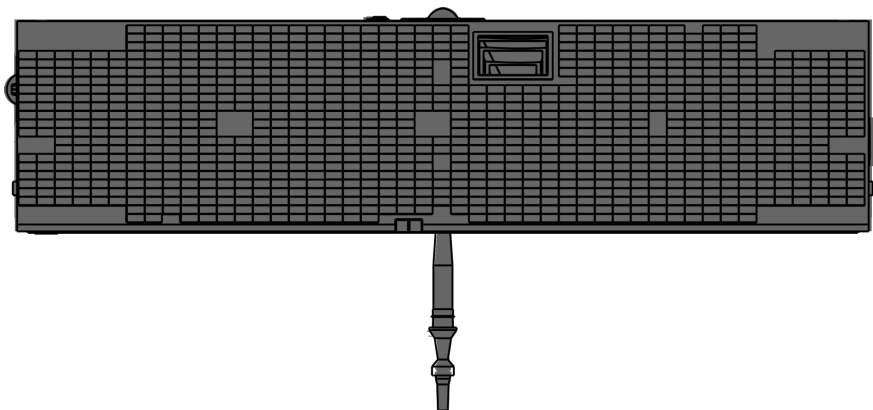


Figure 2.32: Comparison between technical drawing (shaded area) and SPARTA geometry model (black lines) for GRACE. Side view.

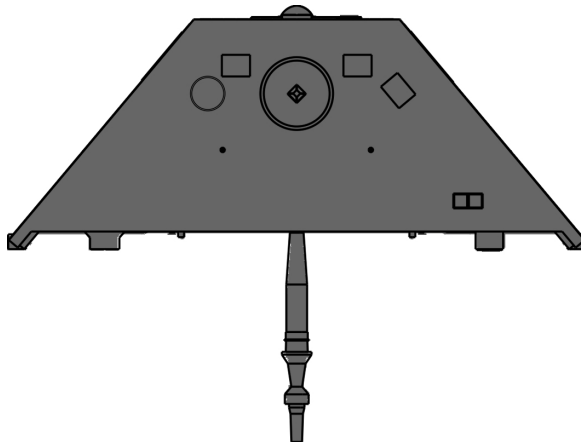


Figure 2.33: Comparison between technical drawing (shaded area) and SPARTA geometry model (black lines) for GRACE. Front view.

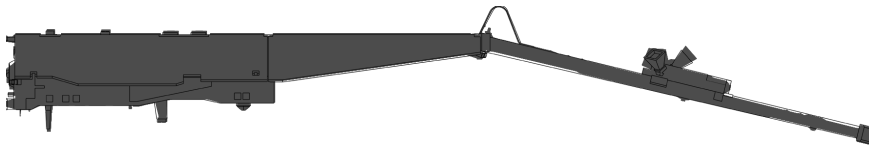


Figure 2.34: Comparison between technical drawing (shaded area) and SPARTA geometry model (black lines) for Swarm. Side view.

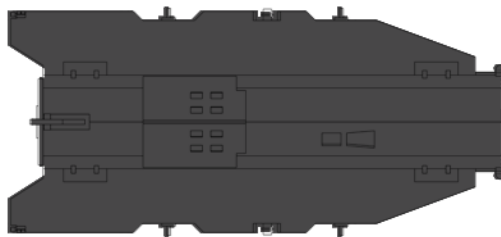


Figure 2.35: Comparison between technical drawing (shaded area) and SPARTA geometry model (black lines) for GOCE. Side view.



# 3

## CHAMP AND GOCE THERMOSPHERIC WIND CHARACTERIZATION WITH IMPROVED GAS-SURFACE INTERACTIONS MODELLING

**G. MARCH, T. VISSER, E.N. DOORNBOS and P.N.A.M. VISSER**

*The CHAMP and GOCE satellites provided high-resolution thermosphere data between 2000 and 2013, improving our knowledge of atmosphere dynamics in the thermosphere–ionosphere region. However, the currently available data sets contain inconsistencies with each other and with external data sets and models, arising to a large extent from errors in the modelling of aerodynamic forces. Improved processing of the wind data for the two satellites would benefit the further development and validation of thermosphere models and improve current understanding of atmospheric dynamics and long-term trends. The first step to remove inconsistencies has been the development of high-fidelity models of the satellite surface geometry. Next, an improved characterization of the collisions between atmospheric particles and satellite surfaces is necessary. In this chapter, the effect of varying the energy accommodation coefficient, which is a key parameter for describing gas-surface interactions (GSI) is investigated. For past versions of the thermosphere*

---

Parts of this chapter have been published in *Advances in Space Research*, **64**(6), 1225–1242, 2019 [March et al. \(2019b\)](#).

*density and wind data from these satellites a value of the energy accommodation coefficient of  $\alpha_E = 0.93$  was selected. The satellite accelerometer measurements, from which the thermospheric data are derived, have now been reprocessed using high-fidelity geometries and a wide range of  $\alpha_E$  values. Lowering the  $\alpha_E$  value used in the processing leads to an increase in the lift over drag ratio for those satellite panels that are inclined to the flow. This changes the direction of the modelled acceleration, and therefore the interpretation of the measured acceleration in terms of wind. The wrong choice of  $\alpha_E$  therefore leads to the introduction of satellite attitude-dependent wind errors. For the CHAMP and GOCE satellites, we have found that values of the energy accommodation coefficient significantly lower than 0.93 (0.85 for CHAMP and 0.82 for GOCE) result in increased consistency of the wind data. A comparison between the two missions and an overview of the influence on the results of filtering for solar activity and seasonal and diurnal variations is presented.*

### 3.1. INTRODUCTION

The accuracy of thermospheric wind data sets derived from satellite accelerations is coupled to satellite aerodynamic modelling. Previously derived thermospheric products have been computed using simplified satellite geometries and gas-surface interaction (GSI) assumptions based on only sparse experimental data (Doornbos, 2011; Sutton, 2008). However, in recent years, an increasing interest in enhanced geometry and satellite aerodynamics modelling has raised the accuracy level of acceleration data processing applied for retrieving thermospheric densities (March et al., 2019a; Mehta et al., 2017; Pilinski, 2011; Pilinski et al., 2016). Weaknesses in the formerly used geometry models turned out to adversely affect the accuracy and consistency of thermospheric products with discrepancies in density up to 32% (March et al., 2019a). However, the observed large scale differences between data sets and atmospheric models are not exclusively connected to inaccurate geometry modelling. Indeed, the characterization of the physics describing the collisions between atmospheric molecules and satellite surfaces plays a crucial role. In this study, we shift the focus from density to wind data. Differently from a study based on the density, the higher sensitivity of the wind data to the aerodynamic model provides a better opportunity to find more optimal GSI settings. The CHAMP (Challenging Minisatellite Payload) and GOCE (Gravity field and steady-state Ocean Circulation Explorer) satellites have been selected in order to provide a better understanding of this influence.

The CHAMP mission was designed to investigate the Earth's gravity and magnetic fields as well as the thermosphere-ionosphere region (Reigber et al., 2002). The mission was initially planned to last for five years, but it provided data from July 2000 to September 2010, covering altitudes between 300–500 km and almost a full solar cycle. The on-board accelerometer measured high-resolution non-gravitational accelerations for a large part of the mission lifetime.

The European Space Agency (ESA) GOCE mission had the primary objective to provide a detailed description of the static part of Earth's gravity field (Floborghagen et al., 2011). In order to do so, the spacecraft, which was in orbit between 2009 and 2013, was equipped with a gradiometer, consisting of six accelerometers positioned along the directions of the body-fixed reference frame. Although this was not the primary objective, the accelerometer data from both missions provide an opportunity for analysis in terms

Table 3.1: List of the mission characteristics for the CHAMP and GOCE satellites.

Satellite	CHAMP	GOCE
<b>Management &amp; operations</b>	GFZ and DLR	ESA
<b>Launch date</b>	15 Jul. 2000	17 Mar. 2009
<b>Reentry date</b>	19 Sept. 2010	11 Nov. 2013
<b>Initial altitude</b>	460 km	270 km
<b>Inclination</b>	87.3 deg	96.7 deg

of satellite aerodynamics.

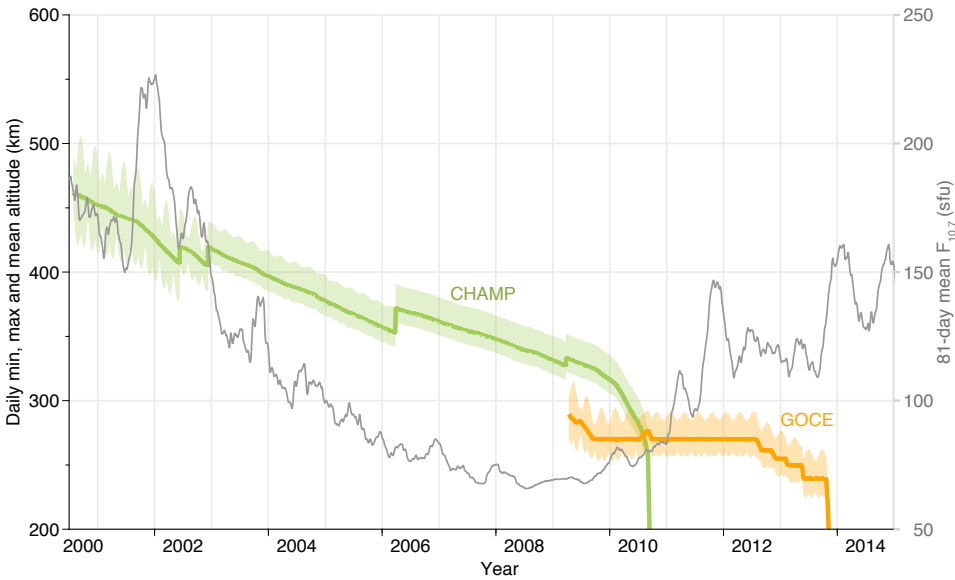


Figure 3.1: CHAMP and GOCE altitude evolution over time, in terms of the daily minimum, mean, and maximum. Solar activity is indicated by the 81-day mean  $F_{10.7}$  flux value.

Table 3.1 lists basic information about both missions, while Fig. 3.1 illustrates the evolution of their altitudes, set against the solar cycle variation. CHAMP encountered higher peaks of solar activity compared to GOCE. This especially occurred at the beginning of its lifetime. GOCE operated at very low altitudes (around 260 km for most of the mission) during low to moderate solar activity. Due to their orbit geometries and coverage of atmospheric conditions, these two satellites were able to provide a complete analysis of thermospheric winds in terms of local time, solar activity and altitude.

At the altitudes of these satellites, the atmosphere is highly rarefied. Collisions between atmospheric particles are negligible with respect to the gas-surface interactions. Physical aerodynamic coefficients can be determined by computing the energy and momentum exchange between atmospheric particles and satellite outer surfaces. The first studies on the interactions between molecules and surfaces arose in the previ-

ous century, when laboratory experiments were developed to measure surface reflection properties (e.g. *Saltsburg et al.*, 1967). Replicating the extremely low densities and high velocities of satellite orbits in the laboratory has remained extremely challenging however. With the advent of space exploration, satellite experiments indicated that surfaces are covered by adsorbed gases and that the nature of reflections might vary depending on the satellite orbit characteristics (*Moe et al.*, 1998). These first measurements were mainly obtained using pressure gauges (*Moe et al.*, 1972; *Moe and Moe*, 1969) and mass spectrometers (*Hedin et al.*, 1973) and indicated that at around 200 km altitude, the accommodation coefficient should be near unity and depends only on the adsorbed gas at the surface (*Moe et al.*, 1993). Unfortunately, there are only very limited direct measurements of the angular distribution of reflected particles. An experiment on the Space Shuttle at 225 km by *Gregory and Peters* (1987) revealed a distribution of 97–98% diffusive reflection ( $\alpha_E=1$ ) and 2–3% quasi-specular reflection ( $0<\alpha_E<1$ ).

More elaborate or more recent dedicated gas-surface interaction experiments in space are not available, but the improvement in satellite instrumentation allows us to investigate this area indirectly, in this case through the effect of gas-surface interactions on thermospheric density and wind retrieval.

In this work, we make use of the higher sensitivity of accelerometer-derived winds to the energy accommodation coefficient. The effect of this parameter on the low–mid latitude wind data is easier to assess than on the density data, because thermospheric winds show far less variation with altitude and solar activity than thermospheric density (*Doornbos*, 2011).

An important premise used in this work is that a wrong value of the energy accommodation adds errors to the wind data, which introduces an erroneous artificial variability on top of the natural wind variability. An estimate of the most suitable energy accommodation coefficient can therefore be found by finding the value for which the wind variability is at a minimum either looking at two similar orbits or comparable seasonal or solar activity conditions. An implied assumption is that energy accommodation related wind errors are uncorrelated with the natural wind variability. We also investigate the sensitivity of this approach to parameters that drive the natural wind variability, such as season, latitude and local time.

### 3.2. GAS-SURFACE INTERACTION MODELING

The satellite aerodynamic model by *Sentman* (*Sentman*, 1961a,b) and modified by *Moe and Moe* (2005) has been implemented for accelerometer data processing by *Sutton* (2009) and *Doornbos et al.* (2010). *Mehta et al.* (2017) introduced the name Diffuse Reflection Incomplete Accommodation (DRIA) for this model. Due to lack of more detailed investigations at the time, both *Sutton* (2009) and subsequently *Doornbos et al.* (2010), adopted the value for the energy accommodation coefficient of  $\alpha_E = 0.93$  used in a numerical example by *Bowman et al.* (2007), as a first effort towards consistency in data processing.

Later, *Mehta et al.* (2017) adopted the gas-surface interaction modelling research by *Pilinski et al.* (2013) and *Walker et al.* (2014) for their updated CHAMP and GRACE data sets. GOCE and Swarm data are not yet processed using this approach however, so aerodynamic modelling inconsistencies between the different missions remain to this day.

Moreover, these papers focused on density data, and an investigation on the effect of gas-surface interaction on wind retrieval has not been performed before.

In the DRIA model, the energy accommodation coefficient is the only GSI model parameter. More sophisticated models, used by [Mehta et al. \(2017\)](#), for example, offer additional parameters and introduce a variability of parameters based on gas conditions (temperature and composition). However, due to a lack of experimental data, as well as lack of measurements of the gas conditions by the current generation of accelerometer-carrying satellites, additional parameters have to be set to assumed values. In our assessment, the current observational data is therefore not suitable for a reliable assessment of such models. We therefore commit to the DRIA model for the remainder of this chapter.

The DRIA approach for gas-surface interaction is based on reflections with a diffusive angular distribution, according to Lambert's cosine law ([Lambert, 1892](#)). The exchanged energy at the surface depends on  $\alpha_E$  values which range between 0 and 1. The energy dissipation can be computed from the incoming and reflected kinetic temperatures ( $T_{k,i}$  and  $T_{k,r}$ ) and the surface wall temperature ( $T_{wall}$ ) as

$$\alpha_E = \frac{T_{k,i} - T_{k,r}}{T_{k,i} - T_{wall}} \quad (3.1)$$

The incoming kinetic temperature is related to the molar mass ( $m$ ) and the incoming velocity ( $V_i$ ) as

$$T_{k,i} = \frac{mV_i^2}{3k_B} \quad (3.2)$$

where  $k_B$  is Boltzmann's constant. The kinetic temperature of the reflected particles can be determined from Eq. 3.1 by

$$T_{k,r} = T_{k,i}(1 - \alpha_E) + \alpha_E T_{wall} \quad (3.3)$$

The lack of measurements or models for the wall temperature introduces an uncertainty in calculations. However, since  $T_{wall} \ll T_{k,i}$ , the sensitivity to this parameter is low and does not particularly affect aerodynamic computations.

The value of  $T_{k,r}$  can be substituted into the equations by [Sentman \(1961b\)](#) for the drag and lift coefficients of a flat plate with one side exposed to the flow. A simple aerodynamic model of a satellite can be build by simply combining several of those plates with appropriate areas and orientations, as described by [Doornbos \(2011\)](#). However, this approach does not provide information on multiple reflections, shadowing and, especially, does not accurately describe all the surface elements of the satellite. A higher-fidelity representation of the satellite outer-surface geometry, such as presented by [March et al. \(2019a\)](#) can be used in combination with gas-dynamics simulation software based on a Monte Carlo method. This approach has been adopted here.

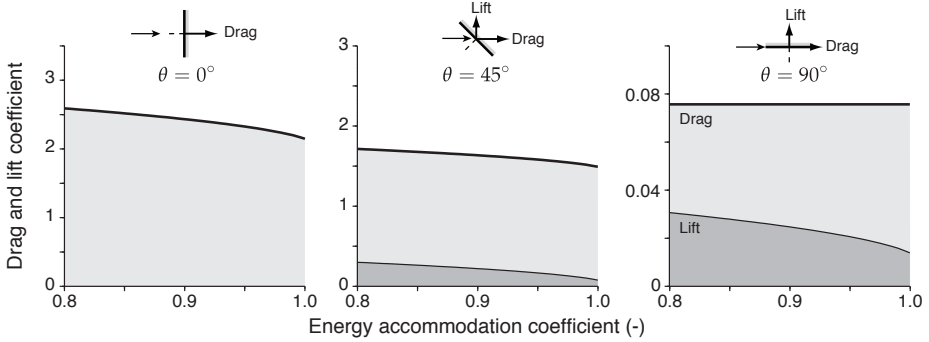


Figure 3.2: Variation of drag and lift coefficients for a one-sided panel as a function of the energy accommodation coefficient in the Diffuse Reflection Incomplete Accommodation (DRIA) satellite aerodynamics model. The variation is shown for three different incidence angles. Note the different Y-axis scale for the rightmost panel.

To understand the effect of the energy accommodation coefficient in the DRIA model, however, we briefly return to the case of a single flat plate. Fig. 3.2 shows how the energy accommodation coefficient  $\alpha_E$  affects the magnitude of the modelled drag force for such a satellite panel. In addition, and more important for this work, it affects the modelled lift over drag ratio of those panels that are inclined to the flow, and therefore the direction of the modelled acceleration. Since the crosswind retrieval is based on matching the direction of the modelled acceleration with the observed one, a wrong value of the energy accommodation coefficient leads to error in the retrieved wind product. This  $\alpha_E$ -induced wind error depends on the orientation of the satellite's panels with respect to the flow, and therefore on the attitude of the satellite as well as the flow velocity vector. On both CHAMP and GOCE, the attitude of the satellites was controlled so that the longitudinal axis of the satellite was kept within a certain range of a few degrees, with respect to the velocity vector. Variation within this range depended on the interplay between the torques exerted by the attitude control actuators on the satellite (magnetic torquers on both satellites and in addition cold gas thrusters on CHAMP) and the external torques, and therefore had a certain degree of randomness. Due to this random element which is more relevant for the CHAMP satellite than for GOCE, an error in the gas-surface interaction used in the data processing will have introduced errors in the wind data that are uncorrelated with the physical wind.

### 3.3. METHODOLOGY

Various authors have dealt with inconsistencies in accelerometer-derived density and wind data by estimating correction factors to apply to the data, to get them in line with other sources (Bowman *et al.*, 2008; Dhady *et al.*, 2017, 2018; Weimer *et al.*, 2018). In order to remove the inconsistencies at the source, however, it was first of all necessary to improve the satellite outer surface modelling. For the CHAMP and GOCE satellites, new geometries have been designed and used as input in the SPARTA gas-dynamics simulator (Gallis *et al.*, 2014), as presented in March *et al.* (2019a). The analysis in this paper was based on full accommodation ( $\alpha_E = 1.00$ ), and the resulting model was applied to

the processing of CHAMP, GRACE, GOCE and Swarm density products. However, the geometry modelling errors are only partially responsible for the discrepancies between the data sets, because the gas-surface interaction modelling also plays a key role. The assumption of full accommodation is most likely not valid and possible alternatives are discussed in the following sections.

Within this study, the algorithms of *March et al. (2019a)* are used for the processing of CHAMP and GOCE thermospheric wind products. The GRACE and Swarm satellite data have not been included. Their data does not meet the criteria in terms of aerodynamic acceleration signal strength. The presence of instrument or platform-related issues for these missions also prevents a reliable wind retrieval.

The equations introduced in Section 3.2 were implemented in the input to the SPARTA code, and subsequently aerodynamic data sets were generated for each satellite. The  $T_{wall}$  was fixed to 400 K in agreement with *March et al. (2019a)*. The SPARTA outputs comprise of a complete coverage of aerodynamic force coefficients, covering different satellite attitudes (attack and side-slip angles) and atmospheric particle composition and temperature, through the speed ratio ( $s$ ), defined as

$$s = \frac{V_{inc}}{\sqrt{\frac{2RT_{inc}}{m}}} \quad (3.4)$$

In order to be able to provide the static temperature  $T_{inc}$  and molecular masses  $m$  of the incoming gas particles, the NRLMSISE-00 model was used (*Picone et al., 2001*).

The role of GSI is investigated by assuming it can be represented by a constant energy accommodation  $\alpha_E$ . In previous work by *Doornbos et al. (2010)*; *Sutton (2008)*  $\alpha_E$  was set to 0.93, and in *March et al. (2019a)* it was set to 1.00. However, in this work, we will be searching for an optimal value, depending on the self-consistency of resulting wind data. Limitations are still present, especially because the NRLMSISE-00 empirical model is used for  $T_i$  and  $m$  in Eq. 3.4. To reduce these uncertainties, independent temperature and composition observations would be required on future accelerometer-carrying satellites.

The natural variability of thermospheric winds depends mainly on season, local solar time, latitude, and geomagnetic activity. Solar activity, in terms of solar extreme ultraviolet (EUV) emission, has a much smaller influence on thermospheric wind than on density, but it is taken into account in the next sections as well. There is also a dependence of wind on longitude and its associated upward propagating waves, which will not be considered in the remainder of the chapter.

Within this work, two different methods are used to gain more insight into CHAMP and GOCE accelerometer-derived thermospheric wind and its sensitivity to GSI modelling. For the GOCE mission, a long period investigation over 3 years (between 2010-2013) is introduced to look at self-consistency over different seasons and solar activity conditions (Section 3.5). For the CHAMP satellite, an enhanced wind consistency is studied through the analysis of the sideways manoeuvre that occurred in November 2002 (Section 3.6).

### 3.4. THERMOSPHERIC WIND DATA

Early studies of wind derivation from accelerometer data started long before the launch of dedicated missions such as CHAMP and GOCE (*Marcos and Forbes, 1985*). More recently, detailed analyses of thermospheric wind have been performed using CHAMP (*Liu et al., 2006, 2009; Lühr et al., 2007a,b*) and GOCE (*Doornbos et al., 2014; Liu et al., 2016*) data sets.

In this chapter, the thermosphere horizontal wind experienced by CHAMP and GOCE is investigated to provide a better consistency and an enhanced understanding of the energy accommodation parameter. The wind retrieval from accelerations is based on the algorithm by *Doornbos et al. (2010)* and because low- and mid-latitude data has been selected, the analyzed cross-track wind component is in the zonal (eastward positive) direction. Errors due to the meridional component of the cross-track wind are negligible for both satellites.

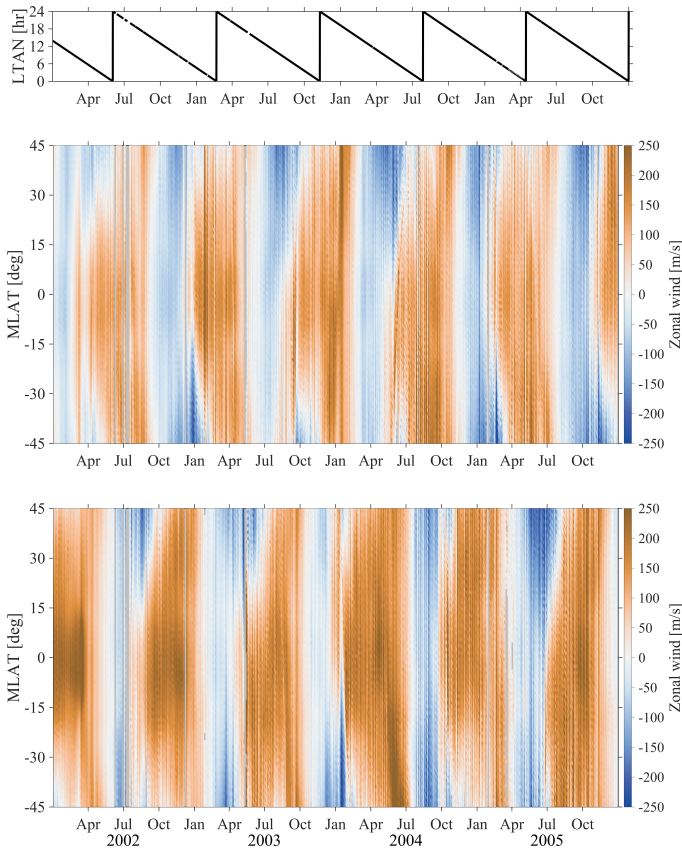


Figure 3.3: Ascending (top) and descending (bottom) mean zonal winds for the CHAMP satellite within the selected period and with  $\alpha_E=0.93$ . The LTAN evolution is also available in the top part of the figure.

In this chapter, the geomagnetic coordinates (quasi-dipole coordinates) were preferred to the geodetic ones in agreement with previous works (e.g. [Xiong et al. \(2015\)](#), [Huang et al. \(2017\)](#)). MLAT ensures an easier description of winds in the polar regions due to the winds nature mostly driven by the energy input that is fed into the thermosphere via magnetic field and, in particular, through field-aligned currents ([Gasperini et al., 2016](#)). Even though the high magnetic latitudes are excluded from the following diagrams, we decided to keep this convention. For the neutral density plots available in this thesis, the argument of latitude was mostly used to mitigate possible misinterpretations of the results due to the altitude variations along the satellite orbit. The change of the signal of the density variability caused by the interaction with currents (e.g. Joule heating, EPP heating) is very small compared to the change in altitude.

In the previous processing at Delft University of Technology, the wind for CHAMP and GOCE have been processed assuming  $\alpha_E$  equal to 0.93 ([Doornbos, 2011](#)). These products were based on low fidelity satellite geometries. Figs. 3.3 and 3.4 show the zonal wind as a function of magnetic latitude (MLAT) and time for the ascending and descending orbit sectors for CHAMP and GOCE. These figures are generated for  $\alpha_E=0.93$ , but with improved high-fidelity geometries from [March et al. \(2019a\)](#).

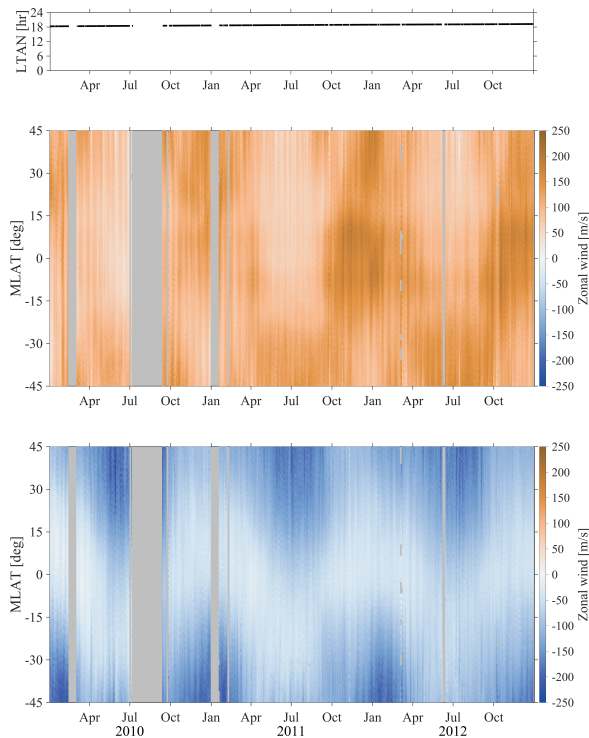


Figure 3.4: Ascending (top) and descending (bottom) mean zonal winds for the GOCE satellite within the selected period and with  $\alpha_E=0.93$ . The LTAN evolution is also available in the top part of the figure.

As a starting point, from these data sets and figures, it is possible to observe the temporal cyclic nature of thermospheric wind as sampled along the satellite orbits and how the magnitude varies with different magnetic latitudes. For GOCE, which had a nearly sun-synchronous orbit, the dominant cycle is the seasonal one. Indeed, similar wind features can be observed with a regular period of one year. Looking at the descending sector zonal wind in Fig. 3.4, it is clear that magnitudes are reaching their peaks around January and July periods respectively for Southern and Northern hemispheres. CHAMP on the other hand, had an orbital plane which precessed with respect to the Sun, completing a full cycle in less than a year and allowing for a 24 h coverage in local time over 130 days. Therefore, although the seasonal cycle is visible in the data, the dominant cycle is due to the winds varying with local solar time. The selected time domains are between 2002-01-01 and 2006-01-01 for CHAMP (Fig. 3.3) and between 2010-01-01 and 2013-01-01 for GOCE (Fig. 3.4). These two intervals guarantee a full description of horizontal wind excluding periods with low aerodynamic accelerations at solar minimum and high altitude, and those with many satellite manoeuvres. The variability of the wind at magnetic latitudes over 45 degrees and below -45 degrees (not shown in the Figures) is much stronger than at lower latitudes. This is due to intense thermosphere/ionosphere/magnetosphere coupling at high latitudes. In Section 3.5, we removed the high latitude data from our analysis, to be able to more clearly discern the natural variability and the variability due to gas-surface interaction model error.

As shown in Fig. 3.5, the two missions sample different local times (LT). The GOCE satellite mainly was flying at LT between 3:00–9:00 and 15:00–21:00 hours, whereas the CHAMP mission provided measurements over the full range of local times. Fig. 3.5 illustrates the wind data for the two missions. The overall wind for the complete range of MLAT values is available on the top, whereas mid–low latitude data are available in the bottom panel for each satellite. The comparison between the two plots for each satellite show that especially high wind measurements are removed, as these usually occur in the highly variable thermospheric conditions at high latitudes.

The two selected satellites are characterized by different orbits. The dusk-dawn orbit of GOCE requires particular attention and, in the following pages, the ascending (dusk) and descending (dawn) orbit sectors are investigated independently. Since the thermospheric wind at low latitude flows predominantly from the day-side to the night-side, the dawn and dusk zonal wind components have opposite signs. The CHAMP data is characterized by a continuous variation in local time, which makes a seasonal analysis more complicated. For this reason, for CHAMP, another approach based on the zonal wind investigation over a sideways manoeuvre is introduced in Section 3.6.

The selected satellite data have been compared also with the Horizontal Wind Model (HWM). This model is based on ground-based, rocket and satellite measurements. The HWM-14 version of the model provides a time-dependent global empirical description of the upper atmospheric general circulation dynamics, with an extremely large number of observations (Drob *et al.*, 2015), including also a subset of the GOCE data. This model was preferred to the older version (HWM-07) especially for the much wider assimilated data set (Drob *et al.*, 2015). The GOCE data in HWM-14 is based on older processing using a lower fidelity satellite geometry and an energy accommodation of 0.93. The HWM-14 model therefore does not provide an independent source of validation of reprocessed

GOCE data. Instead its use here is to investigate the influence of trying to use such a model for lowering the variability in the data. The model can be thought to represent part of the natural variability in the thermospheric wind. When this part is removed, the variability due to errors in the accommodation coefficient used in the data processing will be more clearly visible and easy to assess. The main results are shown in comparison with the HWM-14 model, however in the next section the newly derived zonal winds are also compared with the HWM-07 version for completeness.

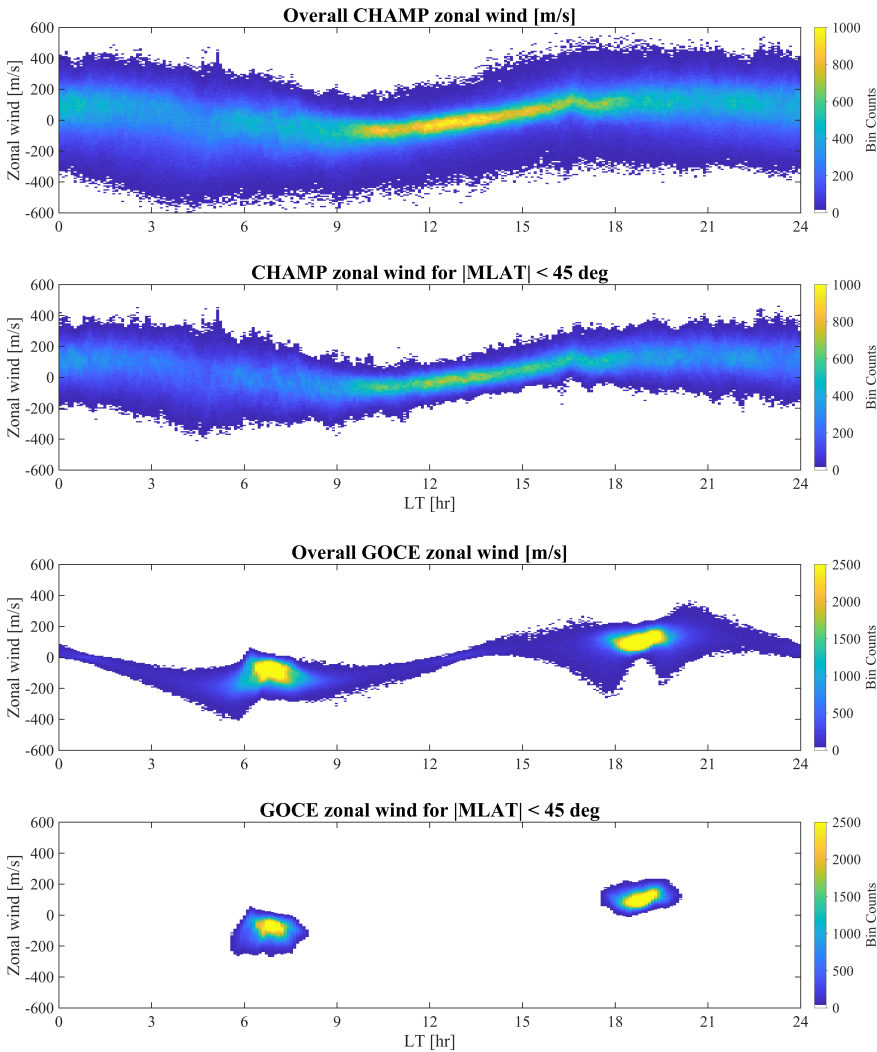


Figure 3.5: Wind data for the CHAMP and GOCE satellites with a full range of magnetic latitudes and with filtering enabled for magnetic latitude below 45 deg. Bins with less than 15 and 40 points are not shown for CHAMP and GOCE, respectively.

In the development of empirical models such as HWM, possible discrepancies between observation data sets are constantly under investigation. Outcomes like those presented in the next sections are important in the improvement process. In Sections 3.5 and 3.6, the results for GOCE and CHAMP are illustrated looking at the newly derived wind themselves and at comparisons with HWM output. An accurate analysis of the two approaches provides an essential input for assessing possible future work in terms of data assimilation and in general for empirical modelling.

## 3

### 3.5. GOCE ANALYSIS

In this section, the observed wind is subdivided into three seasonal bins. Each bin includes four months of data: December solstice (between November and February), Equinox (March, April, September, October) and June solstice (between May and August). In order to purely investigate the GSI features within the new model, the main quantity of interest is the standard deviation of the zonal wind observations ( $\sigma_{WIND}$ ) for the complete spectrum of  $\alpha_E$  values. This quantity of interest was estimated binning the selected data with a resolution of 1 degree in MLAT. Therefore, wind data sets have been generated with an energy accommodation coefficient ranging between 0 and 1. Within this study, we expect an optimal level of consistency in the wind data for a specific accommodation coefficient. If the  $\alpha_E$  value would deviate from the optimal value, this would lead to differences in the direction of the aerodynamic force as a function of the satellite attitude, which would generate a reduction in the consistency in the wind data.

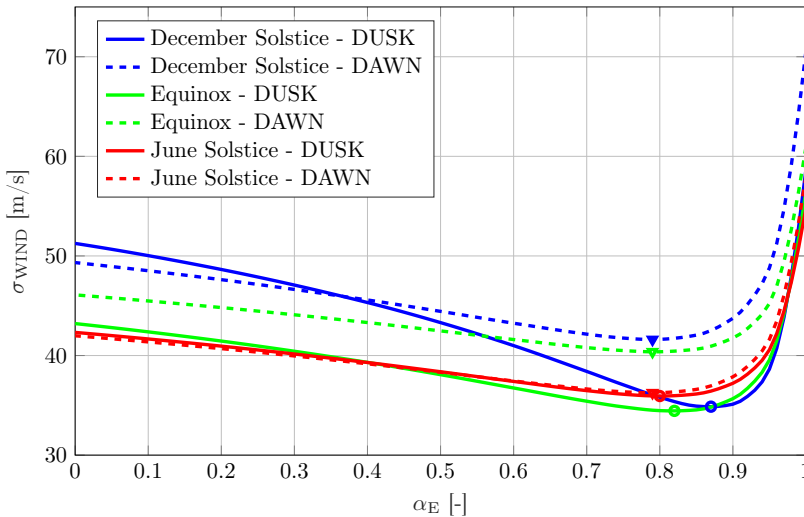


Figure 3.6: Standard deviation of newly derived zonal wind for the GOCE satellite, for data with a maximum geomagnetic latitude of  $\pm 45$  deg. The values are averages over the selected magnetic latitudes and all the sampled local solar times.

The energy accommodation coefficient influence on the standard deviation of the wind data can be observed in Fig. 3.6. The magnetic latitude (MLAT) range is considered

within  $\pm 45$  degrees. The data for the full range of magnetic latitudes are made available as part of the official ESA data dissemination. However, for this analysis the range was limited due to the complex dynamics at the poles which did not provide enough stability in the winds to extract meaningful information regarding the energy accommodation coefficient at high latitudes. The averages over the selected magnetic latitudes are computed for the full range of  $\alpha_E$  values. Markers highlight the minimum points of standard deviation. For the GOCE satellite these values are within the range of 35 to 70 m/s. For energy accommodation coefficients approaching unity, the standard deviation has a steep slope. At full accommodation, lift forces on the satellite are at their minimum (see Figure 3.2), and a cross-track acceleration would instead be erroneously interpreted as a higher wind speed.

Minima in the standard deviation curves appear for  $\alpha_E$  values well below 0.93, in the 0.79–0.87 range for GOCE, depending on the seasonal and local time bins. This indicates that the lift component of the aerodynamic force on satellite panels plays a significant role in thermosphere data processing from satellite accelerations. Computing the average over the selected range of MLAT values (Fig. 3.6), the minimum points converge to an accommodation coefficient of 0.82. This value is in agreement for the three seasonal subsets. The accommodation coefficient ranges between two extreme values of 0.79 (for December solstice and Equinox in dawn) and 0.87 (for December solstice in dusk). This strong seasonal variation is expected to be connected to the low altitude. Further variations for smaller MLAT ranges (below  $\pm 45$ ) or normalizing the standard deviation with the total range of wind speeds did not affect the results.

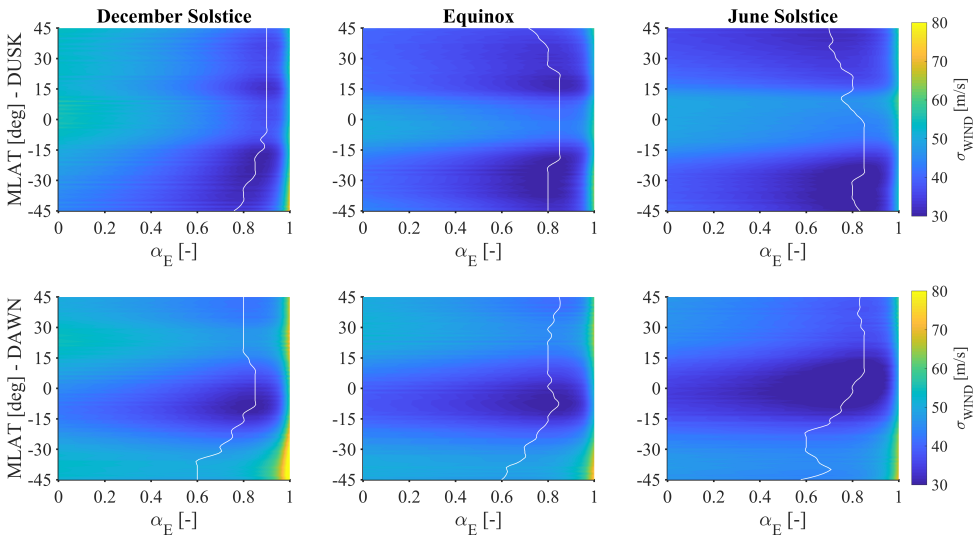


Figure 3.7: Standard deviation of new zonal wind for the GOCE satellite for both dusk and dawn orbit sectors. The white line shows the minimum values computed for each magnetic latitude.

In Fig. 3.7, the standard deviations are further binned according to magnetic latitude. The white lines connect the minimum points along the MLAT and  $\alpha_E$  ranges. The

$\sigma_{WIND}$  has a complex behaviour. The top part shows the results for the dusk sector, whereas in the bottom side, the dawn wind analysis is available. The two sectors are differently characterized within the MLAT and  $\alpha_E$  intervals. This is related to the low altitude and different night–day crossings within the orbits. Looking at the dusk sector, variations within the magnetic latitude range can be observed. In particular for the December and June solstice bins, the white lines appear to be mirrored with respect to the magnetic equator. Whereas, for the Equinox subset, a more symmetric and stable behaviour can be detected. This is slightly visible for the dawn sector as well, however for this second case, the satellite orbit characteristics introduce a wider variance for low latitudes. A wider variation is obtained for the dusk sector. This can be related to the larger presence of eclipse transitions in the dusk sector than in the dawn one independently from the season. This feature introduces errors in the solar radiation pressure, which increases the variability in the observed data. An improvement would be reached with an enhanced solar radiation pressure modelling, which is currently under investigation. Within the selected MLAT interval, the minimum standard deviations are located around an average  $\alpha_E$  of 0.82. We obtain the same value also when reducing the range of magnetic latitudes.

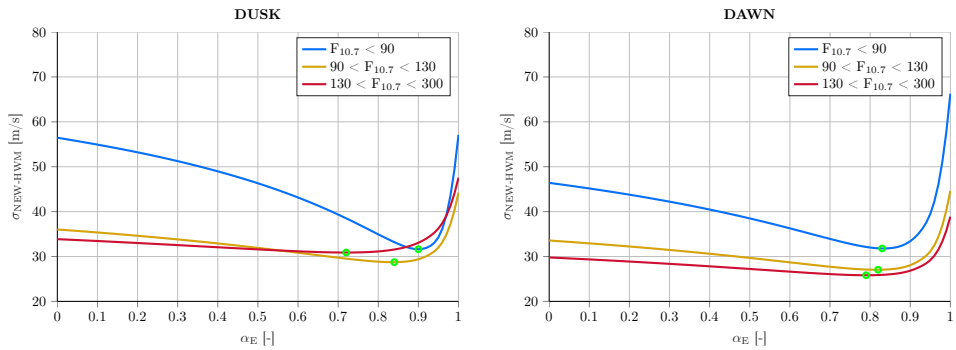


Figure 3.8: Standard deviation of the difference between newly derived zonal wind and HWM-14 results for the GOCE satellite and different  $F_{10.7}$  ranges. The results of dusk and dawn orbit sectors are available on the left and right side respectively.

A comparison and validation against previous results can be performed with an analysis of the HWM-14 wind model. The standard deviation of the difference in wind between the newly derived zonal wind and HWM-14 results is presented in Fig. 3.8. The impact of the solar activity is studied by considering the solar radio flux at 10.7 cm ( $F_{10.7}$ ), which is measured in solar flux units (sfu). Within this analysis, this index is subdivided into three bins: lower than 90 sfu, between 90 and 130 sfu and between 130 and 300 sfu. These ranges describe respectively low, moderate and high solar activities. Within the selected years, the GOCE mission is characterized by a medium to low activity. As shown in Fig. 3.8, for GOCE, the minima are around an average value of 0.81–0.82 of the accommodation coefficient. For GOCE, the number of data points are  $2 \times 10^5$ ,  $3 \times 10^5$  and  $1 \times 10^5$  respectively for low, medium and high solar activity. Comparing these results with the self-consistent  $\sigma_{WIND}$  minimum points (Fig. 3.6), it is observed that the com-

parison with HWM-14 does not change our earlier conclusions. In order to visualize the variations between the HWM-14 and HWM-07 versions, in Fig. 3.9, the zonal wind differences between the newly-derived wind (for  $\alpha_E=0.82$ ) and the modelled ones are available. As expected, the probability density shows a better agreement with the newer model.

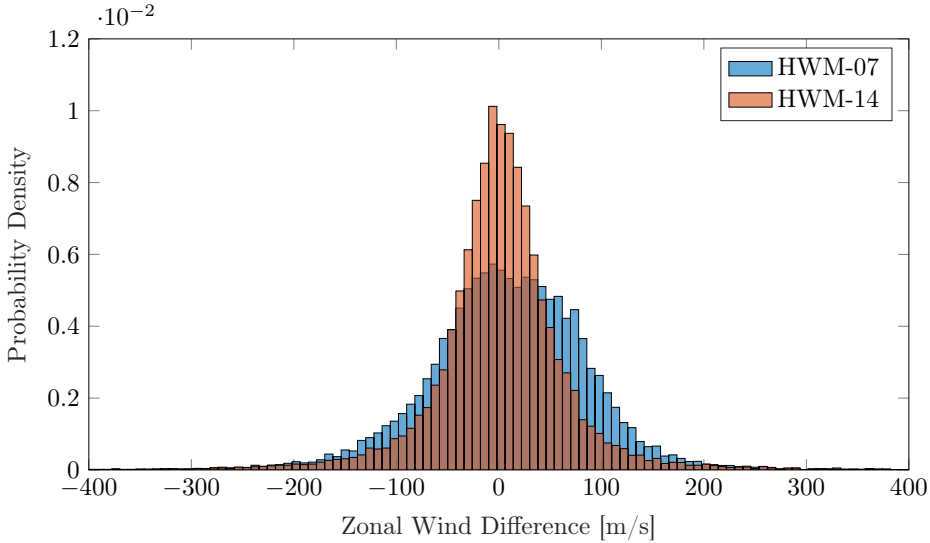


Figure 3.9: Histograms of the difference between the newly-derived wind and the results from the two versions of the HWM model.

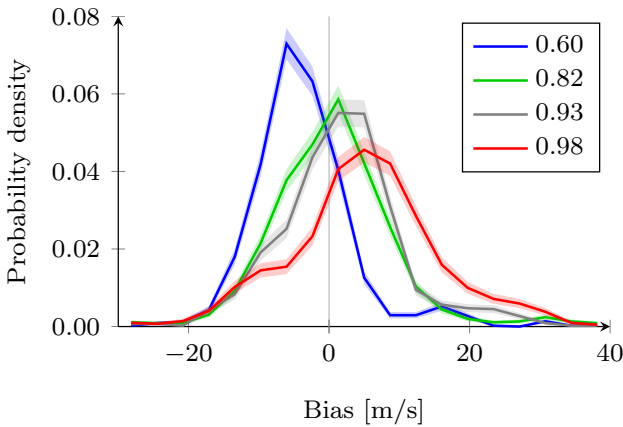


Figure 3.10: Histogram of the bias between force- and torque-derived wind for four different values of energy accommodation coefficient. For side-slip angles between 0 and 4 degrees the deviation of the wind remains within the bounds set by the shaded areas.

Instead of exclusively improving the consistency of the thermospheric wind derived from linear accelerations, these data may also be compared to wind derived from angular accelerations, as suggested by *Visser et al. (2019)*. Implementing their approach for the GOCE satellite, using a range of accommodation coefficients, it is found that the two sets of horizontal wind data are primarily separated by a bias.

Estimating this bias for each full day of data, its probability distribution may be plotted, as displayed in Fig. 3.10 for four values of  $\alpha_E$ . Although the bias does not significantly exceed the reported uncertainty caused by the thruster misalignment angles (see Table 5 of *Visser et al. (2019)*), the distribution is best centered around 0 m/s for a value close to 0.82 accommodation. These results further confirm the improvement in self-consistency of the GOCE data for an energy accommodation coefficient of around 0.82.

## 3

### 3.6. CHAMP MANOEUVRE ANALYSIS

An evaluation of the gas-surface interactions influence over CHAMP zonal wind observations can be performed studying a special manoeuvre made by this satellite. On November 6, 2002, CHAMP performed a sideways flight for about 6 orbits. In Fig. 3.11, the accelerations along the X and Y directions of the satellite body frame are illustrated in the three days between November 5 and 7. In the middle, on November 6, just before noon, the CHAMP satellite moved into sideways flight configuration. Within this time, the accelerometer recorded a greater magnitude of accelerations on the Y axis due to the larger area exposed to the flow. The analysis of the data within and outside the manoeuvre provides the possibility to study two different aerodynamic shapes with respect to the flow within a considerable short time window. A similar analysis was performed in *Doornbos et al. (2010)* with low fidelity geometry and aerodynamic modelling. The following results are based on the newly derived models presented in this chapter.

In Fig. 3.11, we selected six different orbits within similar time windows. With the green and blue colors, the forward flying configurations before and after the manoeuvre respectively are illustrated. The red areas are associated to the orbits with a satellite side-slip angle of 90 degrees. For each of the selected six cases, the 24-hour intervals between the three orbits were chosen so that each passage over high latitude zones would occur within approximately the same magnetic field characteristics. This would allow us to reduce thermospheric variability comparing similar conditions.

Fig. 3.12 shows the zonal wind for the orbits case 4 defined in Fig. 3.11. The winds as a function of the argument of latitude are illustrated for the three orbits. Three energy accommodation coefficients are introduced in order to visualize the direct effect on the zonal wind.

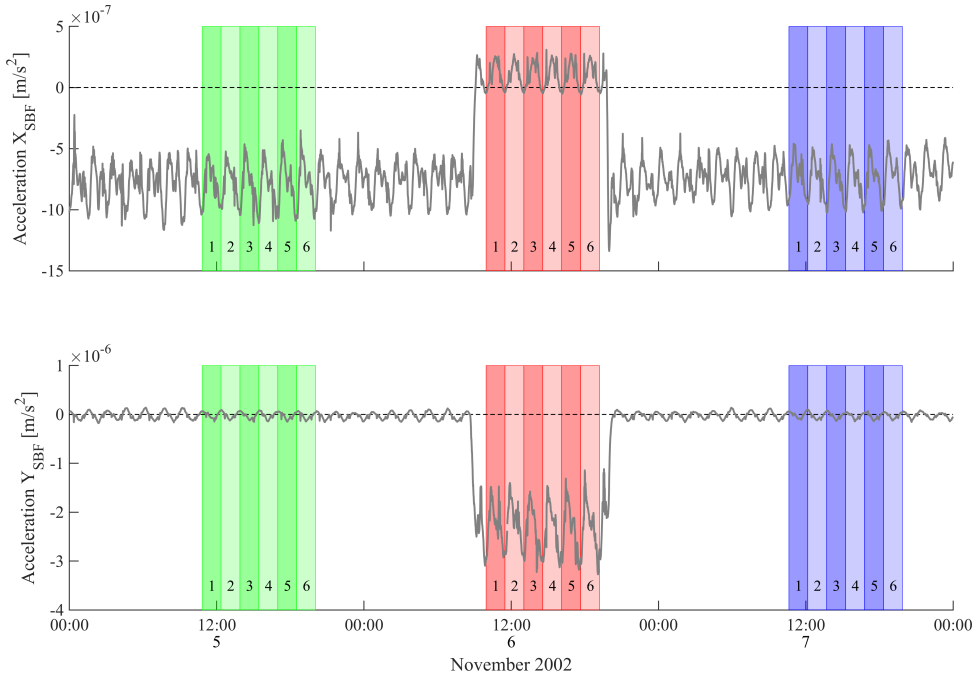


Figure 3.11: CHAMP accelerations for three days in November 2002 surrounding the sideways-flying manoeuvre on November 6 (09:00–20:00 UTC). The shaded areas correspond to all the selected orbits and cases used in Fig. 3.13.

Starting from the top of Fig. 3.12, the selected values are 1.00, 0.93 and 0.85. The first two values have been used in previous works as discussed before. However, the last value is a new coefficient which shows a good agreement between the three orbits and the HWM-14 model result. The HWM model winds at the poles reach peaks of 200–300 m/s, whereas for low- and mid-latitudes the magnitude reduces to less than half. Some peaks can be identified in the auroral regions. The semi-empirical model seems to underestimate the westward winds in the Northern Hemisphere in the auroral region. These strong phenomena are well known and occur quite often in those regions from the day to the night side (Lühr *et al.*, 2007b). The Southern Hemisphere peak has a better agreement between the new computed and modelled winds. For mid and low latitudes, HWM results for the three consecutive days are overlapping. However, looking at the three different plots of Fig. 3.12, it is possible to notice wide variations between the three estimated winds for the accommodation coefficients of 1.00 and 0.93. The differences in winds between the three orbits reduce for an  $\alpha_E$  value around 0.85.

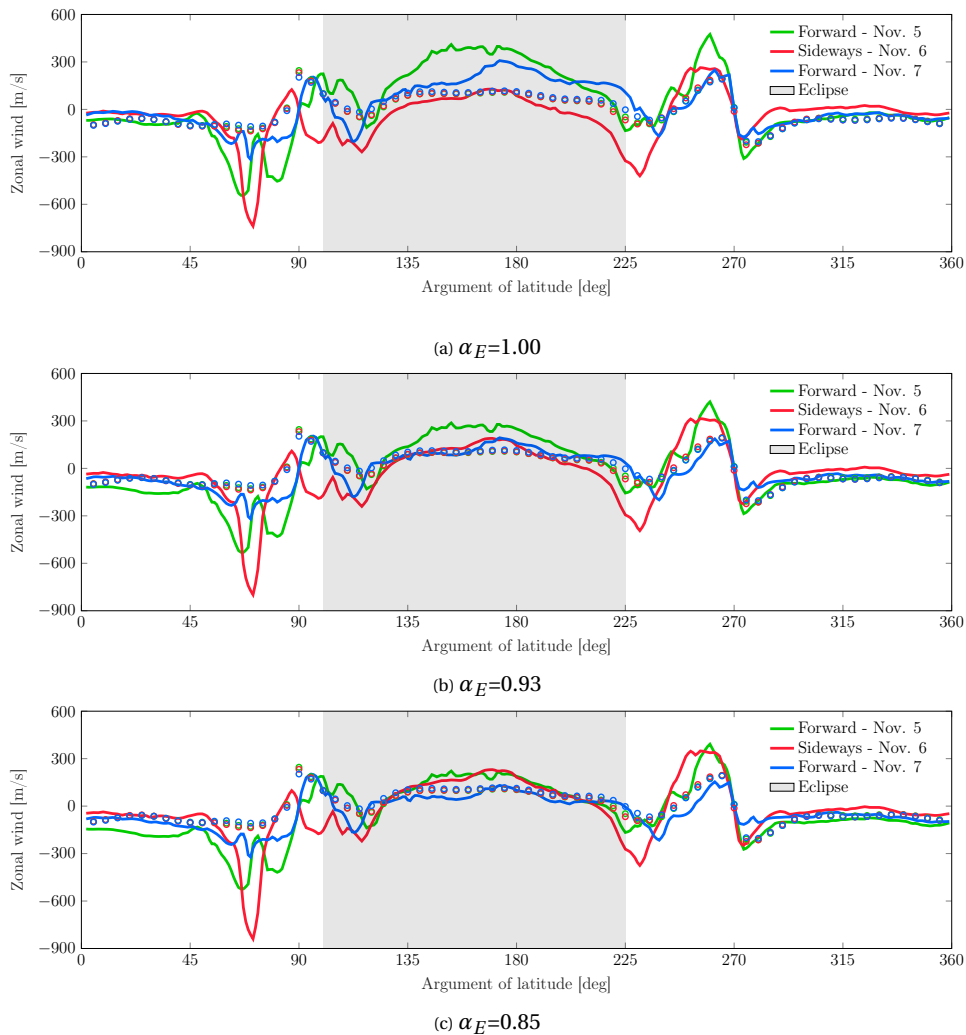


Figure 3.12: Zonal winds for the CHAMP satellite as a function of argument of latitude and different energy accommodation coefficients. The HWM-14 model data are drawn using open circles.

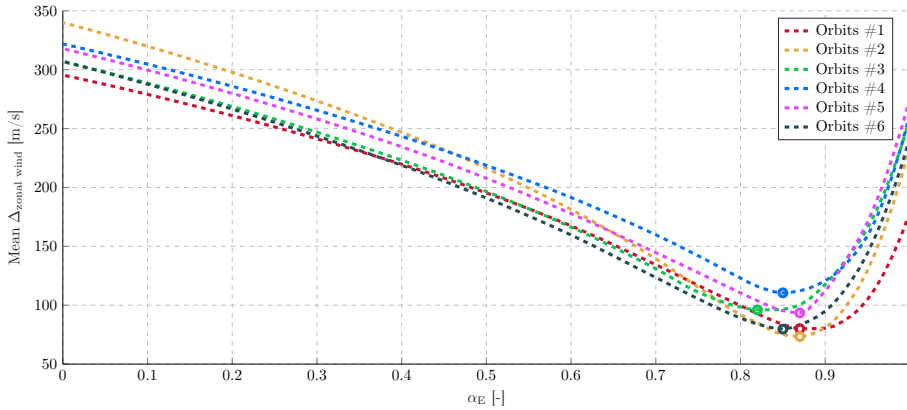


Figure 3.13: CHAMP residual wind as a function of the energy accommodation coefficient for the six selected orbits.

Decreasing the accommodation coefficient from the fully diffusive case ( $\alpha_E=1.00$ ), a minimum in the difference between the three subsets of zonal winds can be detected. The different orientation of the instrument has consequences for the accuracy of the accelerometer calibration (Doornbos, 2011) and the further uncertainties in the solar radiation pressure estimation need to be kept into consideration in the data interpretation. In order to minimize such error sources, it is useful to investigate when the satellite was in eclipse. Within the 100–225 degrees range of argument of latitude, we extracted the mean of the difference between the maximum and minimum wind for each latitude. For all the six selected cases, this quantity of interest is shown as a function of the accommodation coefficient in Fig. 3.13. The minima, similarly to GOCE (in Section 3.5) converge to an accommodation coefficient which is lower than 0.93. In particular for CHAMP, this value fits in the range between 0.82 and 0.87 with an average value of 0.85. For this value, as shown in Fig. 3.12, the derived winds are more consistent within the three days and with the model results. Moreover, for this optimal value the mean difference between the three orbits drops between 70 and 120 m/s. For lower  $\alpha_E$  values the differences can reach values of 300 m/s. For coefficients approaching unity, discrepancies around 200–250 m/s can be obtained with a steep increment due to the misleading distribution of aerodynamic forces. As additional information, in 3.9, a comparison of the newly derived zonal winds with HWM model is available between 2002-01-01 and 2006-01-01. Looking at the results as a function of the magnetic latitude, it is also possible to notice that zonal wind is moving towards westwards direction if the accommodation decreases from unity towards zero. For erroneous low  $\alpha_E$  values, this is a clear effect due to the inaccurate aerodynamic modelling.

### 3.7. SENSITIVITY ANALYSIS

In order to quantify the importance of an accurate accommodation coefficient estimation, in this section and in Fig. 3.14, the GSI parameter influence on horizontal wind nearby the 0.85 and 0.82  $\alpha_E$  values for CHAMP and GOCE is presented. To generate the

plots, first the wind is calculated for the chosen accommodation coefficient, at a specific side-slip angle ( $\beta$ ). Assuming an orbital velocity of 8 km/s this amounts to 560 m/s horizontal wind at 4 degrees side-slip. The resulting aerodynamic acceleration direction vector is stored. As the accommodation is varied, the in-built interior-point algorithm of Matlab<sup>®</sup> is used to find a side-slip angle at which the aerodynamic acceleration vector aligns with the original direction vector. Note that a change in density affects only the acceleration magnitude, not the direction, and is therefore ignored in this process. From the newly found side-slip angle, the horizontal wind can be derived directly. The difference between the wind for the selected accommodation coefficient and the new one, is plotted in Fig. 3.14. The labels reflect the side-slip angle at the reference accommodation coefficient.

If the flow has a direction parallel to the longitudinal axis of the satellite, the side-slip angle is zero. For this condition there is no influence of  $\alpha_E$  on wind, because the wind itself is negligible. However, if there is a larger angle, the GSI parameter has a relevant role in the wind estimation. For GOCE, within the full range of  $\alpha_E$  values, horizontal wind can change up to  $\pm 135$  m/s for  $\beta=4$  degrees, whereas these values are around  $\pm 100$  m/s for CHAMP. The difference in estimated wind is approximately proportional to the side-slip angle, which confirms the observation of [Visser et al. \(2019\)](#) that the accommodation coefficient seems to primarily scale the wind up or down. This is mainly associated to an increase in lift at lower accommodation coefficients. Approaching a full accommodation creates some instabilities in the wind estimation process. This is especially visible for CHAMP, which has a more complex geometry due to the elongated shape and the presence of the frontal boom.

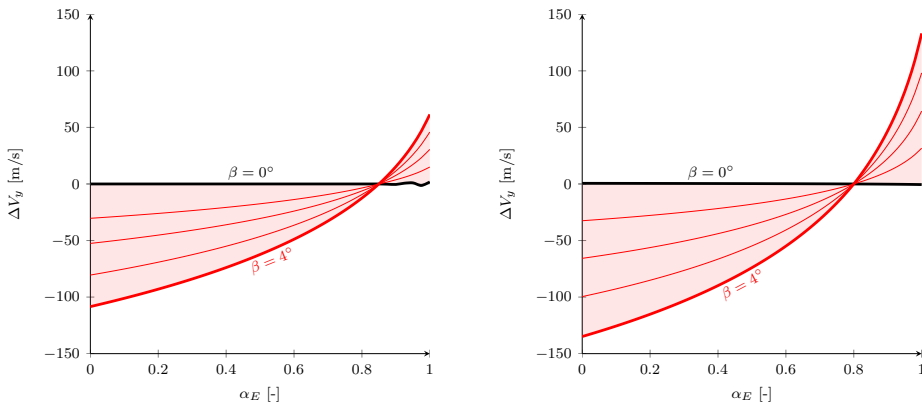


Figure 3.14: CHAMP (left) and GOCE (right) energy accommodation coefficient influence on horizontal wind as a function of  $\alpha_E$  for side-slip angles between 0 degree (black line) and 4 degrees (thick red line) with a step of 1 degree between the included lines.

### 3.8. CONCLUSIONS

This chapter investigates new thermospheric wind estimations using accelerometer-derived measurements from the CHAMP and GOCE satellites. A complete overview

of the influence of different accommodation coefficients on the consistency of thermospheric wind is presented. High-fidelity geometries and the SPARTA rarefied gas-dynamics solver have been used in order to improve the current accuracy level. A diffusive reflection mode with incomplete accommodation was selected and investigated under varying conditions and using different methods. A higher level of self-consistency in the wind data can be found by introducing lower accommodation coefficients with respect to the previously adopted value of 0.93. Investigating the newly generated wind, optimal values of 0.85 and 0.82 are suggested for a higher accuracy in CHAMP and GOCE thermospheric products, respectively. A general overview of the two data sets is available in 3.10. Based on this research, the value of 0.82 for  $\alpha_E$  is used in the V2 GOCE density and wind processing as part of the official ESA production. The newly derived winds are available in the GOCE virtual archive (<http://eo-virtual-archive1.esa.int/GOCE-Thermosphere.html>). The HWM-14 model was not an independent source for the GOCE data, but provided a useful comparison showing a better agreement for lower accommodation coefficient values as well. Seasonal variations are significant for the GOCE satellite, which orbited at low altitudes. Among the three seasonal bins, over the full range of magnetic latitudes, a maximum range within  $\pm 45$  degrees provided a reliable estimation for the energy accommodation coefficient. Outside of this MLAT range, instabilities and high and low wind peaks negatively affected the results. As an outcome of this investigation, a value of 0.82 led to a better consistency within the modelled winds.

The CHAMP sideways manoeuvre provided a great opportunity to investigate the zonal wind consistency as a function of the gas-surface interaction modelling. The results were inter-compared in a short time window and with the HWM-14 model. Consistent wind results were achieved for an energy accommodation coefficient of 0.85.

In order to further improve the current GSI information, an improved solar radiation pressure modelling is necessary. Moreover, in-situ observations of aerodynamic model parameters should be made by independent instruments on accelerometer-carrying satellites. Indeed for future missions, including instrumentation to measure atmospheric and wall temperatures and species concentrations separately, in combination with acceleration observations would be recommended. This would be fundamental in order to quantify current uncertainties. In absence of such missions, future research should be focused on theoretical approaches and laboratory experiments, which would accurately reproduce outer space conditions.

## 3.9. APPENDIX-A: ZONAL WIND COMPARISON WITH HWM-14

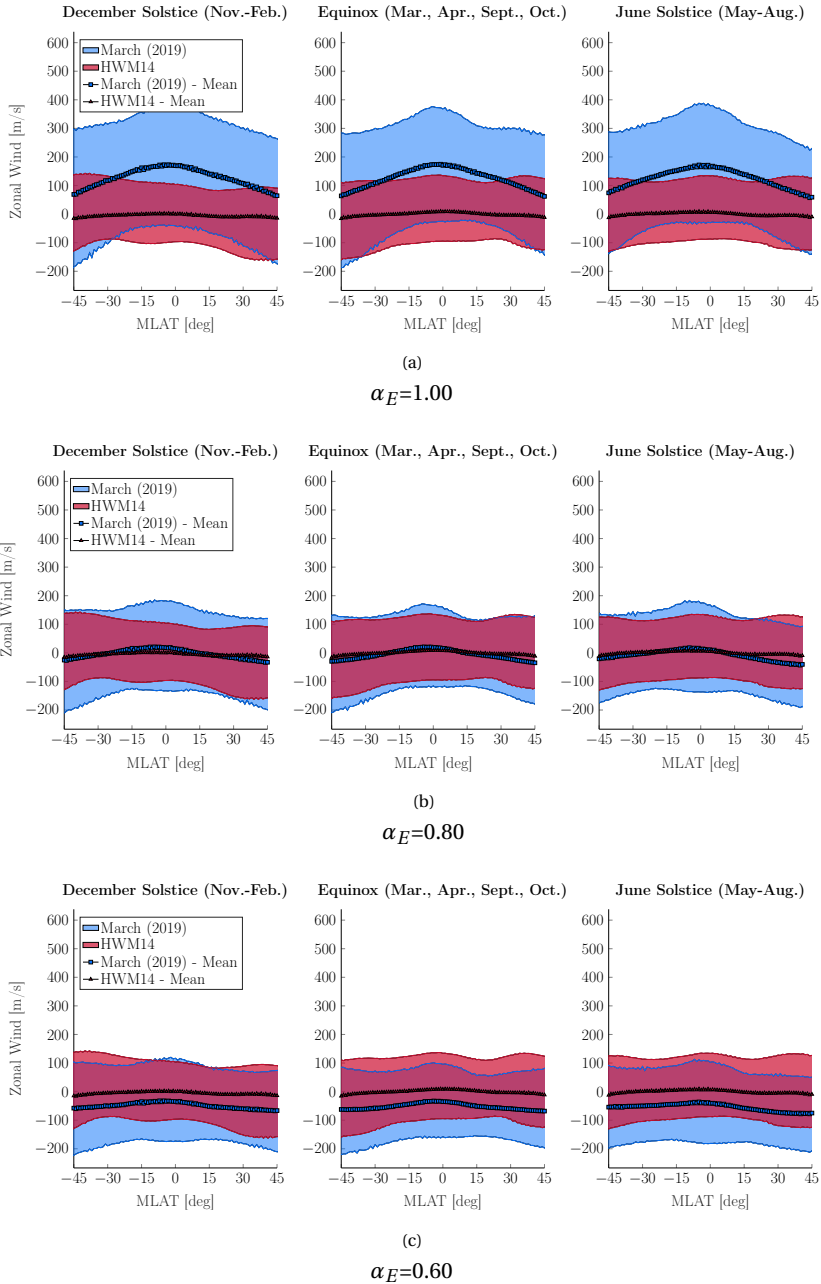
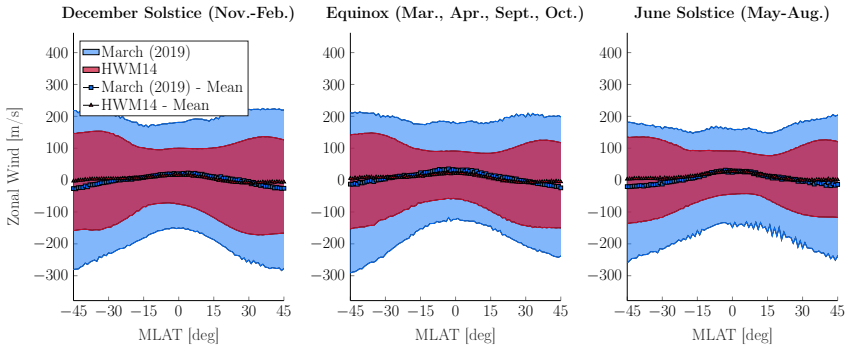
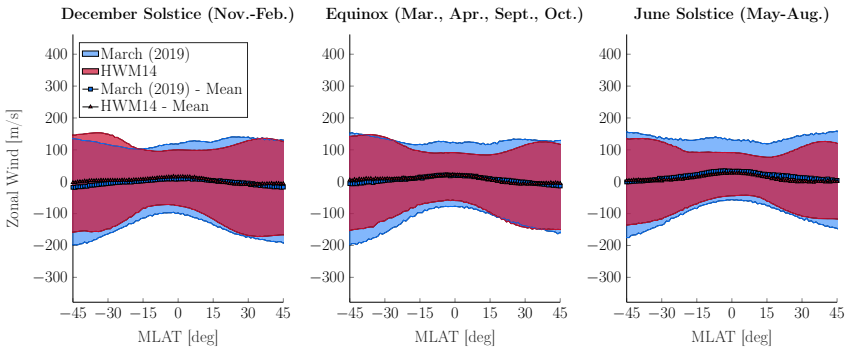


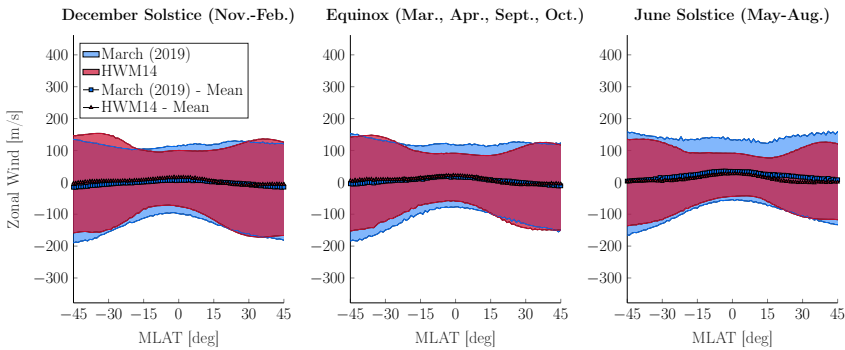
Figure 3.15: Zonal winds for the CHAMP satellite as a function of magnetic latitude and different energy accommodation coefficients between 2002-01-01 and 2006-01-01.



(a)  
 $\alpha_E=1.00$



(b)  
 $\alpha_E=0.80$



(c)  
 $\alpha_E=0.60$

Figure 3.16: Zonal winds for the GOCE satellite as a function of magnetic latitude and different energy accommodation coefficients between 2010-01-01 and 2013-01-01.

### 3.10. APPENDIX-B: NEWLY DERIVED WIND DATA SETS

3

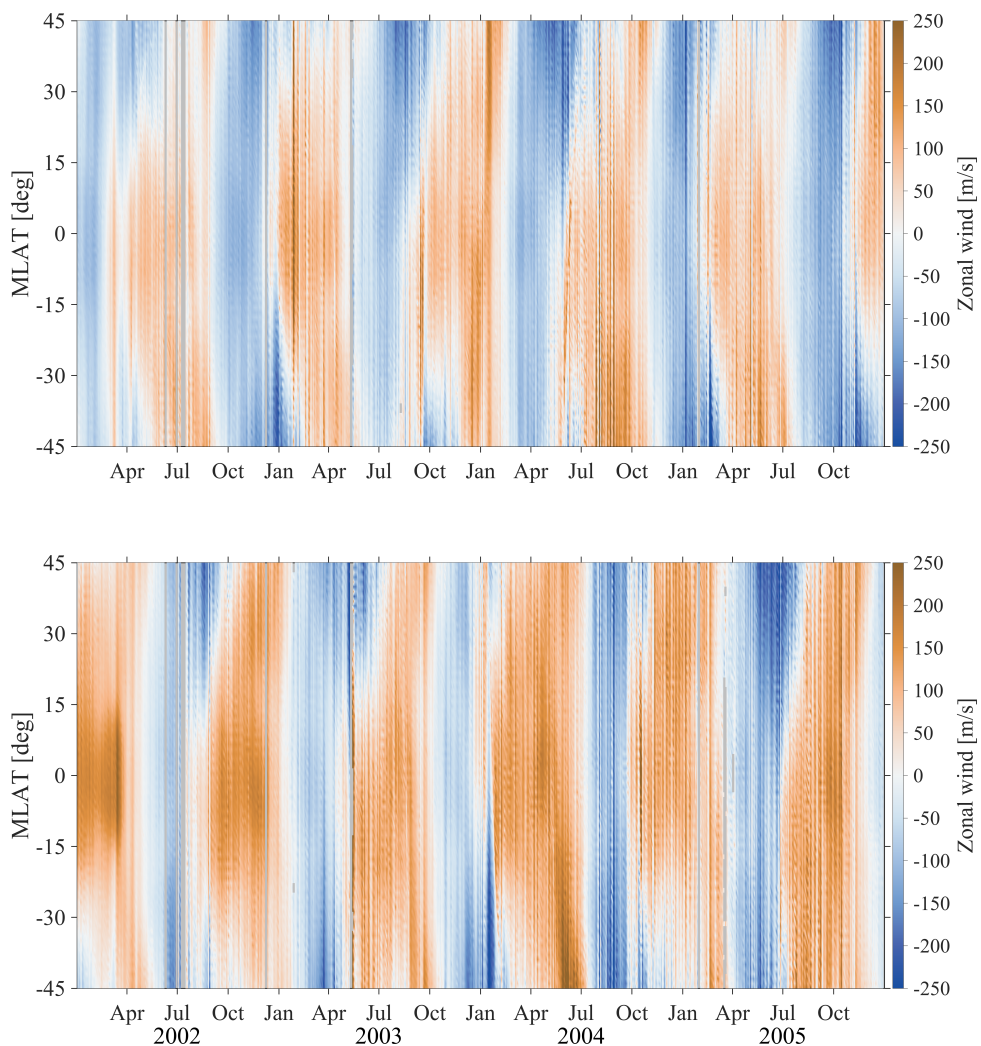


Figure 3.17: Ascending (top) and descending (bottom) mean zonal (eastward) wind for the CHAMP satellite with  $\alpha_E=0.85$ .

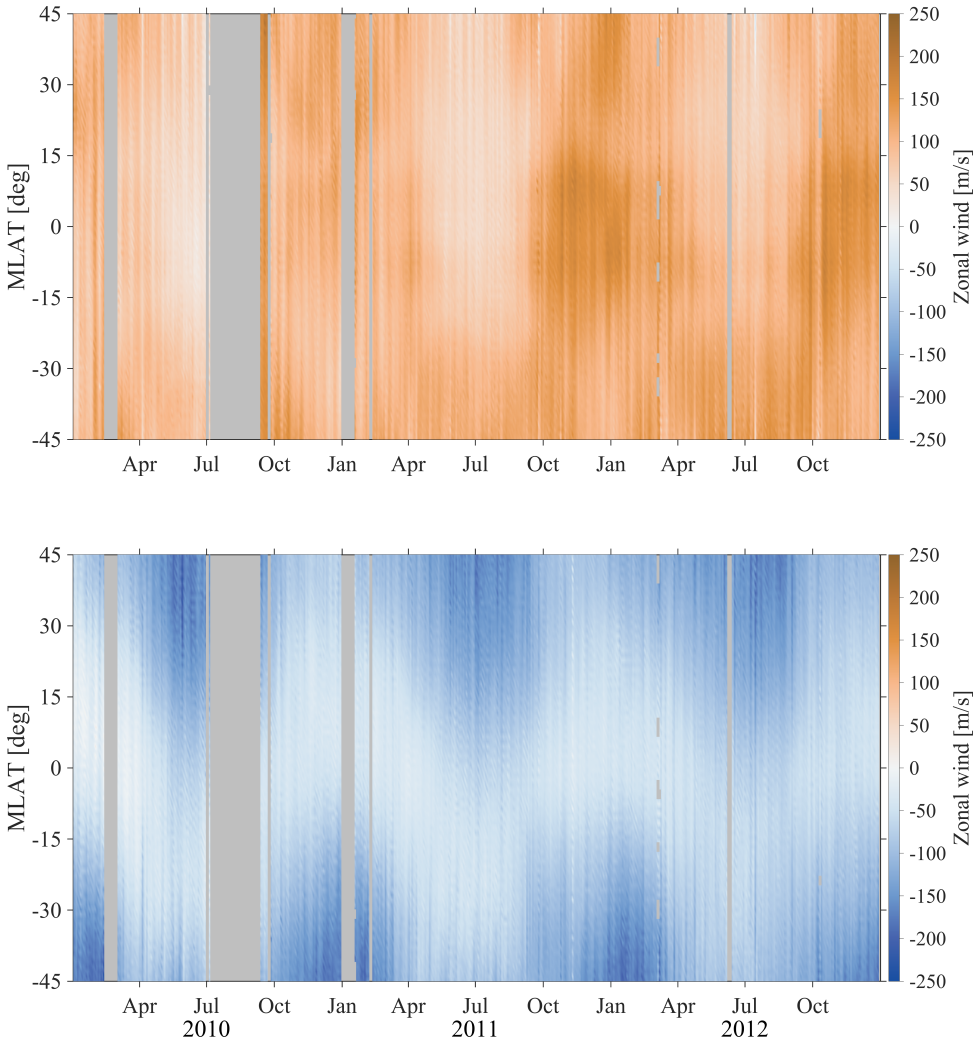


Figure 3.18: Ascending (top) and descending (bottom) mean zonal (eastward) wind for the GOCE satellite with  $\alpha_E=0.82$ .



# 4

## **GAS-SURFACE INTERACTIONS MODELLING INFLUENCE ON THE CHAMP, GRACE, GOCE AND SWARM AERODYNAMIC AND NEUTRAL DENSITY DATA SETS WITH DIFFUSE REFLECTION AND CONSTANT INCOMPLETE ACCOMMODATION**

*The satellite acceleration data from the CHAMP, GRACE, GOCE and Swarm missions provide detailed information of density variations in the thermosphere over the last two decades. Recent work on reducing errors in the modelling of the spacecraft geometry has already greatly reduced scale differences between the thermosphere data sets of these missions. However, residual inconsistencies between the data sets and between data and models are still present. To a large extent, they originate in the modelling of the gas-surface interaction (GSI), which is part of the satellite aerodynamic modelling used in the acceleration to density data processing. Physics-based GSI models require in-situ concentration and temperature data that are not measured by any of the above-mentioned satellites and, as a consequence, rely on thermosphere models for these inputs. To reduce the dependence on existing thermosphere models, we choose in this chapter a GSI model with one constant energy accommodation coefficient per mission, which we optimize to increase the*

*self-consistency of the multi-mission thermosphere data sets. In addition, we make use of a series of attitude manoeuvres performed in May 2014 by the Swarm A and C satellites, which are flying in close proximity, to evaluate the residual inconsistency of the density observations as a function of the energy accommodation coefficient. We find that a value of the energy accommodation coefficient in the range of 0.80–0.85 leads to an improved consistency of density observations across the four missions and Swarm attitudes, compared to the previous 0.93 value assumed at TU Delft and for GOCE and Swarm official products. These numbers are in the same range as our previously published results based on the consistency of wind data from CHAMP and GOCE. A comparison of the mean density ratios between thermosphere models and observations indicates that the NRLMSISE-00 model significantly overestimates the density, and that our constant low accommodation GSI model leads to an overall higher consistency between CHAMP and GRACE densities than the variable accommodation model employed by Mehta et al. (2017).*

## 4.1. INTRODUCTION

The launch of the CHAMP satellite in 2000 marked a new era in which accelerometer measurements were used for producing high-resolution thermosphere density data sets. More satellite missions carrying precise accelerometers into a low-Earth orbit followed soon. The GRACE, GOCE, Swarm, and GRACE-FO missions were launched in 2002, 2009, 2013 and 2018, respectively. Though only the Swarm mission mentions observing thermosphere density as a mission objective, all of the before-mentioned missions provide valuable thermosphere density data sets.

Early generations of CHAMP and GRACE density data sets were based on simplified satellite geometry descriptions and idealised first-guess gas-surface interaction (GSI) parameters (e.g. [Bruinsma and Biancale, 2003](#); [Doornbos, 2011](#); [Sutton, 2008](#)). However, over the last years, a research effort towards improving geometry and rarefied gas-dynamics modelling has raised the level of accuracy of the density data sets ([March et al., 2019a](#); [Mehta et al., 2017](#); [Pilinski et al., 2013, 2016](#)). New models of satellite surface geometries have been constructed in order to improve on the previously used simpler models, which lack a description of shadowing, multiple reflections, and the definition of features such as baffles and antennas. These shortcomings introduced large errors in the scaling of the individual density data sets, leading to inconsistency between the data sets ([March et al., 2019a](#)). However, the scale differences between data sets and atmospheric models are not exclusively due to geometry modelling. The characterization of particle-surface collisions between atmospheric molecules and satellite surfaces is a second fundamental step required in the satellite aerodynamics calculations that are part of the data processing ([March et al., 2019b](#)).

Reducing the current scale differences between the thermosphere data sets is crucial for many reasons. Bias-free measurements are fundamental for inter-comparisons of data from simultaneously flying satellites. They enable accurate data interpolation and extrapolation to different altitudes. Another benefit can be achieved when combining data from multiple satellites for the investigation of scale heights at crossover points and long-term trends (e.g. [Emmert et al., 2008](#)) over multiple solar cycles. More accurate results would also be obtained in the analysis of the thermosphere-ionosphere system's energy budget (e.g. [Wilson et al., 2006](#)). Moreover, orbit analysts of current and future

missions will benefit from improved knowledge of satellite aerodynamics and upper atmospheric variability, which affects orbital lifetime analysis and manoeuvre planning.

The energy accommodation coefficient ( $\alpha_E$ ) is an important parameter of GSI modelling. It describes the energy exchange between the atmospheric molecules and the satellite surfaces. The parameter ranges between the two extreme values of 1 and 0, which describe reflections with and without the ability of the particle's temperature to accommodate to that of the satellite surfaces, respectively. Depending on the different level of absorption of specific atmospheric constituents on satellite surfaces, the GSI can drastically change (Pilinski *et al.*, 2013). Atomic oxygen and helium play a relevant role in satellite aerodynamics (Mehta *et al.*, 2019). The solar cycle is one of the key drivers and influences the chemical composition at the satellite altitude.

Laboratory experiment and in-situ data for GSI are extremely sparse and often limited in practical usability due to the lack of auxiliary data and the use of underlying assumptions. The currently most advanced approach to model GSI in a physically realistic way requires the use of empirical relations between the atomic oxygen concentration and temperature of the gas, and the energy accommodation coefficient (Pilinski *et al.*, 2013). However, in-situ concentration and temperature observations are not available for any of the above-mentioned satellites, so the use of this approach in the data processing from acceleration to thermosphere densities relies completely on the use of an existing thermosphere model for these input parameters. In addition, the parameters used in the aforementioned empirical relations are fitted to past satellite observations that were processed making use of past thermosphere models as well. Therefore, accelerometer data processed with this physics-based GSI approach depends on multiple previous thermosphere models and satellite data sets in complex ways, making it challenging to attribute and reduce the residual inconsistencies between the more modern data sets and models.

In this chapter, we investigate the influence of the GSI modelling on the self-consistency of thermosphere density data sets from the CHAMP, GRACE, GOCE and Swarm missions. This research follows our previously published analyses of neutral wind measurements by CHAMP and GOCE that used the same approach. Our goal has been to self-consistently analyse and process these data sets, and assess the results in combination with thermosphere models that were evaluated along the satellite trajectories.

Due to limitations in the observation data and data/parameter relations for constituents nearby satellite surfaces, the use of the above-mentioned physics-based GSI approach based on oxygen concentration and temperature was incompatible with our self-consistent approach. For this reason, we chose a simpler GSI model with one constant energy accommodation coefficient per mission, which we treat as a free parameter to increase the self-consistency of the thermosphere density data sets.

A similar approach was selected in March *et al.* (2019b) for studying the effect of GSI on thermosphere wind from the CHAMP and GOCE missions. The GSI model is based on diffuse reflections with incomplete accommodation (DRIA), which was adopted in agreement with the current processing algorithms of the GOCE and Swarm missions. However, assuming a constant incomplete accommodation reflections mode introduces an overall mean thermosphere description. Therefore, variations due to different solar activity levels and dayside–nightside differences should be interpreted with caution and

are out of the scope of this study.

Over the last years, numerous works have been performed on satellite aerodynamics by Monte Carlo techniques and there is an increasing interest in processing satellite data with high-fidelity geometries. The SPARCS software (*Pilinski, 2011*), based on the test particle technique, analyzes triangulated meshes to provide aerodynamic coefficients. In *Mehta et al. (2017)*, a similar investigation was performed for the CHAMP and GRACE satellites assuming a variable energy accommodation coefficient. Throughout this work, drag coefficients are based on an extension of the Monte Carlo technique for obtaining free molecular flow aerodynamic coefficients presented in *March et al. (2019a)*.

The density data resulting from this work have been made available to aid in the further development and validation of thermosphere models such as MSIS and DTM, for use in further scientific research as well as space mission operations analysis and planning.

The methodology is summarized in Section 4.2. Information on the GSI influence on the satellite aerodynamics can be found in Section 4.3. Section 4.4 describes the GSI modelling effects on the thermospheric neutral density. Results and comparison with external data sets and models are available in Sections 4.5 and 4.6. Section 4.7 provides conclusions and an outlook on future work.

## 4.2. METHODOLOGY

This study is based on the use of output from the Stochastic PARallel Rarefied-gas Time-accurate Analyzer (SPARTA) software (*Gallis et al., 2014*), in combination with the new high-fidelity satellite geometries from *March et al. (2019a)*. The atmospheric flow is considered to be in the free molecular regime and therefore collisions between particles are neglected. This allowed for a simplification resulting in a faster convergence of the simulations. All analyzed cases cover the most common mission scenarios including a wide range of attitude angles with respect to the incoming flow, satellite velocity and chemical compositions. A full data set was generated for four energy accommodation coefficient values. Afterwards, the data sets for the additional  $\alpha_E$  values have been generated in the post-processing phase using a least-squares method. Though the satellite surface is covered with a variety of materials, we could unfortunately not associate different surface properties to different parts of the triangulated geometry due to software limitations. Therefore, GSI are assumed to be independent from the different surface materials. The main simulations settings are fully described in *March et al. (2019a)*. However, as a difference with respect to that work, the gas-surface collisions are not assumed to always use the energy accommodation coefficient  $\alpha_E = 1$ , which represents the case in which the temperature of the impinging particles on the satellite fully accommodates to the surface temperature. In this work, we allow an incomplete accommodation of the temperature, i.e. the energy accommodation coefficient  $\alpha_E$  is allowed to differ from unity. In the following sections and within this research, the energy accommodation coefficient is the key parameter to characterize the GSI models. Indeed, this parameter provides tangible information on the energy exchange between atmospheric particles and satellite surfaces. Its value can be estimated from the incoming and reflected kinetic tempera-

tures ( $T_{k,i}$  and  $T_{k,r}$ ) and the satellite surface temperature ( $T_{wall}$ ) according to

$$\alpha_E = \frac{T_{k,i} - T_{k,r}}{T_{k,i} - T_{wall}} \quad (4.1)$$

and may assume values ranging from 0 to 1. The two extremes  $\alpha_E = 0$  and  $\alpha_E = 1$  represent reflections where the particle temperature does not accommodate and fully accommodates to the satellite surface temperature, respectively.

In Section 4.3, the influence of  $\alpha_E$  on the satellite aerodynamics is investigated for the CHAMP, GRACE, GOCE and Swarm satellites. In Section 4.4 the effects on the resulting thermospheric neutral density are investigated. In both analyses the values of  $\alpha_E$  are studied in the range between 0 and 1. However, from a few experimental observations (*Gregory and Peters, 1987; Hedin et al., 1973; Moe et al., 1993*), this value is suggested to be closer to unity than to zero. Unfortunately, the reliability of older observation methods is uncertain. The chemical constituents play a crucial role for the adsorption properties of the satellite surfaces. The amount of adsorbed chemical molecules on the satellite surface can be implemented in the Cercignani-Lampis-Lord (CLL) model (*Cercignani and Lampis, 1971*). This approach is widely used for the GSI modelling (*Mehta et al., 2017; Walker et al., 2014*). The scattering distribution of the particles after the collisions is based on the accommodation coefficients for the tangential velocity ( $\sigma_t$ ) and the normal kinetic energy ( $\alpha_n$ ). The total energy accommodation coefficient for the CLL model ( $\alpha_{CLL}$ ) is defined as

$$\alpha_{CLL} = \frac{\alpha_n + \sigma_t}{2} \quad (4.2)$$

The Response Surface Model (RSM) developed by *Mehta et al. (2017)* was designed as an implementation of the CLL GSI model applied to the CHAMP and GRACE satellites. In the RSM model, the energy accommodation coefficient is assumed to be variable and an improved geometry of the satellites was used to calculate the drag coefficients. This was done assuming quasi-specular collisions and satellite surfaces covered by adsorbed atomic oxygen. Adopting these assumptions, within the CLL method  $\sigma_t$  is set to unity (*Sutin et al., 1973*) and the normal component can be estimated with

$$\alpha_n = \frac{6\mu}{(1 + \mu)^2} - 1 \quad (4.3)$$

where  $\mu$  is the ratio of the mass of the atmospheric gas constituents to the mass of the satellite surface material. However,  $\mu$  and  $\alpha_n$  are difficult to estimate without in-situ observations of the atmospheric composition. Unfortunately, no satellite mission provides all required observations. Therefore, we prefer to infer information on the energy accommodation coefficient by changing its value and analyzing the effect on the self-consistency of the density and wind data. This was already done by *March et al. (2019b)* for thermosphere wind for the CHAMP and GOCE satellites. In particular, for CHAMP, an attitude manoeuvre performed in November 2002 provided detailed information on the energy accommodation coefficient. Studying the consistency of the thermosphere wind within similar orbit and magnetic field conditions, but using different satellite orientations, a higher self-consistency was achieved for  $\alpha_E = 0.85$ . Zonal winds within the analysed attitude manoeuvre had a lower variability under similar conditions for this

improved  $\alpha_E$  value. Also for GOCE, a study based on seasonal dependency resulted in a lower energy accommodation coefficient than the currently adopted value of 0.93 at TU Delft and for part of the official ESA mission products. Indeed, a greater consistency was achieved for an optimal value of 0.82. This value is currently adopted in the new GOCE data release (<http://eo-virtual-archive1.esa.int/GOCE-Thermosphere.html>, January, 2020).

Unfortunately, attitude manoeuvres are not common, and, in particular, the ones that guarantee a stable flight configuration without thruster activation, or with sufficient time windows between different attitude orientations are even more rare. In order to provide reliable information, these manoeuvres need to be in periods of high to medium solar activity and at relatively low altitudes (i.e. below 400–450 km) to ensure a good aerodynamic acceleration signal in relation to error sources such as radiation pressure acceleration and instrument bias mismodelling. Investigating these manoeuvres is particularly useful for thermosphere wind studies.

Neutral density is more sensitive to variations in the solar extreme ultraviolet (EUV) emissions. For this reason, studying densities for the optimization of the energy accommodation coefficient is more challenging and requires satellites with characteristics as similar as possible. The Swarm mission provides an opportunity for such a comparison. The Swarm A and C satellites are flying side-by-side at the same altitude (between 450–500 km) with up to  $1.4^\circ$  separation in longitude over the equator and 4–10 seconds (30–75 km) separation in along-track direction, providing nearly identical density observations. If, within a certain time window, these satellites perform attitude manoeuvres exposing a different side of their body to the atmospheric flow, it is possible to inter-compare the two data sets and deduce information on GSI modelling parameters like the energy accommodation coefficient. This will be further explained in the Section 4.5.

### 4.3. GAS-SURFACE INTERACTIONS INFLUENCE ON SATELLITE AERODYNAMICS

In this section, the aerodynamic coefficients for the CHAMP, GRACE, GOCE and Swarm satellites are introduced, and variations with attack and side-slip angles are examined. The selected aerodynamic coefficients are estimated in the satellite reference frame and have been normalized with a reference area set to  $1 m^2$  for all missions. This fixed reference area does not depend on the attack and side-slip angles, and therefore variations of the true exposed satellite area do not need to be independently calculated, as they are included in the normalized force coefficients. The  $C_x$ ,  $C_y$  and  $C_z$  force coefficients are computed along the axes of the satellite reference frame, which in nominal attitude correspond to the longitudinal (along-track), horizontal sideways (cross-track) and vertical downward (anti-radial) directions of the satellite reference frame, respectively. In this analysis, the GSI influence is investigated with six different values of the energy accommodation coefficient (0.0, 0.2, 0.4, 0.6, 0.8 and 1.0). The value of 1.0 represents reflections with full accommodation to the spacecraft wall temperature, while the value 0.0 is for collisions without thermal energy exchange and accommodation to the surface temperature. The data sets are obtained as a function of attack and side-slip angles and

a range of speed ratio values. In particular, the speed ratio, defined as

$$s = \frac{v_{inc}}{\sqrt{\frac{2RT_{inc}}{m}}} \quad (4.4)$$

is a fundamental parameter, which allows to simulate different satellite velocities, but also different chemical compositions and atmospheric temperatures. From Eq. 4.4, it is possible to notice that this parameter is directly connected with the relative velocity between satellite and atmosphere ( $v_{inc}$ ), local atmospheric temperature ( $T_{inc}$ ), molecular mass ( $m$ ) and gas constant ( $R$ ). In the generated data sets, this ratio ranges between 0.5 and 14 and this interval fully describes all possible encountered mission scenarios.

Figures 4.1, 4.2 and 4.3 show the aerodynamic coefficients for the GRACE, CHAMP and Swarm satellites for a wide range of side-slip angles. The  $C_x$ ,  $C_y$  and  $C_z$  components are available in the figure for the same range of  $\alpha_E$  values. During mission lifetime, the attack angle is mainly centered around the nominal flight configuration of  $0^\circ$  in attack, while the side-slip angle is usually less stable, and varies over the full domain from approximately  $0$  to  $180^\circ$  during manoeuvres. The three plots of Figures 4.1, 4.2 and 4.3 show that the coefficients are lower in magnitude when the collisions are closer to the fully accommodated mode. Moreover, looking at the constant step of 0.2 in  $\alpha_E$ , it is clear that between 0.8 and 1.0 the difference in the aerodynamic forces is much larger than between 0.0 and 0.2. A description of the computed discrepancies varying the attack and side-slip angles are available in Tables 4.1 and 4.2, respectively. The higher sensitivity for coefficients nearby the fully diffusive mode was already observed in the zonal wind analysis by [March et al. \(2019b\)](#). The shape of the aerodynamic force coefficient curves remains the same without relevant differences. However, the main change, as expected, is a bias between the different computed values within the selected  $\alpha_E$  range. When we inspect the differences between non-accommodated and fully diffusive modes, the percentage difference reaches up to 84.5% for CHAMP, 84.0% for GRACE, 52.0% for GOCE and 82.1% for Swarm (Tables 4.1 and 4.2). For the study of the attack angle variation the highlighted coefficients are  $C_x$  and  $C_z$ . The cross-track component of the aerodynamic force ( $C_y$ ) is negligible. The plots for the side-slip angle variation show the  $C_x$ ,  $C_y$  coefficients. The  $C_z$  coefficients are one order of magnitude lower or negligible (for GOCE). For this reason only the most relevant aerodynamic contributions are shown in the enclosed plots. However, for the quantitative analysis of Table 4.2, the results for the Z-component are also provided. Among the possible representations, the polar plots shown in Figures 4.1, 4.2 and 4.3 provide a clear overview of the different coefficients for GRACE, CHAMP and Swarm, respectively. In Fig. 4.1, the nearly symmetrical shape of the lobes for the  $C_x$ ,  $C_y$  and  $C_z$  coefficients can be observed for the GRACE satellite. Whereas, for CHAMP and Swarm, Figs. 4.2 and 4.3 show the asymmetric shape of the  $C_x$  and  $C_z$  coefficient lobes which is a consequence of the presence of booms (boom pointing into flight direction for CHAMP and into anti-flight direction for Swarm). A different sensitivity to the energy accommodation coefficient can also be observed depending on the nominal or backward orientation of the satellite. When both CHAMP and Swarm have their boom pointing into flight direction, the drag coefficients are less dependent on the accommodation coefficient value. If the satellite exposes the large side to the incoming flow, the

collisions are playing a crucial role in the force coefficients determination.

4

$\alpha_E$ range	0.0-0.2			0.8-1.0			0.0-1.0		
Satellite	$C_x$ [%]	$C_y$ [%]	$C_z$ [%]	$C_x$ [%]	$C_y$ [%]	$C_z$ [%]	$C_x$ [%]	$C_y$ [%]	$C_z$ [%]
CHAMP	1.6	-	7.9	5.8	-	42.9	13.7	-	66.2
GRACE	3.0	-	6.6	11.2	-	32.3	24.8	-	55.5
GOCE	2.4	-	5.2	8.6	-	22.8	19.8	-	43.5
Swarm	2.9	-	5.5	11.3	-	24.6	24.6	-	46.0

Table 4.1: Force coefficient differences for different  $\alpha_E$  ranges along X and Z satellite reference frame axes for the selected attack angle variation range.

$\alpha_E$ range	0.0-0.2			0.8-1.0			0.0-1.0		
Satellite	$C_x$ [%]	$C_y$ [%]	$C_z$ [%]	$C_x$ [%]	$C_y$ [%]	$C_z$ [%]	$C_x$ [%]	$C_y$ [%]	$C_z$ [%]
CHAMP	1.5	3.2	10.0	5.0	12.2	67.6	12.0	26.7	84.5
GRACE	2.1	3.1	10.9	7.5	11.8	63.1	17.6	25.9	84.0
GOCE	2.4	6.2	-	8.6	29.3	-	19.8	52.0	-
Swarm	0.9	3.1	9.8	3.1	11.8	63.8	7.7	25.8	82.1

Table 4.2: Force coefficient differences for different  $\alpha_E$  ranges along X, Y and Z satellite reference frame axes for the selected side-slip angle variation range.

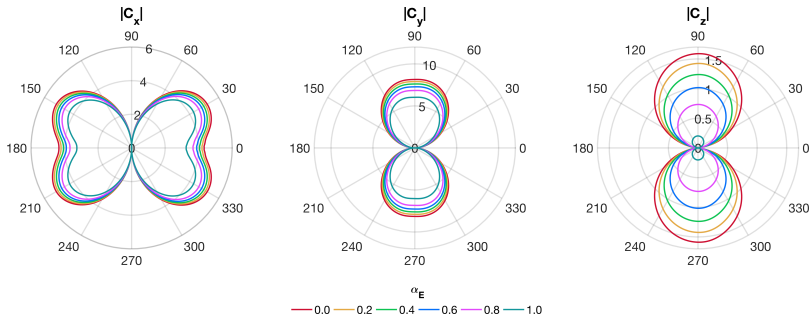


Figure 4.1: Polar plots of the aerodynamic coefficients as a function of the side-slip angle (between  $0^\circ$  and  $360^\circ$ ) and energy accommodation coefficient for the GRACE satellite.

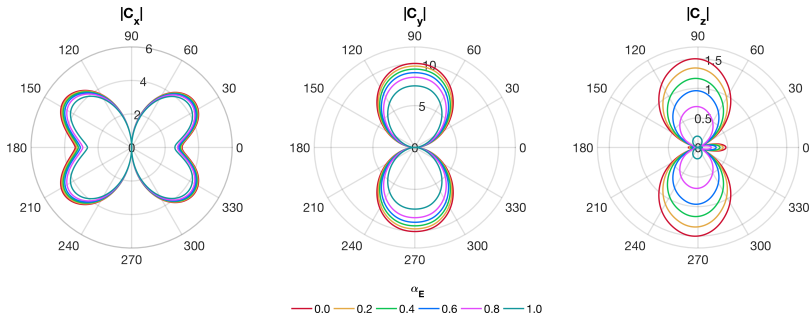


Figure 4.2: Polar plots of the aerodynamic coefficients as a function of the side-slip angle (between  $0^\circ$  and  $360^\circ$ ) and energy accommodation coefficient for the CHAMP satellite.

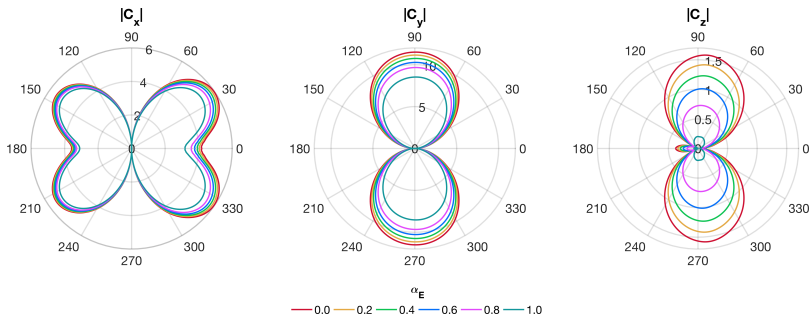


Figure 4.3: Polar plots of the aerodynamic coefficients as a function of the side-slip angle (between  $0^\circ$  and  $360^\circ$ ) and energy accommodation coefficient for the Swarm satellites.

In 3.9, the force coefficients for the CHAMP, GRACE, GOCE and Swarm satellites are shown for different attack and side-slip angles. Within the GOCE mission, large attitude manoeuvres were not performed. Therefore, the side-slip angle range is smaller (between  $-16^\circ$  and  $16^\circ$ ). All these figures (including the previous polar plots) are obtained

for a speed ratio of 7. A complete analysis which shows the different coefficients for the complete analyzed range of speed ratios is provided in 3.10. In this additional section, the  $C_x$ ,  $C_y$  and  $C_z$  coefficients are shown in the 0.5–14 speed ratio range and for different side-slip angle configurations (i.e.  $0^\circ$ ,  $45^\circ$  and  $90^\circ$ ).

As a further investigation, it is interesting to study the influence of how the latitude variations influence the satellite aerodynamics. In Fig. 4.4, the CHAMP force coefficients along the satellite longitudinal axis are shown for three different solar activity levels. The three days were already selected by (March *et al.*, 2019a). High, moderate and low activities correspond to 2002-10-27, 2005-05-15 and 2009-08-28, respectively. From this analysis, it is possible to notice that peaks in drag are reached at the equator for 0 and 180 degrees in argument of latitude. This is especially clear for high and low activity cases. Relevant trend differences among different values of  $\alpha_E$  are not present. Indeed, averaging the full day of observations, between different energy accommodation coefficients a mean bias can be identified as main effect on the satellite aerodynamics.

The figures and analyses of this section and mentioned annexes aim to provide insight for further aerodynamic studies and possible experimental campaigns investigating orbital aerodynamics. The presented aerodynamic data sets for the selected satellites are available as part of the publication's supplemental material.

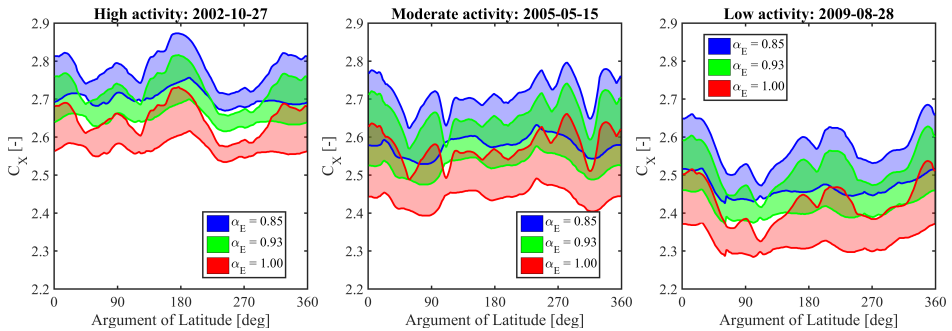


Figure 4.4: CHAMP force coefficients along the longitudinal axis as a function of the argument of latitude in three selected days describing high, moderate and low solar activity.

## 4.4. GAS-SURFACE INTERACTIONS INFLUENCE ON NEUTRAL DENSITY

The thermospheric density is retrieved with the algorithm discussed in [Doornbos \(2011\)](#) and [March et al. \(2019a\)](#). The methodology is based on the processing of the accelerations derived from satellite observations. The CHAMP, GRACE and GOCE on-board accelerometers provided high-precision information. Unfortunately, for the Swarm satellites, many anomalies occurred in the accelerometer measurements ([Siemes et al., 2016](#)) and for this reason a new density product based on GPS-derived accelerations was introduced as part of the official ESA documentation ([van den IJssel et al., 2020](#)). For CHAMP and GOCE the cross-track component can be investigated. However, for GRACE and Swarm, winds are difficult to retrieve due to the high altitudes (around 500 km) and the lack of sufficiently precise accelerometer measurements as previously mentioned.

In this chapter, the optimal  $\alpha_E$  values from [March et al. \(2019b\)](#) are implemented in the density processing in order to generate the newly derived data sets. Quickly comparing the new and the previously adopted  $\alpha_E$  value of 1.00 from [March et al. \(2019a\)](#), the average difference between new and previous densities is around 6% for CHAMP and 11% for GOCE. The comparisons with semi-empirical models are influenced by solar and geomagnetic activity, because models perform differently for different geomagnetic and solar activity conditions ([Emmert, 2015](#)). The semi-empirical models are commonly closer to the observed density during periods of high solar activities and, within this condition, the agreement with the new results is better. However, when these models are introduced for comparisons the results provide a qualitative information which needs to be interpreted carefully. The presented results are fundamental for atmospheric scientists and modellers that constantly improve empirical and physics-based available models.

Analyzing long time periods, it is possible to investigate the sensitivity of the energy accommodation coefficient on the new density data with respect to the fixed output of a semi-empirical model. In [Fig. 4.5](#), the density ratio with respect to the NRLMSISE-00 model is shown for three different solar activity levels. The high activity is represented by  $F_{10.7}$  values between 130 and 300 solar flux units (sfu). The medium activity is in the range between 90 and 130 sfu, while the low solar activity is chosen for values of  $F_{10.7}$  under 90 sfu. The selected time periods are between January 2003 and January 2006 for CHAMP and GRACE, January 2010 and January 2013 for GOCE and July 2014 and July 2017 for Swarm, respectively. Comparing the three subsets, it is possible to notice a deterioration of the agreement between different satellites for low values of  $F_{10.7}$ . This is due to the lower signal magnitude, the larger error in the solar radiation pressure modelling, but also to the lower performances of the semi-empirical model during deep-low solar activity. However, for the results for high activity, a clear optimal value of the accommodation coefficient which guarantees a higher consistency or lower variabilities among different missions cannot be identified. This is mostly due to the large uncertainties of the MSIS model.

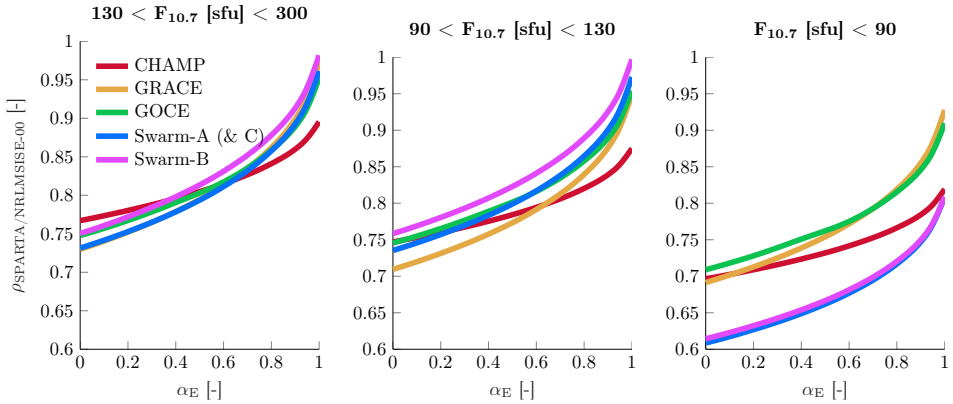


Figure 4.5: Long period density ratios with respect to the NRLMSISE-00 model for different ranges of  $F_{10.7}$ .

For fully accommodated reflections ( $\alpha_E = 1.0$ ), the maximum in variability among the satellites is registered. This further confirms that the optimal accommodation coefficient is not the full accommodation case. From this analysis, as explained before, it is not possible to retrieve an optimal  $\alpha_E$  coefficient, and it is shown just in order to provide characteristics of the new modelled data in comparison with a semi-empirical model and the energy accommodation coefficient. However, exploiting the particular manoeuvres of the Swarm constellation, as outlined in the next Section, it is possible to further assess the neutral density and provide additional information on the energy accommodation coefficient determination.

The new density presented in this work is based on a constant energy accommodation coefficient. This creates a constraint in specific features like differences in chemical composition during day–night transitions and along the orbit. To quantify the difference with other models like the CLL, a comparison with other densities is performed for the CHAMP satellite. In Figures 4.6, 4.7 and 4.8, a comparison between different models is analysed for high, moderate and low solar activity, respectively. The new density from this work is compared with the one obtained with the same SPARTA modelling with full accommodation (March *et al.*, 2019a) and the ones by Mehta *et al.* (2017) and Doornbos (2011). Mehta *et al.* (2017) adopts an approach based on the CLL model, while Doornbos (2011) uses the DRIMA model applied to a simplified macromodel geometry. Only the first three hours for each selected day are shown to fully appreciate the variations within around two orbits. As expected, the densities by March *et al.* (2019a) are greater than the others. This is due to the higher energy accommodation coefficient set to unity. However, it is clear from the density ratio plot that the difference between the SPARTA simulations for full accommodation and the  $\alpha_E = 0.85$  case are not purely differing with a bias over short periods. This is related to the different collisions physics implemented with the new  $\alpha_E$  value. Comparing the new density with the ones derived with the CLL model by Mehta *et al.* (2017), larger variations can be noticed. The recorded discrepancies have a periodic behaviour associated to the satellite location. The greater peaks are over the poles and reach a maximum difference with respect to the new results of around 10–15%. Higher fluctuations in densities and their ratios are also localized nearby polar regions,

this is mostly due to the complex dynamics in those areas. A more stable behaviour can be shown for the densities by [Doornbos \(2011\)](#), which similarly to the previous results by [March et al. \(2019a\)](#) are characterized by low frequency variations with respect to the new density. This is associated to the use of the same chemistry inputs from the NRLMSISE-00 model. With this comparison it is possible to quantify the discrepancies between CLL and DRIA models. Most of the times, orbit variations are within  $\pm 10\%$ , however peaks can reach up to 15% over poles. These cyclic variations are expected to be associated to the different chemical constituents adsorbed over satellite surfaces along the orbit.

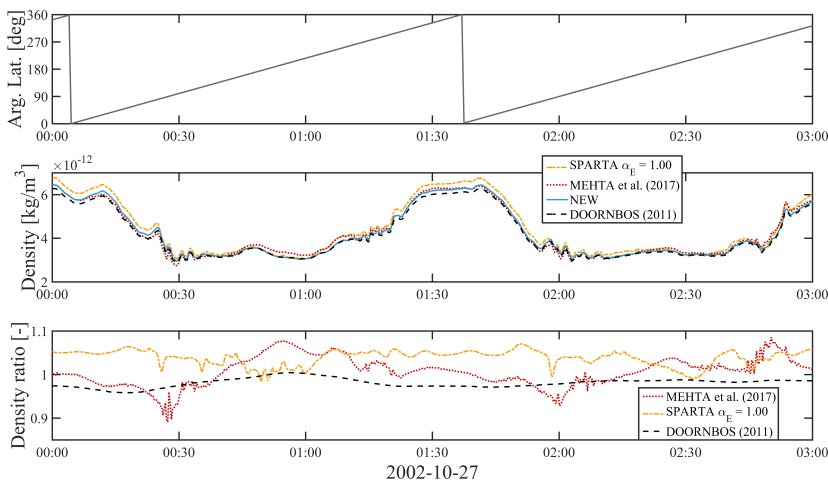


Figure 4.6: Comparison between the new densities and the ones derived by [March et al. \(2019a\)](#), [Mehta et al. \(2017\)](#), and [Doornbos \(2011\)](#) for the CHAMP satellite under high solar activity condition.

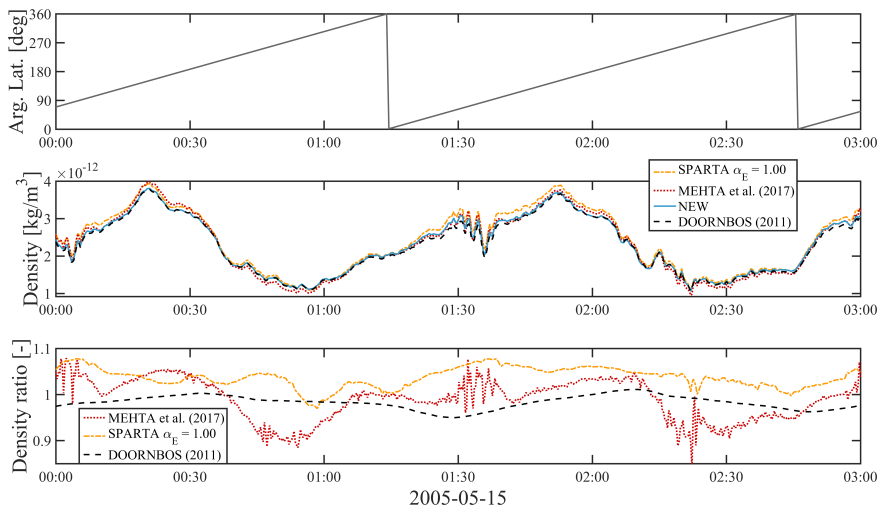


Figure 4.7: Comparison between the new densities and the ones derived by [March et al. \(2019a\)](#), [Mehta et al. \(2017\)](#), and [Doornbos \(2011\)](#) for the CHAMP satellite under moderate solar activity condition.

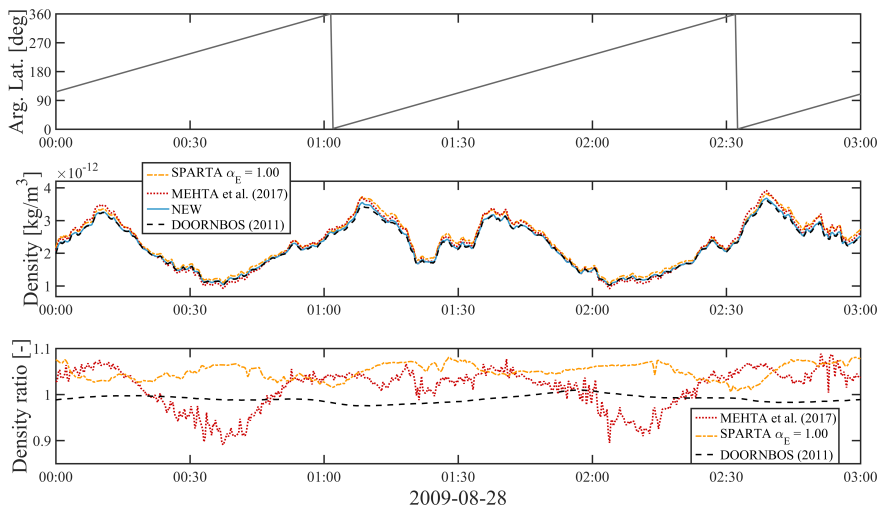


Figure 4.8: Comparison between the new densities and the ones derived by [March et al. \(2019a\)](#), [Mehta et al. \(2017\)](#), and [Doornbos \(2011\)](#) for the CHAMP satellite under low solar activity condition.

## 4.5. DENSITY CONSISTENCY FOR SWARM-A AND -C

In the time window between the 13th and 14th of May 2014, the Swarm A and C satellites performed multiple attitude manoeuvres. The main objective of the four 90° yaw slew rotations was focused on investigating differences between the measurements of the vector and absolute magnetometers. However, it is possible to exploit these changes of satellite orientation with respect to incoming atmospheric flow to retrieve information on the satellite aerodynamics. An animation of the manoeuvres and associated data and models that were used in this Section is available as part of the supplemental material for [March et al. \(2020\)](#).

Looking at a single satellite at a time, the thermospheric variability affects the density comparison in time. However, since Swarm A and C were flying next to each other, the simultaneous measurements of the two satellites can be compared. It is fair to assume that the extracted densities would be nearly identical. This assumption is especially justified during high solar activity, when the signal strength is suitable for further processing. Indeed, during high activity the average ratio between the two densities are consistent to within 1%, and these small differences in density generally agree with the expected diurnal density gradient. For the current very low solar activity data, this density ratio can reach values up to 50%. If the experiment with the attitude manoeuvre were to be repeated, it would therefore be necessary to wait for when high solar activity conditions and/or significantly lower orbit altitudes are reached by the mission.

In the two analyzed days in 2014, the average  $F_{10.7}$  value was around 165 sfu, which is characterized by high solar activity conditions. The absence of geomagnetic activity events provided a suitable time window without undesired spikes in the data. In Fig. 4.9, the performed manoeuvre is represented by the absolute value of the yaw angles for both satellites. The coloured shaded areas highlight the orbits that are taken into account for the analysis. All orbits containing large slew rates have been discarded because of high thruster activity and uncertainty induced by the Kalman-filter approach in the GPS-derived accelerations. In the bottom part of Fig. 4.9, the density ratio between Swarm A and C measurements is illustrated as a function of the energy accommodation coefficient. Each line corresponds to one of the selected orbits following the same color specified in the top part. Varying the accommodation coefficients, it is possible to notice a variation in the slope of the density ratios. With the green markers, the intersections between different periods are highlighted. The intersections appear to be concentrated around the value of 0.85.

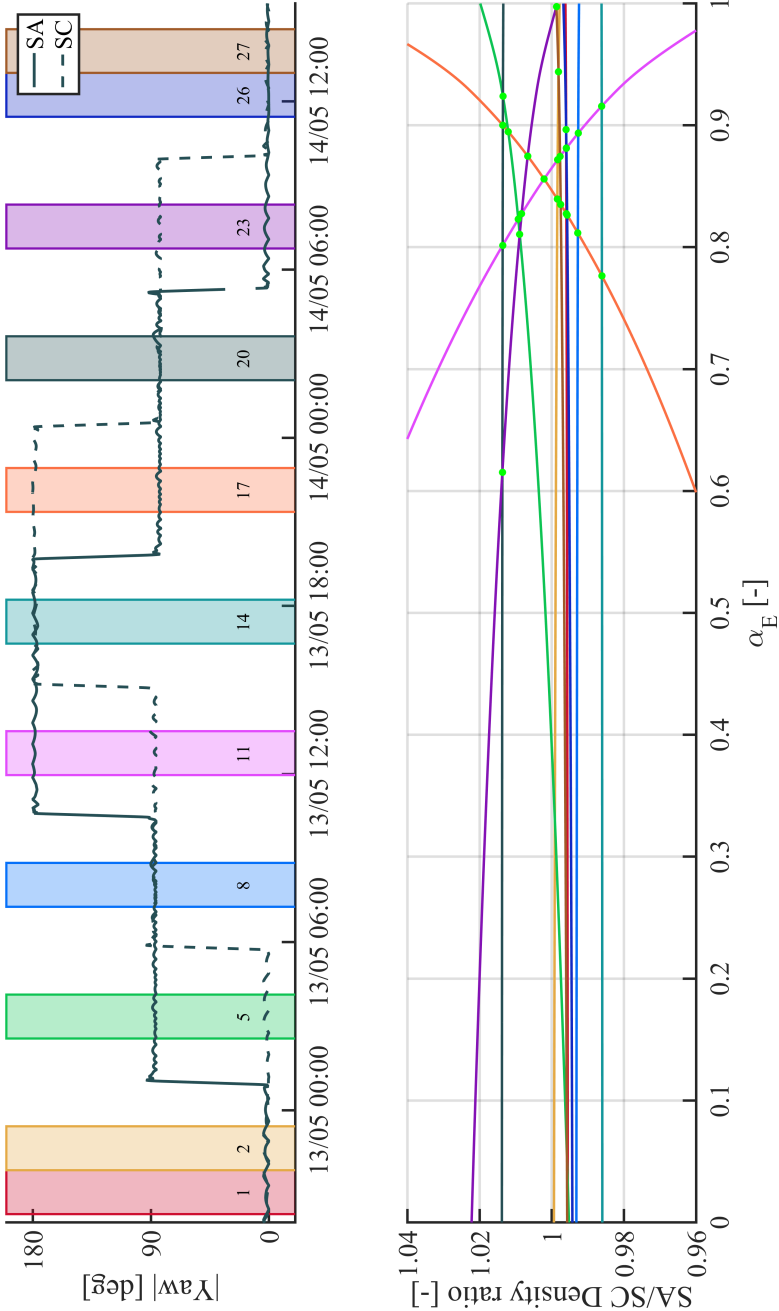


Figure 4.9: Yaw angle variations and density ratios between Swarm-A and Swarm-C measurements during the May 2014 manoeuvre. Selected orbit numbers are available in the top part of the figure.

Particular attention needs to be focused on the orbits which, at the same time, are characterized by different satellite shapes with respect to the flow. Two of these orbits are numbered 11 and 17. For these two specific cases, the satellites are respectively in backwards and sideways orientation with respect to the nominal flight. Having the capability to estimate the densities within the range of 0–1 for  $\alpha_E$ , it is possible to create a map of density ratios within the two orbits, setting a different accommodation coefficient for each satellite. The two maps for the two selected orbits are available in Fig. 4.10. In this representation in the  $\alpha_E$  values for Swarm A and C, an area can be identified where the density ratio between the two satellites is close to one. Highlighting the optimal ratios with dashed lines, the intersections for both orbits with the diagonal of the map coincide with an  $\alpha_E$  value of 0.85. Similar conclusions can be drawn looking at other interesting periods as the orbits number 5 and 23. In this case the two satellites are in the nominal and sideways configurations. For these two periods an intersection is achieved for an  $\alpha_E$  value of 0.81. Similar results can be found including all the remaining selected orbits (Fig. 4.11). All values found are below the currently adopted  $\alpha_E$  value of 0.93.

The results coincide with the values obtained from the accelerometer-derived wind analysis of the CHAMP and GOCE satellites in *March et al. (2019b)*, which showed optimal  $\alpha_E$  of around 0.85 and 0.82 for the two missions, respectively. Looking at the overall intersections available in Fig. 4.9 and the other results from this section, a value of 0.85 is recommended for future Swarm density processing. Comparing the current densities processed with a value of 0.93 for the accommodation coefficient (available at <https://swarm-diss.eo.esa.int/>), the new data would be slightly lower in magnitude with a 4–5% difference. This new presented  $\alpha_E$  value will be adopted in the future ESA product releases.

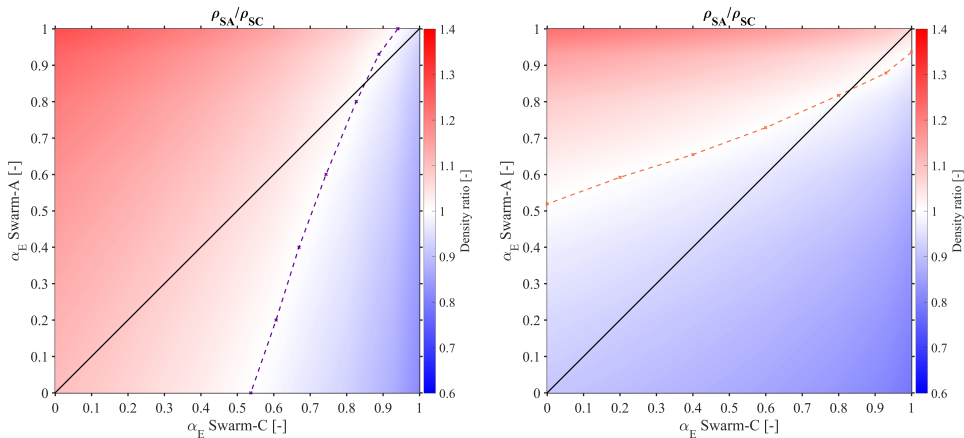


Figure 4.10: Swarm A and C density ratios for periods 11 and 17 (on the left and right side, respectively). The optimal density ratios for which satellites are in better agreement are highlighted with dashed lines.

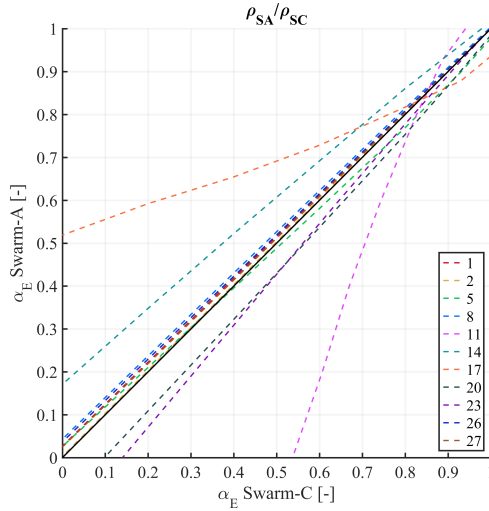


Figure 4.11: Swarm A and C optimal density ratios for May 2014 manoeuvres and selected periods.

#### 4.6. COMPARISONS WITH ATMOSPHERIC MODELS

In order to compare and validate the new density data, a further analysis is performed using the results from the NRLMSISE-00 and the WACCM-X models. The choice of these two models was based on their wide use among scientific users and their applications to past and current TU Delft and ESA projects.

The WACCM-X model is a physics-based model developed at the High Altitude Observatory (HAO) of the National Center for Atmospheric Research (NCAR) (*Liu et al., 2018*). In order to have an overview of the newly generated neutral densities, the outputs are compared for specific conditions. The simulated scenarios represent three different periods with high, medium and low solar activity. One month of data for each subset are investigated and shown in Fig. 4.12. The new results are normalized with the NRLMSISE-00 model at the altitude of 400 km for the CHAMP and Swarm satellites. This procedure was already used with the DTM2000 model in *Bruinsma et al. (2006)*. For GOCE, the normalization is performed at 250 km in order to provide a more representative altitude for that mission. This normalization was especially necessary for the Swarm satellites because the WACCM-X upper pressure level altitude boundary extends to around 500 km altitude. The monthly time window was selected to limit the computational cost of the physics-based model simulations.

For the GRACE satellites, the relatively large density error due to the high altitude of this mission impedes the investigation of an optimal accommodation coefficient. For this reason, within this section no further details about new density data of GRACE satellites are available. Additional studies would require a deeper investigation after reprocessing current GRACE data. This would be especially useful for the second phase of the mission, which was characterized by a dramatic degradation of accelerometer measurements (*Klinger and Mayer-Gürr, 2016*).

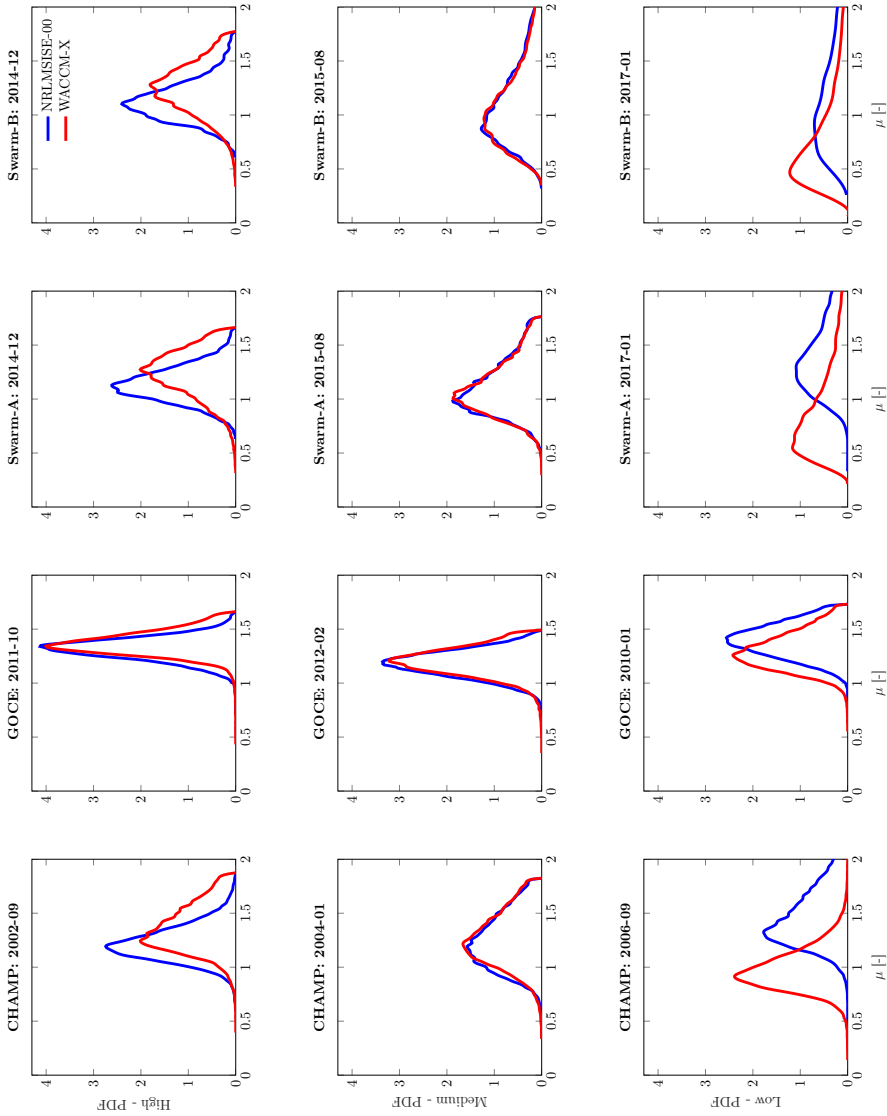


Figure 4.12: Comparison of the density ratios between the newly derived density and the NRLMSISE-00 and WACCM-X models results. The densities are normalized at 400 km altitude except for GOCE, which is normalized at 250 km.

As shown in Fig. 4.12, which shows the Probability Density Function (PDF) of the density ratios between the new and the modelled densities, both models are currently providing higher estimates of the neutral density than the satellite data especially under high and moderate solar activities. For low solar activity periods, the differences in the ratios between NRLMSISE-00 and WACCM-X compared with the new data are much larger. These comparisons are difficult to interpret because of the large atmospheric models' errors which allow just for a qualitative representation. For GOCE, the density ratios show high agreement for both NRLMSISE-00 and the physics-based model, however for both a bias of about 30–40% can be noticed. A similar behavior between the two introduced models and the new densities is verified for the moderate solar activity levels. This is valid for all the selected satellites. If we look at the low activity periods, very different values can be detected for both models. This is especially the case for Swarm B which is highly affected by the low signal magnitude in deep-low solar activity. Imperfections in the solar radiation pressure modelling have a strong contribution. An improvement of this additional contribution would enhance the quality of derived neutral densities and this is currently under investigation.

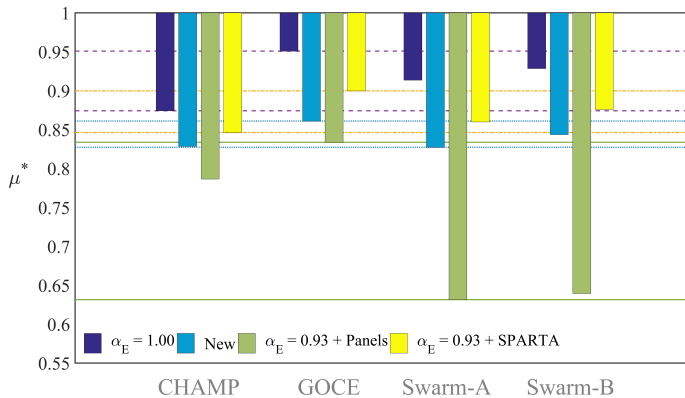


Figure 4.13: Comparison between the mean density ratios ( $\mu^*$ ) between the NRLMSISE-00 model and the full accommodation (March et al., 2019a) and the newly generated densities with the new  $\alpha_E$  values for the CHAMP, GOCE and Swarm satellites. The density ratios computed with  $\alpha_E=0.93$  are also available for the old panels method (0.93 + Panels) and the new SPARTA modelling (0.93 + SPARTA), always compared to NRLMSISE-00. Dashed lines indicate the maximum variability range among the satellites.

In order to provide an overview over longer periods, the average density ratios with respect to the NRLMSISE-00 model have been computed (Fig. 4.13). The illustrated periods are between 2003 and 2005 for CHAMP, 2010 and 2012 for GOCE and July 2014 and February 2019 for the Swarm satellites. The newly derived densities are compared with the previous results from March et al. (2019a) for fully accommodated reflections ( $\alpha_E = 1.00$ ). Fig. 4.13 shows that the new densities are lower with respect to the ones presented in March et al. (2019a). However, even if the agreement with the semi-empirical models is not improving, the results are found to be more consistent among the selected missions. Indeed, the scale with respect to the NRLMSISE-00 model is now more constant across the missions. As highlighted with the dashed lines, the new  $\alpha_E$  bars are within

3% of the variation among the satellites, whereas for the previous version of the data this value reached 8%. Introducing the  $\alpha_E = 0.93$  value, with the old panel method differences reach 23%. The variability decreases to 5–6% when the new geometries and the SPARTA modelling are adopted. Therefore, for the newly presented GSI modelling a higher degree of consistency seems to be achieved although it is necessary to take the empirical model uncertainties into account for more quantitative investigations. This study provides an indication that the new data are more consistent also when compared with an empirical model, but especially when the densities are inter-compared among different missions. However, it is necessary to take into consideration that the uncertainties associated with the semi-empirical models do not allow to use such an approach for the energy accommodation coefficient determination. This analysis indicates that satellite drag data processed with improved geometry and aerodynamic modelling can be used to enhance current semi-empirical and physics-based models.

To compare the presented density observations with those produced with a GSI model based on a variable energy accommodation coefficient, we obtained CHAMP and GRACE density observations from *Mehta et al. (2017)*. Figure 4.14 illustrates the consistency of the two density observation data sets with two representative thermosphere models. We selected the NRLMSISE-00 model (top panel), which is widely used, and the DTM-2013 model (bottom panel), which is one of the most recent thermosphere models. The figure shows the mean density ratio ( $\mu^*$ ) of the model and the observations as an index of their consistency. In the legend of the figure, we provide the difference  $\Delta$  between the CHAMP and GRACE mean density, which is a measure of the self-consistency of the multi-mission observations. The figure is based on the period between 2003-01-01 and 2004-12-31, when the solar activity was high. This enhances the accuracy of the analysis because of the higher aerodynamic signal level and better atmospheric model performance during such high solar activity conditions. The new GRACE density observations were computed with  $\alpha_E = 0.85$ , which is a preliminary assumption introduced to equally compare to the CHAMP results under the same conditions. For a more quantitative analysis, this assumption needs a dedicated investigation, which is out of the scope of this chapter.

Since our primary objective is a high self-consistency of the multi-mission density observations, we focus in the discussion of Fig. 4.14 on the the differences  $\Delta$ . The highest self-consistency is achieved for the density observations presented in this work, where the difference between the two missions is 2.87% for the NRLMSISE-00 model and 2.66% for the DTM-2013. Using the fully accommodated condition  $\alpha_E = 1$  as in *March et al. (2019a)* leads to differences of more than 7% for both thermosphere models. For a fixed energy accommodation coefficient  $\alpha_E = 0.93$ , the differences are still around 7% when a panel model is used, which is reduced to 4–5% when the panel model is substituted by the SPARTA model. Introducing a variable accommodation coefficient in the density processing as in *Mehta et al. (2017)* gives differences around 4.4% for both density models.

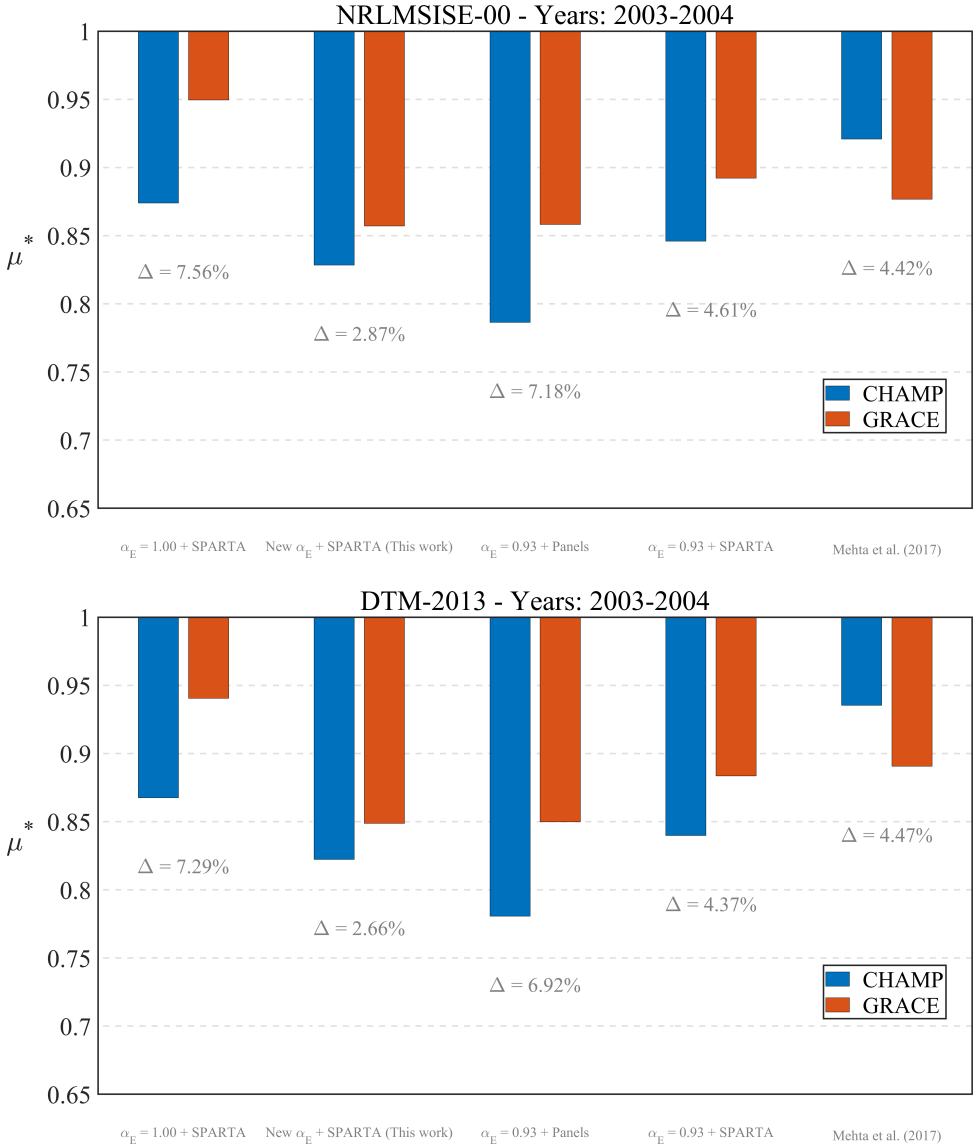


Figure 4.14: Comparison of the mean ratios ( $\mu^*$ ) between the densities according to the NRLMSISE-00 (top) and DTM-2013 (below) models and the observed densities resulting from the full accommodation (March et al., 2019a), the newly generated densities with the new  $\alpha_E$  value of 0.85 for the CHAMP and GRACE satellites. The density ratios computed with  $\alpha_E = 0.93$  are also available for the old panels method (0.93 + Panels) and the new SPARTA modelling (0.93 + SPARTA). Variable energy accommodation coefficient densities are obtained from Mehta et al. (2017). Note that the 0.85 coefficient for GRACE is introduced just for inter-comparing equal conditions with CHAMP.

The low percentages achieved within this work need a careful interpretation due to the uncertainties associated with the atmospheric models. However, the high degree of self-consistency between the CHAMP and GRACE density observations for both thermosphere models is a promising result. It could be a starting point for further enhancing both fixed and variable accommodation coefficient approaches.

The newly derived density data for CHAMP, GOCE and Swarm A and B are illustrated in Section 4.10. The GRACE satellites were excluded because the energy accommodation needs further study and the accelerometer data processing requires further improvement.

## 4.7. CONCLUSIONS

In the presented research, the influence of GSI on aerodynamic and density modelling is investigated. This study provides new data sets for satellite aerodynamics, which are made available to the science community as part of the supplemental material and on the new website <http://thermosphere.tudelft.nl>. The possibility to further validate this work with dedicated test campaigns is given through the new aerodynamic coefficients described in Section 4.3. New neutral density data sets for the CHAMP, GOCE and Swarm satellites are obtained and investigated as a function of the energy accommodation coefficient. This parameter plays a crucial role in the GSI modelling. The commonly adopted value of 0.93, which was used in the past at TU Delft in the processing of density observations, is higher than the optimal values that are found in this research and in *March et al. (2019b)*. Based on a study of the neutral winds presented in *March et al. (2019b)*, a value of 0.85 for CHAMP and 0.82 for GOCE are recommended, which is already implemented in the data sets available on the above-mentioned webpage.

All of our comparisons of thermosphere models and observations show that the models overestimate density. Introducing these models in the density data processing, and knowing that these might be biased by past decisions on satellite aerodynamic modelling based on orbital decay data, prevents quantitative analyses of the energy accommodation coefficient. So far, such analyses are limited to studying attitude manoeuvres and exploiting synergies between satellites. This is demonstrated through the analysis of the Swarm A and C manoeuvre in May 2014. The two satellites provided the unique opportunity to compare simultaneous measurements at high solar activity with large aerodynamic signal magnitude. Through investigating the density ratios, the optimal value of the energy accommodation coefficient is found to be in the range of 0.80–0.90. This is in agreement with the previous analysis of thermosphere wind observed by the CHAMP and GOCE satellites. For the Swarm satellites, we recommend to use an average value of 0.85 for the energy accommodation coefficient in future data processing. The new Swarm densities are lower in magnitude than the ones that we obtained with  $\alpha_E = 0.93$  and are presently available on the before-mentioned website as well as in ESA's Swarm data archive. The difference in magnitude is expected to be around 5%. In the future, further exploitation of the Swarm A and C synergy is strongly encouraged. However, at the currently low solar activity in combination with the altitude, the aerodynamic signal magnitude is too low for additional meaningful analyses.

The presented research would strongly benefit from an improved solar radiation pressure modelling, especially for the GRACE and Swarm satellites, which have spent

a significant portion of their lifetime at relatively high altitude during solar minimum. Our efforts to augment the new high-fidelity satellite geometries with surface properties for improving the solar radiation pressure models are currently on-going.

We also see potential to improve our processing of the GRACE accelerometer data, which would aid among others GSI investigations as presented in this chapter. In particular the accelerometer data calibration for the last 7 years of the mission has a great potential for improvement. The reason is that from April 2011 onward, the thermal control of the accelerometer was deactivated to save battery life, which resulted in significant perturbations related to the fluctuating instrument temperature.

The assumption that the energy accommodation coefficient is constant for all solar and geomagnetic conditions needs to be further investigated as well. This is an open issue, which deserves a deeper investigation to further characterize the impact of the chemical composition, which changes significantly during the solar cycle and dayside–nightside transitions, on GSI parameters and, thus, density observations. An improved level of accuracy of thermosphere data is expected when using GSI models based on variable accommodation coefficients. However, accurate in-situ measurements of the chemical composition are needed to reliably estimate these GSI parameters. In particular, additional information on Helium and atomic Oxygen adsorbed by the satellite surfaces is crucial in this context. Dedicated satellite missions are strongly recommended to remove current uncertainties. As shown in this research, GSI can currently only be investigated in an indirect and imperfect way, making use of scarce data from satellite constellations, manoeuvres and seasonal analysis. Nevertheless, some steps forward can be made with such analyses to improve the self-consistency of the thermosphere data sets. More data of these types will certainly be helpful for further investigations. However, new experiments with more extensive instrumentation will be necessary to resolve open issues.

In the future, dedicated satellite thermosphere density and satellite drag experiments will need to measure not only the accelerations (using accelerometers, GNSS receivers and star cameras as on the satellites analysed here), but also to independently and accurately measure the temperature, composition, wind and density on the same platform as input to the satellite aerodynamic model. Ideally, such experiments would eventually have to cover all possible temperature and composition environments, by spanning both solar minimum and maximum conditions, as well as a wide range of altitudes, including the nearly unexplored region below 200 km.

4.8. APPENDIX-A: NEW AERODYNAMICS DATA SETS

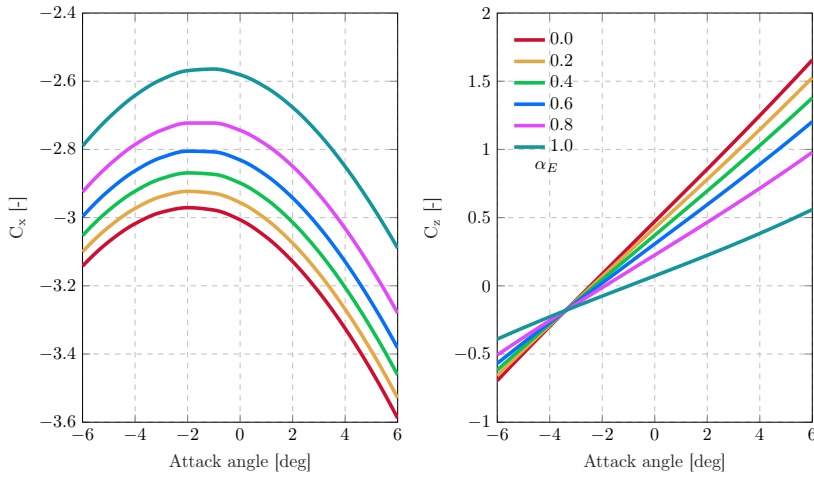


Figure 4.15: Aerodynamic coefficients in the satellite reference frame as function of the attack angle and energy accommodation coefficient for the CHAMP satellite.

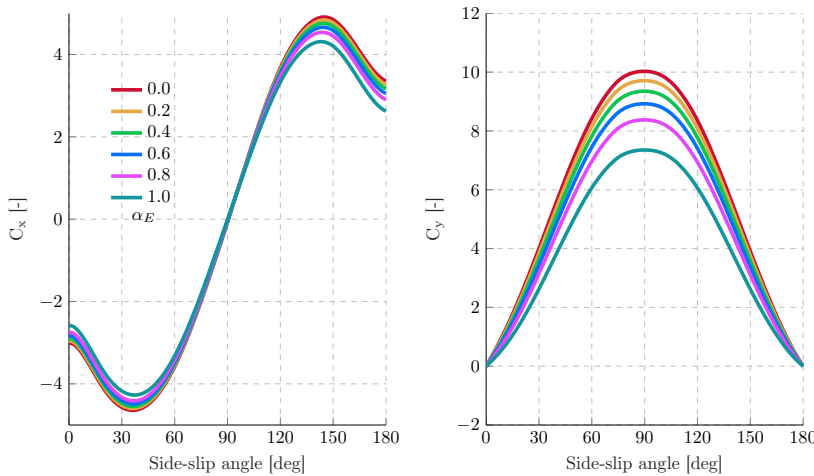


Figure 4.16: Aerodynamic coefficients in the satellite reference frame as function of the side-slip angle and energy accommodation coefficient for the CHAMP satellite.

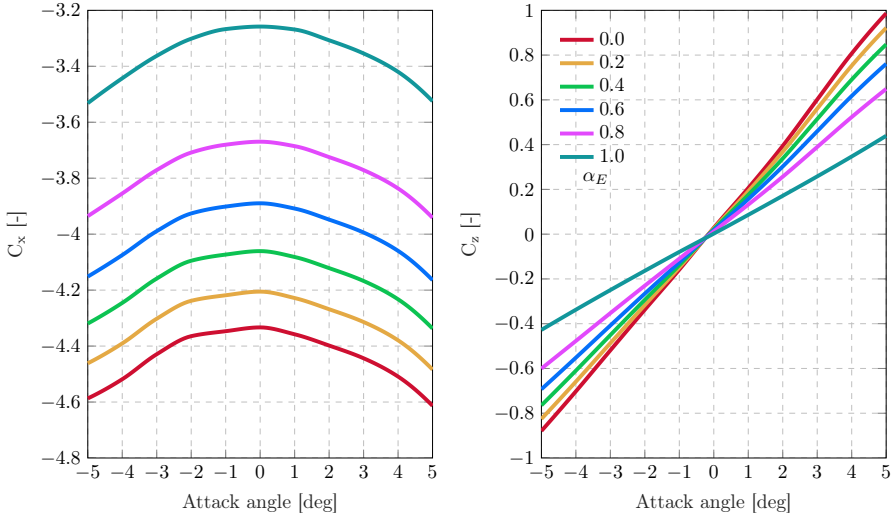


Figure 4.17: Aerodynamic coefficients in the satellite reference frame as function of the attack angle and energy accommodation coefficient for the GRACE satellite.

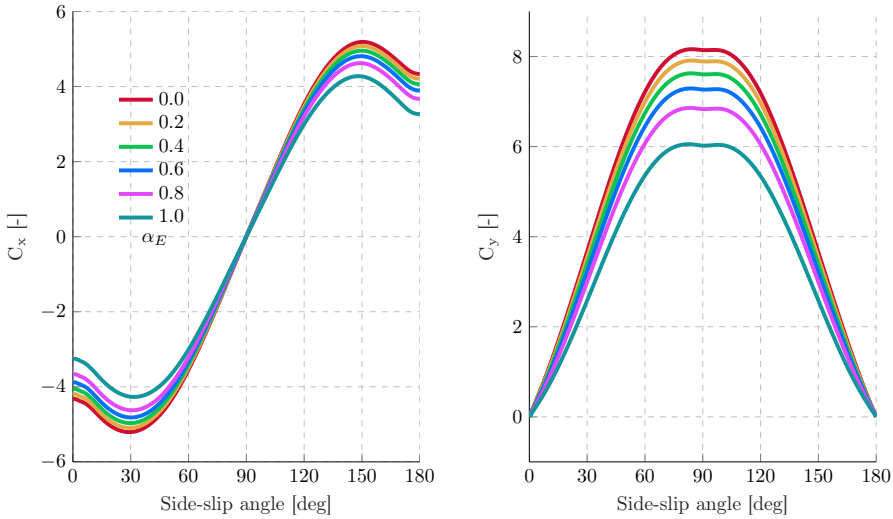


Figure 4.18: Aerodynamic coefficients in the satellite reference frame as function of the side-slip angle and energy accommodation coefficient for the GRACE satellite.

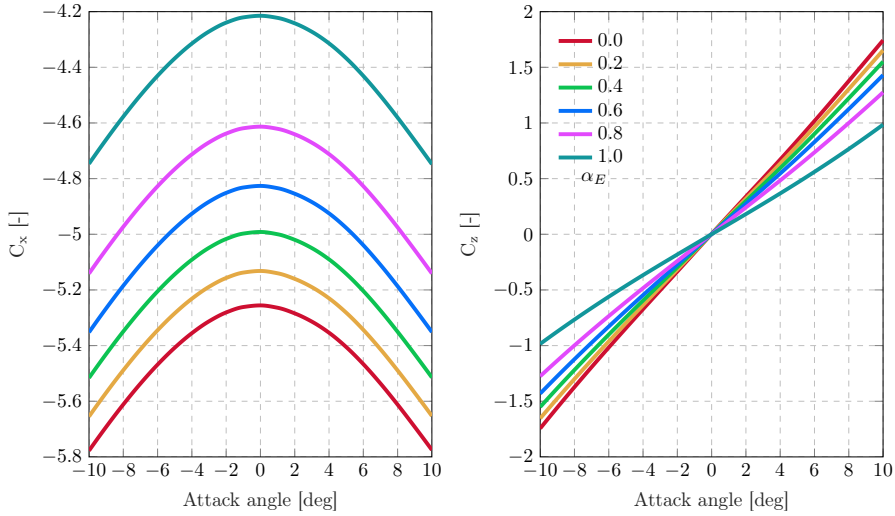


Figure 4.19: Aerodynamic coefficients in the satellite reference frame as function of the attack angle and energy accommodation coefficient for the GOCE satellite.

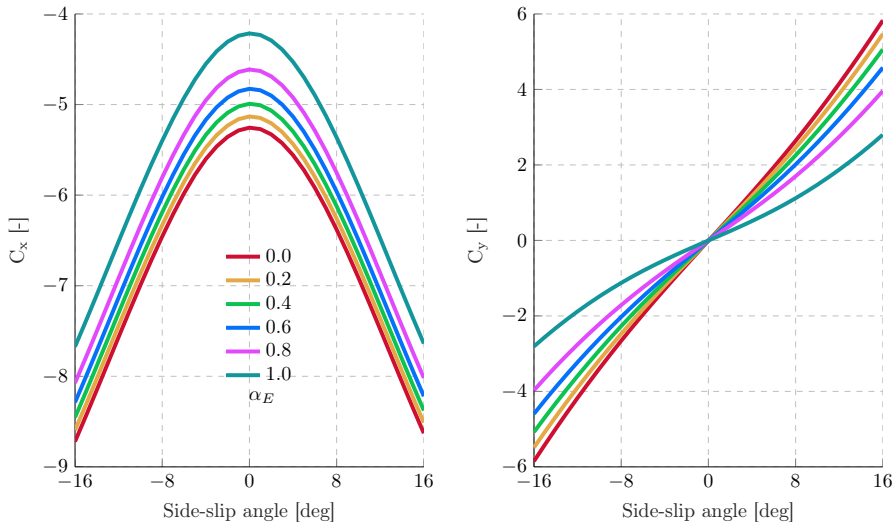


Figure 4.20: Aerodynamic coefficients in the satellite reference frame as function of the side-slip angle and energy accommodation coefficient for the GOCE satellite.

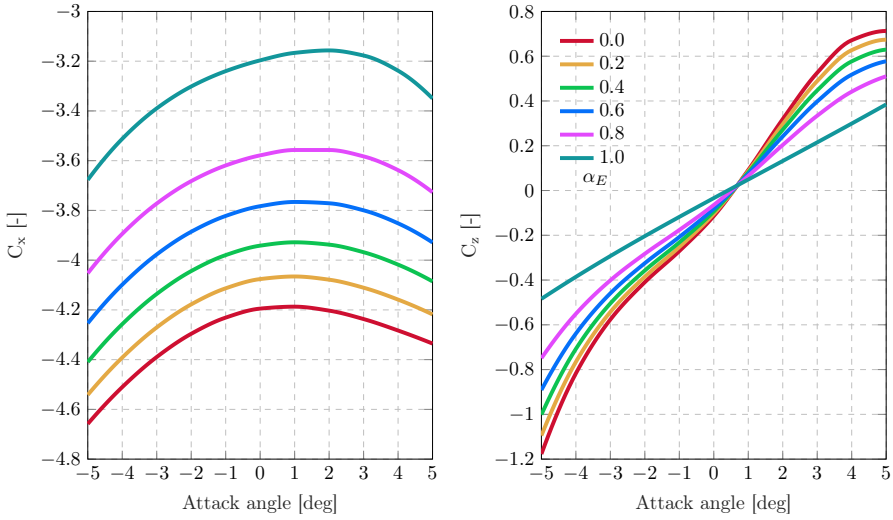


Figure 4.21: Aerodynamic coefficients in the satellite reference frame as function of the attack angle and energy accommodation coefficient for the Swarm satellites.

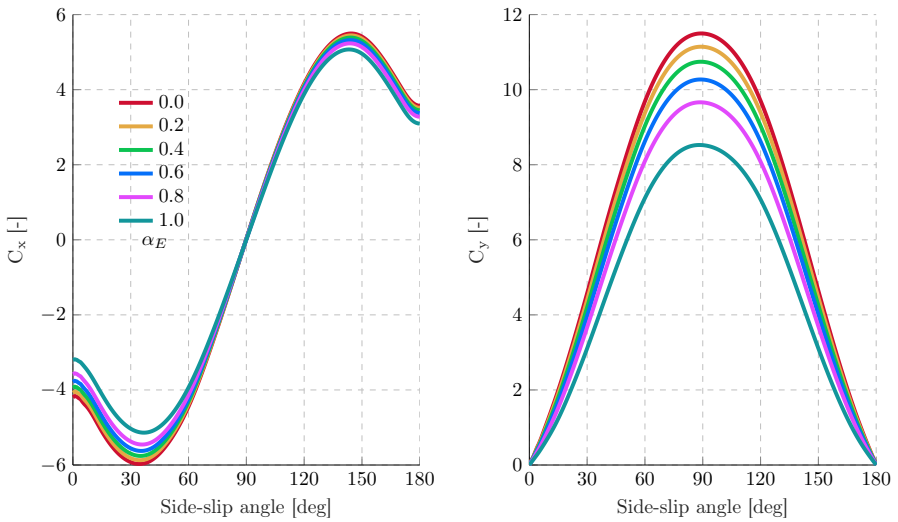


Figure 4.22: Aerodynamic coefficients in the satellite reference frame as function of the side-slip angle (between 0° and 360°) and energy accommodation coefficient for the Swarm satellites.

## 4.9. APPENDIX-B: SPEED RATIO INFLUENCE OVER SATELLITE AERODYNAMICS

The following figures show that an attitude variation affects the sensitivity of the aerodynamic forces to the speed ratio and energy accommodation coefficient. For low values of speed ratio (i.e. below 4) the force coefficients reach high magnitudes. Moreover, the force coefficients converge for very low speed ratios ( $s < 2$ ), i.e. the drag coefficient is then less sensitive to the energy accommodation coefficient. The drag coefficient approaches a constant value towards higher speed ratios. However, due to the different collisions the convergence can vary depending on the satellite attitude. For GOCE, the Z-component is not included because of the symmetric shape of the satellite with respect to the X–Y plane.

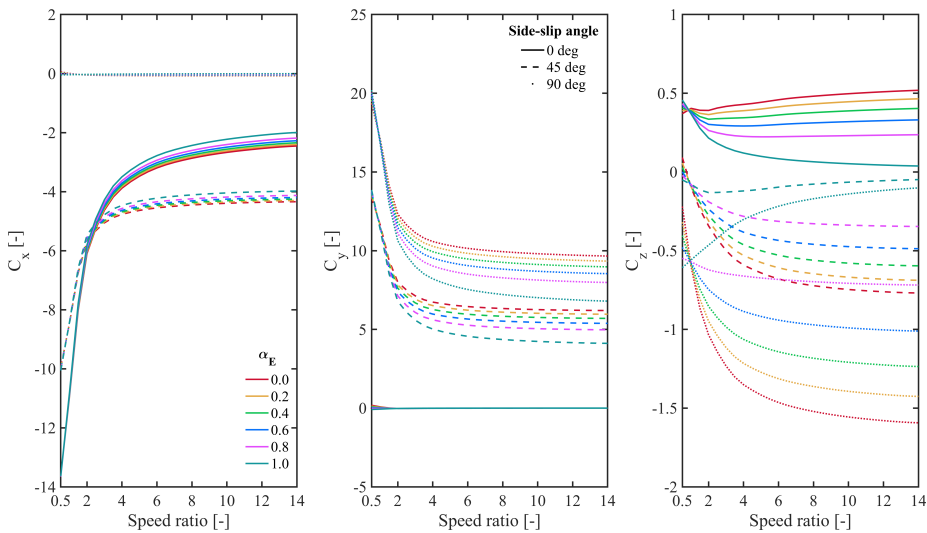


Figure 4.23: Aerodynamic coefficients in the satellite reference frame as function of the speed ratio and energy accommodation coefficient for the CHAMP satellite for fixed side-slip angles.

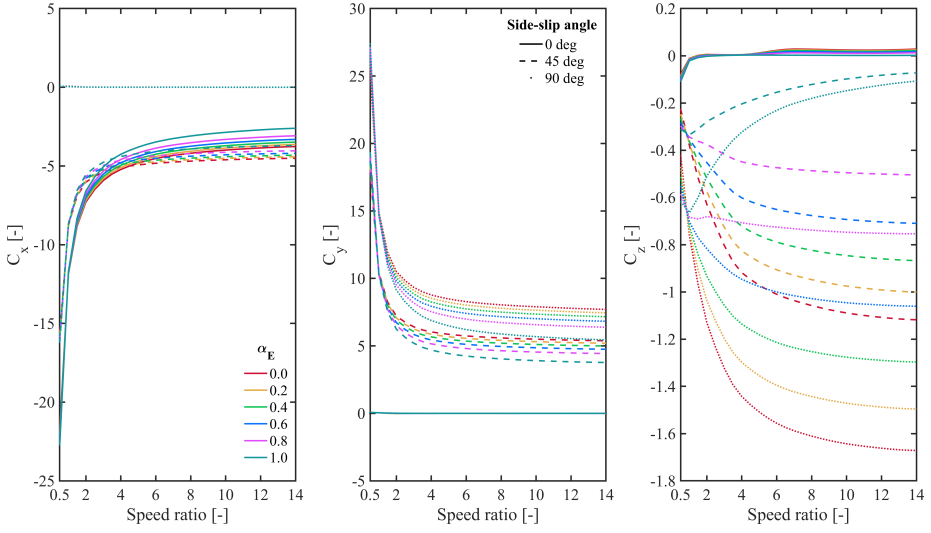


Figure 4.24: Aerodynamic coefficients in the satellite reference frame as function of the speed ratio and energy accommodation coefficient for the GRACE satellite for fixed side-slip angles.

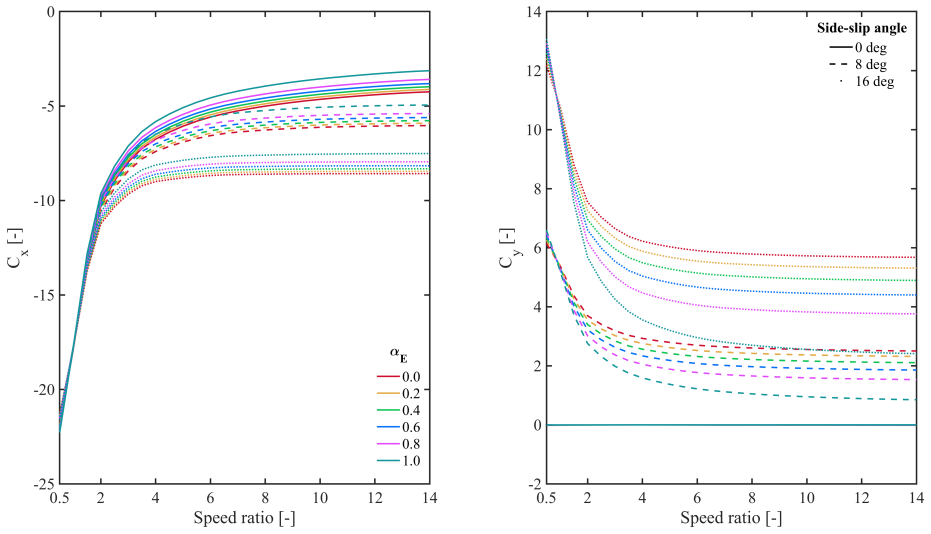


Figure 4.25: Aerodynamic coefficients in the satellite reference frame as function of the speed ratio and energy accommodation coefficient for the GOCE satellite for fixed side-slip angles.

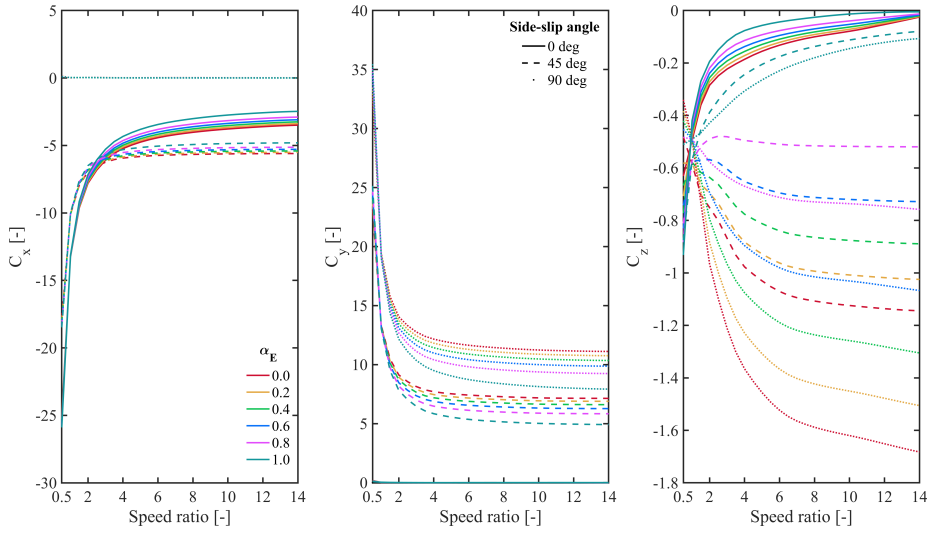


Figure 4.26: Aerodynamic coefficients in the satellite reference frame as function of the speed ratio and energy accommodation coefficient for the Swarm satellites for fixed side-slip angles.

## 4.10. APPENDIX-C: NEWLY GENERATED DENSITY DATA SETS

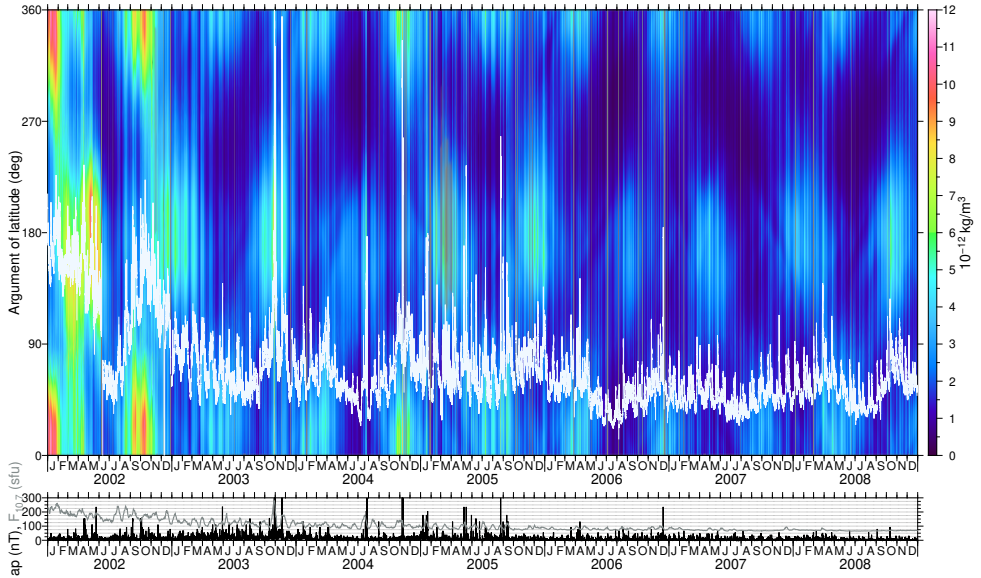


Figure 4.27: Newly generated density for the CHAMP satellite between 2002-01-01 and 2009-01-01. The white line shows the orbit mean density.

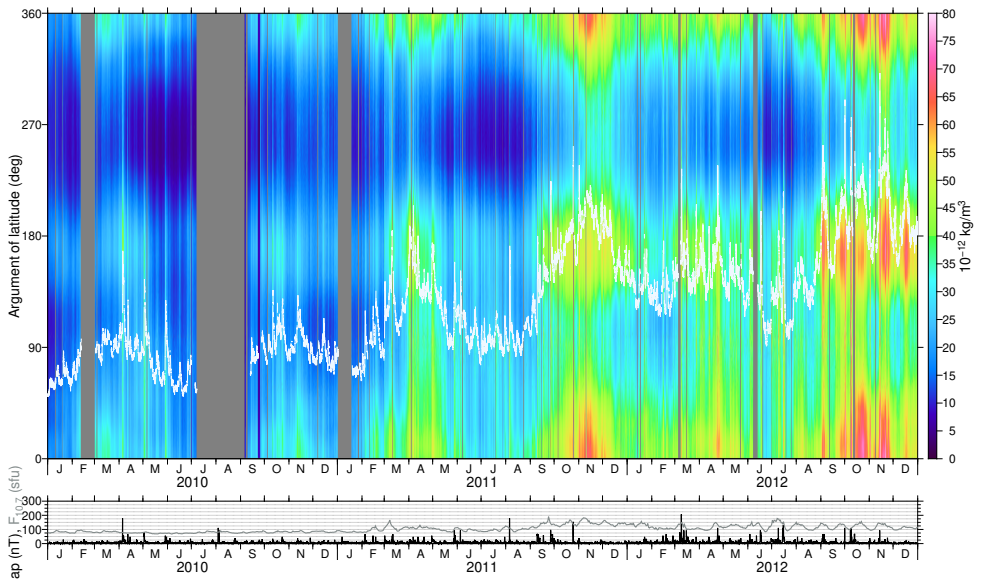


Figure 4.28: Newly generated density for the GOCE satellite between 2010-01-01 and 2013-01-01. The white line shows the orbit mean density.

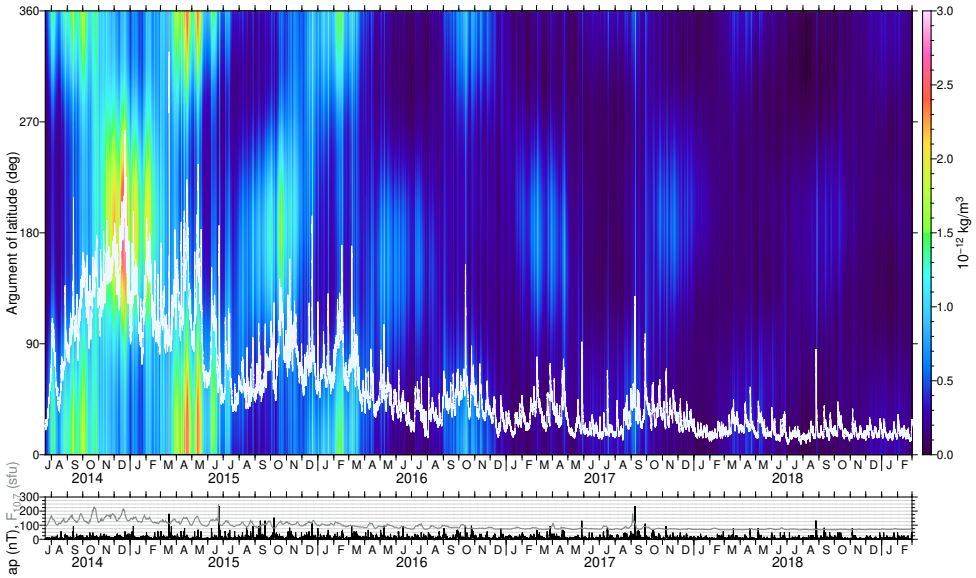


Figure 4.29: Newly generated density for the Swarm-A satellite between 2014-07-20 and 2019-03-01. The white line shows the orbit mean density.

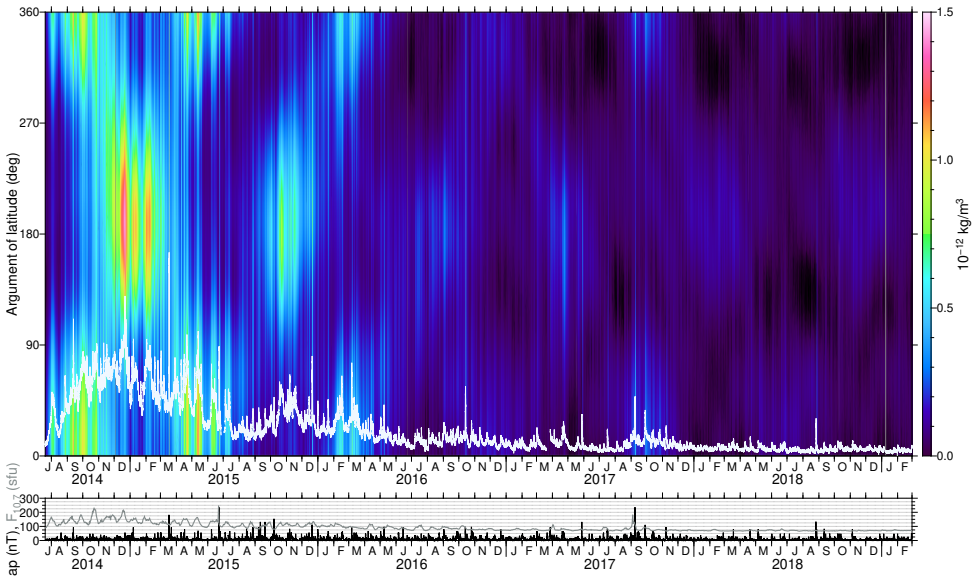


Figure 4.30: Newly generated density for the Swarm-B satellite between 2014-07-20 and 2019-03-01. The white line shows the orbit mean density.



# 5

## CONCLUSION

The previous Chapters 2, 3 and 4 already provided preliminary conclusions on their specific content. In this chapter a general overview of conclusions is presented together with recommendations for follow-on research. Section 5.1 provides answers to the research questions posed at the beginning of this dissertation. Next, in Section 5.2, the new thermospheric data sets are addressed together with their possible applications. Finally, ideas for further work are offered in Section 5.3 with a detailed list of recommendations.

### 5.1. RESEARCH QUESTIONS AND GOAL

Following the structure of the dissertation, the research questions have been addressed and mainly answered in Chapters 2, 3 and 4. In this section all previous conclusions are combined.

#### 5.1.1. QUESTION 1

*What is the influence of high-fidelity geometry inputs on satellite aerodynamics and the derivation of neutral thermospheric density?*

The effects of high-fidelity geometries on satellite aerodynamics and density products have been analyzed and quantified. This coincided with the required study to answer the first research question posed in Section 1.5. In the study presented in Chapter 2, the high-fidelity surfaces, designed using technical drawings and pre-launch photographs, raised the accuracy level of the geometry modelling. Physics-based drag coefficients were obtained with the use of a DSMC simulator, and a quantitative analysis on the improvements with respect to the previous approaches resulted in new thermospheric density data sets. The new data are in better agreement with the empirical models and results reached a higher level of consistency among different missions over long periods, and within short time intervals analyzing single missions. Indeed, analyzing manoeuvres, densities in short time periods turned out to be more consistent. From

density discrepancies of around 40%, the new densities reached a variability down to 1–2% within short time periods. The newly derived densities turned out to be higher in magnitude than the previous generation based on simple panel models. Indeed, differences of +11% for CHAMP, +5% for GRACE, +9% for GOCE and +32% for Swarm have been detected. These values showed high correlation between differences and satellite geometry complexity. Simpler geometries, like the one for GRACE, indeed had smaller differences with respect to other complex satellites (e.g. Swarm and CHAMP).

Therefore, concerning the first primary question of Section 1.5, it can be concluded that the geometry fidelity level has a large influence on aerodynamics and derivation of density. The enhanced geometry models provide a great improvement in the consistency of density data with also a better agreement with the empirical models. The implementation of new geometries were used to determine density scale factors, which were applied to an intermediate version of the official Swarm data. These data were based on ideal gas-surface interactions assumptions and needed a further development. More realistic gas-surface interactions are described in Chapters 3 and 4.

## 5

### 5.1.2. QUESTION 2

*What are the enhanced gas-surface interactions parameters which allow for more consistent thermospheric data products?*

Once the geometry modelling was implemented in the thermospheric products generation, it was necessary to improve the description of the gas-surface interactions. This research was covered by the studies presented in Chapters 3 and 4. The associated investigations focused on finding enhanced gas-surface interactions parameters which allow for more consistent thermospheric data products. In Chapter 3, the study included neutral wind estimations using accelerometer-derived measurements from the CHAMP and GOCE satellites selecting a single value of the energy accommodation coefficient  $\alpha_E$  from the full range of possible gas-surface interactions parameters. An overview of the influence of different accommodation coefficients on the consistency of thermospheric wind was shown. The combination with the high-fidelity geometries previously designed helped to improve the accuracy level of wind estimations. A diffusive reflection mode with incomplete accommodation was introduced to replace the previous fully accommodated condition ( $\alpha_E = 1$ ) used in Chapter 2. Analyzing seasonal variations and particular attitude manoeuvres, it was possible to achieve a higher level of self-consistency in the wind data. This was the result of introducing a lower energy accommodation coefficient with respect to the commonly adopted value of 0.93. Indeed, this analysis provided optimal  $\alpha_E$  values of 0.85 and 0.82 for the CHAMP and GOCE thermospheric products, respectively. This mainly produced more accurate and consistent data with a decrease of wind magnitude for both missions.

In Chapter 4, the same research question was addressed studying the gas-surface interactions influence on the aerodynamics and density modelling. For this study the CHAMP, GOCE and Swarm satellites were reintroduced. This chapter described the new data sets for satellite aerodynamics and density. This was possible due to the selection of a single energy accommodation coefficient for all the selected missions. An overview

of the effects of different gas-surface interactions modes was provided for the selected missions. Once again, the originally and currently adopted  $\alpha_E$  value of 0.93 turned out to be higher than the new values that were found to be more optimal in this chapter. A value of 0.85 for Swarm-A and -C satellites is now recommended based on the investigation on the attitude manoeuvres in May 2014. Indeed, aiming for identical density values between the two satellite measurements, it was possible to find a more accurate value of the energy accommodation coefficient between 0.80 and 0.90 with an average value of 0.85. This is in agreement with the previous wind analysis for CHAMP and GOCE (Chapter 3). Following these results, the new density values are lower in magnitude than the previous generation introduced in Chapter 2. The magnitude with respect to the products with  $\alpha_E=0.93$  is around 5% lower. Density ratios with respect to atmospheric model densities decrease with a lower accommodation coefficient. However, comparing the ratios among the selected missions and the NRLMSISE-00 atmospheric model, the variability is now limited to 3% of variation within the selected missions. This variability was around 8% for the intermediate results before improving the gas-surface interactions modelling. Therefore, a further improvement was achieved with the new values for the  $\alpha_E$  coefficients.

### 5.1.3. GOAL

*The goal of this dissertation is to improve estimates of aerodynamic parameters and assess the quality of accelerations-derived thermospheric density and wind data, by introducing high-fidelity geometry and aerodynamic information with a special focus on the gas-surface interactions.*

With this work, a detailed description of the satellite aerodynamics is now available. This was possible because of the introduction of the new high-fidelity geometries and the capability to model different collision modes for the atmospheric particles hitting the satellite. As shown in this dissertation the gas-surface interactions can be investigated in an indirect way, exploiting the data from satellite constellations, manoeuvres and seasonal cycles. Enhancements can be reached with such analyses to improve thermospheric products consistency. This enabled addressing all the research questions and achieving the overarching goal of this dissertation. As an outcome of this research, new and more consistent thermospheric data sets were produced. The developed algorithms can be applied to any LEO satellite with accelerometers and/or GPS instrumentation.

## 5.2. THE NEWLY DERIVED THERMOSPHERIC DATA SETS

New thermospheric density and wind data sets based on the high-fidelity geometries and new energy accommodation coefficients were generated and can be downloaded at <http://thermosphere.tudelft.nl>. On this website, further information on the aerodynamic data sets and geometry models for the CHAMP, GRACE, GOCE and Swarm satellites are now publicly accessible (status May 2020).

The retrieved information will enhance the existent and new atmospheric models and provide an improved knowledge of the atmosphere dynamics. The previous density bias differences between different satellite missions are now reduced and this allows for

working on multiple data sets providing the possibility to compare and combine consistent information. This aspect is particularly useful when combining data from simultaneously flying missions. Using the new derived products, thermospheric analyses will benefit from a minimal bias difference. A similar enhancement can be obtained for studies of long term change in the thermosphere-ionosphere region. Spanning several solar cycles requires data from multiple missions and reduced inter-missions density scale inconsistencies are going to improve current models. Unbiased data sets are also required when studying coupling between different systems like the thermosphere-ionosphere-magnetosphere; for example, the density scale needs to be unbiased to compute the influence of heating currents on the magnetosphere-ionosphere system. Therefore, the presented data are going to help clarifying also the effects between different couplings of atmosphere and magnetosphere regions.

Introducing more practical applications, the decoupling of the absolute scale of the thermosphere density and physical drag coefficients modelling are important for drag analyses following a reverse approach. In the design of new missions and manoeuvres planning, satellite drag estimations are indeed crucial for reducing the uncertainties in predicted lifetime and fuel consumption.

The new data are also excellent inputs for data assimilation in the physics-based models. The multiple solar and geomagnetic conditions in the investigated years are indeed fully representing all possible atmospheric scenarios. This allows for a deep characterization of thermospheric density and winds.

5

### 5.3. OUTLOOK FOR FUTURE RESEARCH

The research described in this dissertation resulted in more consistent thermospheric density and wind data sets for several satellites. It is however expected that further enhancements are possible by future research and new satellite missions. Open issues that arose from the dissertation introduce the following suggested tasks. The listed points include recommendations on how further improvements can be achieved and how the open issues can be further addressed.

- **Provide an improved macro model based on new high-fidelity geometries.**

The performed research was based on the combination of high-fidelity geometries with a DSMC rarefied gas-dynamic solver. The computational cost for performing the large number of simulations was relatively high. Therefore, for preliminary and quick analyses, it would be recommended to update the original macro models with the information gained with the new detailed surfaces. Applying analytic solutions to the new macro models would not reach the fidelity level described in this research, but would be an improvement of the past panel models applied to the macro geometries, which require a low computational cost and are commonly used by the scientific community. This will be beneficial especially for satellites with complex and elongated shapes.

- **Develop a new Solar Radiation Pressure (SRP) modelling with the new high-fidelity geometry information.**

Missions like GRACE and Swarm would highly benefit from this new SRP model. Indeed, at relatively high altitudes ( $> 500$  km) and in low solar activity periods, the accelerations due to the solar radiation pressure are comparable in magnitude with the aerodynamic contribution (Figures 5.1 and 5.2). This is especially visible in Fig. 5.2 for the Swarm-B satellite which flies about 50 km higher than Swarm-A and -C.

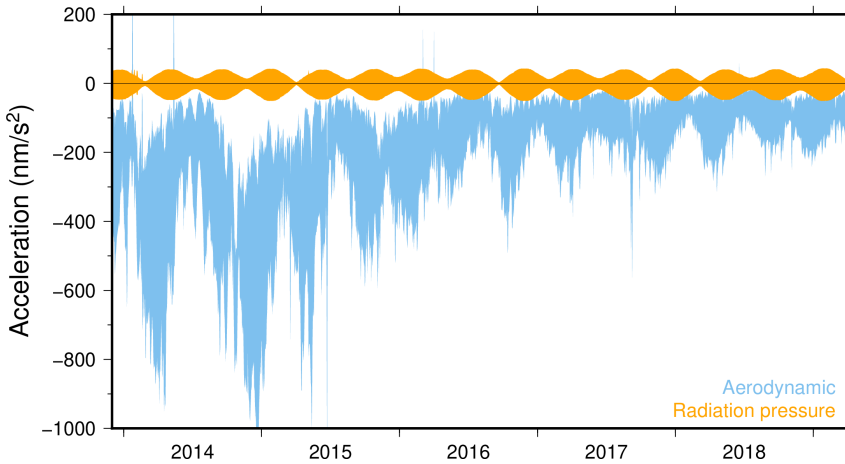


Figure 5.1: Time series of modelled aerodynamic and solar radiation pressure accelerations for Swarm-A (*van den IJssel et al., 2020*).

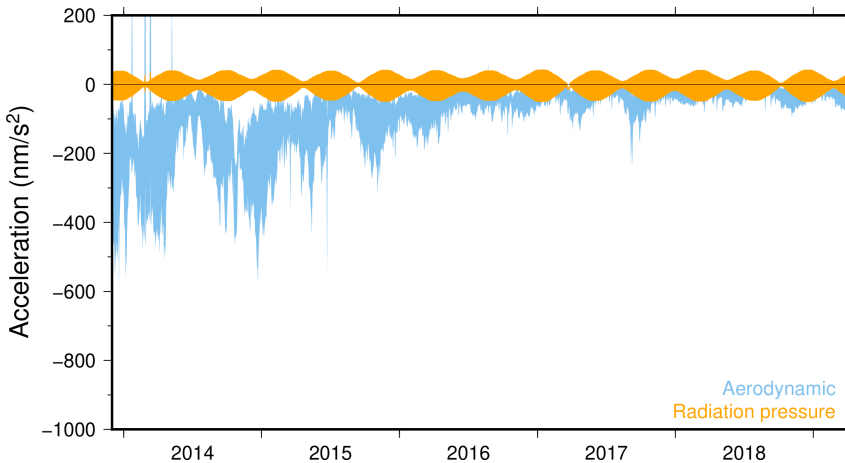


Figure 5.2: Time series of modelled aerodynamic and solar radiation pressure accelerations for Swarm-B (*van den IJssel et al., 2020*).

Moreover, the SRP modeling for high altitude and low solar activity is the predominant error source in density and wind retrieval (*van den IJssel et al., 2020*). Improved solar radiation satellite force models can be generated based on the new detailed satellite surfaces. Accelerations due to the direct solar radiation can be easily modeled. Additional contributions from albedo and infrared emissions can be also introduced. Such an approach would fully exploit the high-fidelity geometries, with an accurate description of shadowing and surface areas. A validation with simple geometries (e.g. spheres, cubes) will be necessary, afterwards further implementations in the processing software will be also required to generate new products from the CHAMP, GRACE, GOCE and Swarm satellites.

- **Provide a detailed uncertainty quantification for density and wind.**

A detailed quantification of the overall modelling uncertainties needs to be defined for a better understanding of the quality of derived density and wind. This process also involves the uncertainty in inputs regarding atmospheric chemical compositions, temperatures and solar flux and geomagnetic indexes, which are so far based on empirical models and ground or space observations. Improving the current solar radiation pressure modelling would allow for a detailed uncertainty estimation, which is suggested to be performed together with the SRP modelling enhancement. In particular, it is recommended to analyze the variations in density and winds within a range of the  $F_{10.7}$  input values and within a specific percentage of difference from the molar masses obtained with the NRLMSISE-00 model.

- **Attitude manoeuvres and variable energy accommodation coefficient analyses.**

Unluckily, only a few suitable manoeuvres for Swarm and CHAMP missions can be fully exploited. In order to provide significant extra information, these manoeuvres need to have long periods between thruster activations. This helps in providing data without big gaps due to thruster accelerations. Therefore, the estimated density and winds within multiple orbits can potentially provide useful information for comparisons between data with the same attitude orientation and time windows. In this research the analyzed periods were characterized by high solar activity. This provided high quality measurements because the drag signal is strong during such periods. It would be extremely useful to study similar manoeuvres in solar minimum conditions. However, this could be challenging because, for example, instead of 1–2% in density differences between Swarm-A and -C measurements, with the current low solar activity the estimated densities can differ up to 50%. It would be valuable if these manoeuvres could be repeated once or twice a year. This will help to validate and provide more data for GSI investigations. If accelerometers with higher precision will be adopted in future missions, it will be interesting to investigate the solar activity influence on the energy accommodation coefficient. For the presented study the energy accommodation coefficient is fixed to a specific value for the complete duration of each mission. This approach has been widely used for density and wind data sets together with a simplified geometry modelling. However, this assumption might create alterations in the thermospheric products for periods far from the conditions for which optimal values are retrieved. Studying the influence of

different solar activity conditions would provide a further enhancement of the presented data sets.

- **GRACE and GRACE-FO (re)processing.**

Many scientists are interested in the reprocessing of the GRACE density data with the application of high-fidelity models and improved GSI assumptions. This could also include the second part of the mission (after 2009), which contains many anomalies due to the batteries deterioration which affected the temperature and the on-board accelerometers. New geometry and GSI modelling can be applied together with the new accelerometer calibration parameters provided via private communication from the Centre National d'Etudes Spatiales (CNES, France) in order to process new density products. With these new parameters it is possible to process the data until the end of 2016. Currently, at TU Delft the calibration parameters are only available until the end of 2009. GRACE-FO would require a new geometry model and the density data set and the aerodynamic model generation can be based on the SPARTA simulator. The developed expertise from this research can be easily applied to this task.

- **New dedicated missions with accelerometers and mass spectrometers.**

Current uncertainties in the local chemistry of the atmosphere are mainly associated to the errors in the empirical models. Within this dissertation the NRLMSISE-00 model was used to generate the inputs in mass composition for the main atmospheric species. If on-board measurements about species concentrations would be available, this would benefit the scientific studies on thermospheric density and winds. The combination of mass spectrometers with accelerometers would be highly preferred instead of having only a mass spectrometer. The state of the art in the accelerometer processing is highly developed and provides a solid base for density and wind processing. Additional information based on spectrometry would provide the complementary information to highly enhance current thermospheric estimations. This coincides with the opportunity provided by the Daedalus Earth Explorer candidate mission (*Sarris et al., 2019*). Indeed, this mission will be equipped with a mass spectrometer in combination with an accelerometer. The very low altitudes ( $\leq 150$  km) which are planned to be investigated along an elliptical orbit with an apogee between 2000–3000 km can further cover unexplored altitudes. This will create a great opportunity for improving current density and wind models. Beyond on-board instrumentation, it is always recommended to exploit the data from multiple satellites covering multiple local times and altitudes. Therefore, a constellation of two or three (or more) satellites is highly recommended instead of a single-satellite mission.



## REFERENCES

- Astafyeva, E., I. Zakharenkova, J. D. Huba, E. Doornbos, and J. van den IJssel (2017), Global Ionospheric and Thermospheric Effects of the June 2015 Geomagnetic Disturbances: Multi-Instrumental Observations and Modeling, *Journal of Geophysical Research: Space Physics*, 122(11), doi:10.1002/2017JA024174.
- Bettadpur, S. V. (2007), Gravity Recovery and Climate Experiment Product Specification Document (Rev 4.5 – February 20, 2007), *Tech. Rep. GRACE 327-720/CSR-GR-03-02*, Center for Space Research, The University of Texas at Austin.
- Bettadpur, S. V. (2012), GRACE Product Specification Document, *Tech. Rep. GRACE 327-720 (CSR-GR-03-02)*, Center for Space Research, The University of Texas at Austin.
- Bird, G. A. (1994), *Molecular Gas Dynamics and the Direct Simulation of Gas Flows*, vol. 42, 458 pp., Oxford Science Publications, ISBN: 9780198561958.
- Bowman, B., F. Marcos, K. Moe, and M. Moe (2007), Determination of drag coefficient values for CHAMP and GRACE satellites using orbit drag analysis, in *Astrodynamics Specialist Conference, American Astronomical Society, 19–23 August 2007*, Mackinac Island, Michigan.
- Bowman, B., W. K. Tobiska, F. Marcos, C. Huang, C. Lin, and W. Burke (2008), A new empirical thermospheric density model JB-2008 using new solar and geomagnetic indices, in *AIAA/AAS Astrodynamics Specialist Conference and Exhibit, Guidance, Navigation, and Control and Co-located Conferences*, Honolulu, Hawaii.
- Bruinsma, S. (2015), The DTM-2013 thermosphere model, *Journal of Space Weather and Space Climate*, 5(A1), doi:10.1051/swsc/2015001.
- Bruinsma, S., and R. Biancale (2003), Total Densities Derived from Accelerometer Data, *Journal of Spacecraft and Rockets*, 40(2), 230–236, doi:10.2514/2.3937.
- Bruinsma, S., D. Tamagnan, and R. Biancale (2004), Atmospheric densities derived from CHAMP/STAR accelerometer observations, *Planetary and Space Science*, 52(4), 297–312, doi:10.1016/j.pss.2003.11.004.
- Bruinsma, S., J. M. Forbes, R. S. Nerem, and X. Zhang (2006), Thermosphere density response to the 20–21 november 2003 solar and geomagnetic storm from CHAMP and GRACE accelerometer data, *Journal of Geophysical Research: Space Physics*, 111(A6), doi:10.1029/2005JA011284.
- Burke, W. J., C. S. Lin, M. P. Hagan, C. Y. Huang, D. R. Weimer, J. O. Wise, L. C. Gentile, and F. A. Marcos (2009), Storm time global thermosphere: A driven-dissipative

- thermodynamic system, *Journal of Geophysical Research: Space Physics*, 114(A6), doi: 10.1029/2008JA013848.
- Cercignani, C., and M. Lampis (1971), Kinetic models for gas-surface interactions, *Transport Theory and Statistical Physics*, 1(2), 101–114, doi:10.1080/00411457108231440.
- Cometto, F. (2007), GOCE models data bank document (DCG No.: EN-18 April 30, 2007), GO-TN-AI-0081, *Tech. rep.*, Alcatel Alenia Space.
- Davis, D. (1960), Monte Carlo calculation of molecular flow rates through a cylindrical elbow and pipes of other shapes, *Journal of Applied Physics*, 30, 69–76.
- Dhadly, M., J. Emmert, D. Drob, M. Conde, E. Doornbos, G. Shepherd, J. Makela, Q. Wu, R. Niciejewski, and A. Ridley (2017), Seasonal dependence of northern high-latitude upper thermospheric winds: A quiet time climatological study based on ground-based and space-based measurements, *Journal of Geophysical Research: Space Physics*, 122(2), 2619–2644, doi:10.1002/2016JA023688.
- Dhadly, M. S., J. T. Emmert, D. P. Drob, M. G. Conde, E. Doornbos, G. G. Shepherd, J. J. Makela, Q. Wu, R. J. Niciejewski, and A. J. Ridley (2018), Seasonal dependence of geomagnetic active-time northern high-latitude upper thermospheric winds, *Journal of Geophysical Research: Space Physics*, 123(1), 739–754, doi:10.1002/2017JA024715.
- Doornbos, E. (2006), NRTDM Final Report - Near Real-Time Density Model (NRTDM) - ESOC contract 18576/04/D/HK(SC), *Tech. rep.*, Delft Institute for Earth-Oriented Space Research.
- Doornbos, E. (2011), Thermospheric Density and Wind Determination From Satellite Dynamics, Ph.D. thesis, Delft University of Technology, ISBN: 978-90-9026051-8.
- Doornbos, E., M. Foerster, B. Fritsche, T. van Helleputte, J. van den IJssel, G. Koppenwallner, H. Lühr, D. Rees, and P. Visser (2009), Air density models derived from multi-satellite drag observations - Final Report, *Tech. Rep. ESTEC contract 21022/07/NL/HE*, DEOS/TU Delft scientific report 01/2009.
- Doornbos, E., J. van den IJssel, H. Lühr, M. Foerster, G. Koppenwallner, S. Bruinsma, E. Sutton, J. M. Forbes, F. Marcos, and F. Perosanz (2010), Neutral Density and Cross-wind Determination from Arbitrarily Oriented Multiaxis Accelerometers on Satellites, *Journal of Spacecraft and Rockets*, 47, 580–589, doi:10.2514/1.48114.
- Doornbos, E., S. Bruinsma, B. Fritsche, G. Koppenwallner, P. Visser, J. van den IJssel, and J. Teixeira da Encarnação (2014), GOCE+ Theme 3: Air density and wind retrieval using GOCE data Final report, *Technical Report*, , doi: 10.1016/S0278-6915(82)80248-2.
- Doornbos, E., J. van den IJssel, and E. Iorfida (2017), GPS-derived density data for the Swarm satellites during the declining phase of the solar cycle, Banff, Canada, fourth Swarm Science Meeting and Geodetic Missions Workshop.

- Dow, J., R. Neilan, and G. Gendt (2005), The international GPS Service: Celebrating the 10th anniversary and looking to the next decade, *Advances in Space Research*, 36(3), 320–326, doi:<https://doi.org/10.1016/j.asr.2005.05.125>.
- Drob, D. P., J. T. Emmert, G. Crowley, J. M. Picone, G. G. Shepherd, W. Skinner, P. Hays, R. J. Niciejewski, M. Larsen, C. Y. She, J. W. Meriwether, G. Hernandez, M. J. Jarvis, D. P. Sipler, C. A. Tepley, M. S. O'Brien, J. R. Bowman, Q. Wu, Y. Murayama, S. Kawamura, I. M. Reid, and R. A. Vincent (2008), An empirical model of the Earth's horizontal wind fields: HWM07, *Journal of Geophysical Research: Space Physics*, doi:10.1029/2008JA013668.
- Drob, D. P., J. T. Emmert, J. W. Meriwether, J. J. Makela, E. Doornbos, M. Conde, G. Hernandez, J. Noto, K. A. Zawdie, S. E. McDonald, J. D. Huba, and J. H. Klenzing (2015), An update to the horizontal wind model (HWM): The quiet time thermosphere, *Earth and Space Science*, 2(7), 301–319, doi:10.1002/2014EA000089.
- Emmert, J. (2015), Thermospheric mass density: A review, *Advances in Space Research*, 56(5), doi:10.1016/j.asr.2015.05.038.
- Emmert, J. T. (2009), A long-term data set of globally averaged thermospheric total mass density, *Journal of Geophysical Research: Space Physics*, 114(6), doi:10.1029/2009JA014102.
- Emmert, J. T., J. M. Picone, and R. R. Meier (2008), Thermospheric global average density trends, 1967–2007, derived from orbits of 5000 near-earth objects, *Geophysical Research Letters*, 35(5), doi:10.1029/2007GL032809.
- Floberghagen, R., M. Fehringer, D. Lamarre, D. Muzi, B. Frommknecht, C. Steiger, J. Piñeiro, and A. da Costa (2011), Mission design, operation and exploitation of the Gravity field and steady-state Ocean Circulation Explorer mission, *Journal of Geodesy*, 85(11), 749–758, doi:10.1007/s00190-011-0498-3.
- Flury, J., S. Bettadpur, and B. D. Tapley (2008), Precise accelerometry onboard the GRACE gravity field satellite mission, *Advances in Space Research*, 42(8), 1414–1423, doi:10.1016/j.asr.2008.05.004.
- Forbes, J. M., S. Bruinsma, X. Zhang, and J. Oberheide (2009), Surface-exosphere coupling due to thermal tides, *Geophysical Research Letters*, 36(15), doi:10.1029/2009GL038748.
- Gallis, M. A., J. R. Torczynski, S. J. Plimpton, D. J. Rader, and T. Koehler (2014), Direct Simulation Monte Carlo: The quest for speed, *AIP Conference Proceedings*, 1628, 27–36, doi:10.1063/1.4902571.
- Gasperini, F., J. M. Forbes, E. N. Doornbos, and S. L. Bruinsma (2016), Synthetic thermosphere winds based on champ neutral and plasma density measurements, *Journal of Geophysical Research: Space Physics*, 121(4), 3699–3721, doi:10.1002/2016JA022392.

- Gini, F., M. Otten, T. Springer, W. Enderle, S. Lemmens, and T. Flohrer (2015), Precise Orbit Determination of the GOCE Re-Entry Phase, in *5th International GOCE User Workshop, ESA Special Publication*, vol. 728, p. 21.
- Gregory, J. C., and P. N. Peters (1987), A measurement of the angular distribution of 5 eV atomic oxygen scattered off a solid surface in earth orbit, in *Proceedings of the 15th international symposium on rarefied gas dynamics*, vol. 1, edited by V. Boffi and C. Cercignani, pp. 644–656, B.G. Teubner, Stuttgart, ISBN: 3519026236 9783519026235.
- Hammond, R. (2006), Satellite External Layout - DT0217691, *Tech. rep.*, ASTRIUM.
- Harding, B. J., J. J. Makela, J. Qin, D. J. Fisher, C. R. Martinis, J. Noto, and C. M. Wrasse (2017), Atmospheric scattering effects on ground-based measurements of thermospheric vertical wind, horizontal wind, and temperature, *Journal of Geophysical Research: Space Physics*, 122(7), 7654–7669, doi:10.1002/2017JA023942.
- Harris, I., and W. Priester (1962), Time-dependent structure of the upper atmosphere, *Journal of Atmospheric Science*, 19(4), 286–301, doi:10.1175/1520-0469(1962)019%3C0286%3ATDSOTU%3E2.0.CO;2.
- Hedin, A. E., B. B. Hinton, and G. A. Schmitt (1973), Role of gas-surface interactions in the reduction of OGO 6 neutral particle mass spectrometer data, *Journal of Geophysical Research*, 78(22), 4651–4668, doi:10.1029/JA078i022p04651.
- Hele, D. G. K., and H. S. W. Massey (1959), Analysis of the orbits of the Russian satellites, *Proceedings of the Royal Society of London. Series A. Mathematical and Physical Sciences*, 253(1275), 529–538, doi:10.1098/rspa.1959.0218.
- Hele, D. G. K., and D. M. C. Walker (1958), An irregularity in the atmospheric drag effects on Sputniks 2 and 3 (Satellites 1957 $\beta$ , 1958 $\delta$ 1 and 1958 $\delta$ 2), *Nature*, 182, doi:10.1038/182860a0.
- Hess, C. (2001), GR00-00000A00A GRACE S/C Flight Configuration, *Tech. rep.*, Astrium GmbH.
- Huang, T., H. Lühr, H. Wang, and C. Xiong (2017), The relationship of high-latitude thermospheric wind with ionospheric horizontal current, as observed by champ satellite, *Journal of Geophysical Research: Space Physics*, 122(12), 12,378–12,392, doi: 10.1002/2017JA024614.
- Jacchia, L. G. (1965), Static Diffusion Models of the Upper Atmosphere with Empirical Temperature Profiles, *Smithsonian Contributions to Astrophysics*, 8, 215.
- Klinger, B., and T. Mayer-Gürr (2016), The role of accelerometer data calibration within GRACE gravity field recovery: Results from ITSG-Grace2016, *Advances in Space Research*, 58(9), 1597 – 1609, <https://doi.org/10.1016/j.asr.2016.08.007>.
- Koppenwallner, G. (2009), Energy accommodation coefficient and momentum transfer modeling, *Tech. Rep. HTG-TN-08-11*, HTG, Katlenburg Lindau.

- Kornfeld, R. P., B. W. Arnold, M. A. Gross, N. T. Dahya, W. M. Klipstein, P. F. Gath, and S. Bettadpur (2019), Grace-fo: The gravity recovery and climate experiment follow-on mission, *Journal of Spacecraft and Rockets*, 56(3), 931–951, doi:10.2514/1.A34326.
- Lambert, J. (1892), *Lamberts Photometrie: Photometria, sive De mensura et gradibus luminis, colorum et umbrae*, W. Engelmann.
- Liu, H., H. Lühr, S. Watanabe, W. Köhler, V. Henize, and P. Visser (2006), Zonal winds in the equatorial upper thermosphere: Decomposing the solar flux, geomagnetic activity, and seasonal dependencies, *Journal of Geophysical Research*, 111, doi:10.1029/2005JA011415.
- Liu, H., H. Lühr, and S. Watanabe (2009), A solar terminator wave in thermospheric wind and density simultaneously observed by CHAMP, *Geophysical Research Letters*, 36, doi:10.1029/2009GL038165.
- Liu, H., E. Doornbos, and J. Nakashima (2016), Thermospheric wind observed by GOCE: wind jets and seasonal variations: Thermospheric winds in lower F-region, *Journal of Geophysical Research: Space Physics*, pp. 6901–6913, doi: 10.1002/2016JA022938.
- Liu, H., C. G. Bardeen, B. T. Foster, P. Lauritzen, J. Liu, G. Lu, D. R. Marsh, A. Maute, J. M. McInerney, N. M. Pedatella, L. Qian, A. D. Richmond, R. G. Roble, S. C. Solomon, F. M. Vitt, and W. Wang (2018), Development and validation of the whole atmosphere community climate model with thermosphere and ionosphere extension (WACCM-X 2.0), *Journal of Advances in Modeling Earth Systems*, 10(2), 381–402, doi:10.1002/2017MS001232.
- Liu, H.-L., B. T. Foster, M. E. Hagan, J. M. McInerney, A. Maute, L. Qian, A. D. Richmond, R. G. Roble, S. C. Solomon, R. R. Garcia, D. Kinnison, D. R. Marsh, A. K. Smith, J. Richter, F. Sassi, and J. Oberheide (2010), Thermosphere extension of the whole atmosphere community climate model, *Journal of Geophysical Research: Space Physics*, 115(A12), doi:10.1029/2010JA015586.
- Lühr, H. (2000), CH-IT-DID-0001 - Personal Communication, *Tech. rep.*, Daimler-Benz Aerospace.
- Lühr, H. (2002), CHAMP reference systems, transformations and standards, *Tech. Rep. CH-GFZ-RS-002*.
- Lühr, H., K. Häusler, and C. Stolle (2007a), Longitudinal variation of F region electron density and thermospheric zonal wind caused by atmospheric tides, *Geophysical Research Letters*, 34, doi:10.1029/2007GL030639.
- Lühr, H., S. Rentz, P. Ritter, H. Liu, and K. Häusler (2007b), Average thermospheric wind pattern over the polar regions, as observed by CHAMP, *Annales Geophysicae*, 25(5), 1093–1101, doi:10.5194/angeo-25-1093-2007.
- March, G., E. Doornbos, and P. Visser (2019a), High-fidelity geometry models for improving the consistency of CHAMP, GRACE, GOCE and Swarm thermospheric density data sets, *Advances in Space Research*, 63(1), 213–238, doi:10.1016/j.asr.2018.07.009.

- March, G., T. Visser, P. Visser, and E. Doornbos (2019b), CHAMP and GOCE thermospheric wind characterization with improved gas-surface interactions modelling, *Advances in Space Research*, 64(6), 1225–1242, doi:10.1016/j.asr.2019.06.023.
- March, G., T. Visser, J. van den IJssel, E. Iorfida, C. Siemes, P. Visser, and E. Doornbos (2020), Gas-surface interactions modelling influence on the CHAMP, GRACE, GOCE and Swarm aerodynamic and neutral density data sets with diffuse reflection and constant incomplete accommodation, *Journal of Space Weather and Space Climate*, Under internal review.
- Marcos, F. A., and J. M. Forbes (1985), Thermospheric winds from the satellite electrostatic triaxial accelerometer system, *Journal of Geophysical Research*, 90, 6543–6552, doi:10.1029/JA090iA07p06543.
- Masutti, D., G. March, A. J. Ridley, and J. Thoemel (2016), Effect of the solar activity variation on the global ionosphere thermosphere model (GITM), *Annales Geophysicae*, 34(9), 725–736, doi:10.5194/angeo-34-725-2016.
- Mehta, P. M., C. A. McLaughlin, and E. K. Sutton (2013), Drag coefficient modeling for GRACE using Direct Simulation Monte Carlo, *Advances in Space Research*, 52(12), 2035–2051, doi:10.1016/j.asr.2013.08.033.
- Mehta, P. M., A. C. Walker, E. K. Sutton, and H. C. Godinez (2017), New density estimates derived using accelerometers on board the CHAMP and GRACE satellites, *Space Weather*, 15(4), 558–576, doi:10.1002/2016SW001562.
- Mehta, P. M., R. Linares, and E. Sutton (2019), Data-driven inference of thermosphere composition during solar minimum conditions, *Space Weather*, doi:10.1029/2019SW002264.
- Moe, K., and M. M. Moe (2005), Gas-surface interactions and satellite drag coefficients, *Planetary and Space Science*, 53(8), 793–801, doi:10.1016/j.pss.2005.03.005.
- Moe, K., M. M. Moe, and N. W. Yelaca (1972), Effect of surface heterogeneity on the adsorptive behavior of orbiting pressure gauges, *Journal of Geophysical Research*, 77(22), 4242–4247.
- Moe, K., M. M. Moe, and S. D. Wallace (1998), Improved satellite drag coefficient calculations from orbital measurements of energy accommodation, *Journal of Spacecraft and Rockets*, 35, 266–272, doi:10.2514/2.3350.
- Moe, K., M. M. Moe, and C. J. Rice (2004), Simultaneous analysis of multi-instrument satellite measurements of atmospheric density, *Journal of spacecraft and rockets*, 41(5), 849–853.
- Moe, M. M., and K. Moe (1969), The roles of kinetic theory and gas-surface interactions in measurements of upper-atmospheric density, *Planetary and Space Science*, 17(5), 917–922, doi:10.1016/0032-0633(69)90097-X.

- Moe, M. M., S. D. Wallace, and K. Moe (1993), Refinements in determining satellite drag coefficients: Method for resolving density discrepancies, *Journal of guidance, control, and dynamics*, 16(3), 441–445.
- Newton, G., and D. Pelz (1973), Neutral thermosphere temperatures from density scale height measurements, *Journal of Geophysical research*, 78(4), 725–732.
- Olsen, N., E. Friis-Christensen, R. Floberghagen, P. Alken, C. D. Beggan, A. Chulliat, E. Doornbos, J. T. da Encarnação, B. Hamilton, G. Hulot, J. van den IJssel, A. Kuvshinov, V. Lesur, H. Lühr, S. Macmillan, S. Maus, M. Noja, P. E. H. Olsen, J. Park, G. Plank, C. Püthe, J. Rauberg, P. Ritter, M. Rother, T. J. Sabaka, R. Schachtschneider, O. Sirol, C. Stolle, E. Thébault, A. W. P. Thomson, L. Tøffner-Clausen, J. Velínský, P. Vigneron, and P. N. Visser (2013), The Swarm Satellite Constellation Application and Research Facility (SCARF) and Swarm data products, *Earth, Planets and Space*, 65(11), 1, doi:10.5047/eps.2013.07.001.
- Pardini, C., L. Anselmo, K. Moe, and M. M. Moe (2010), Drag and energy accommodation coefficients during sunspot maximum, *Advances in Space Research*, 45(5), 638–650, doi:10.1016/j.asr.2009.08.034.
- Pardini, C., K. Moe, and L. Anselmo (2012), Thermospheric density model biases at the 23rd sunspot maximum, *Planetary and Space Science*, 67(1), 130–146, doi:10.1016/j.pss.2012.03.004.
- Pearlman, M., J. Degnan, and J. Bosworth (2002), The international laser ranging service, *Advances in Space Research*, 30(2), 135–143, [https://doi.org/10.1016/S0273-1177\(02\)00277-6](https://doi.org/10.1016/S0273-1177(02)00277-6).
- Perosanz, E., R. Biancale, S. Loyer, J.-M. Lemoine, A. Perret, P. Touboul, B. Foulon, G. Pradels, L. Grunwald, T. Fayard, N. Vales, and M. Sarrailh (2003), *On Board Evaluation of the STAR Accelerometer*, pp. 11–18, Springer Berlin Heidelberg, Berlin, Heidelberg, doi:10.1007/978-3-540-38366-6\_2.
- Peymirat, C., A. D. Richmond, B. A. Emery, and R. G. Roble (1998), A magnetosphere-thermosphere-ionosphere electrodynamic general circulation model, *Journal of Geophysical Research: Space Physics*, 103(A8), 17,467–17,477, doi:10.1029/98JA01235.
- Picone, J. M., A. E. Hedin, D. P. Drob, and A. C. Aikin (2001), NRLMSISE-00 empirical model of the atmosphere: Statistical comparisons and scientific issues, *Journal of Geophysical Research: Space Physics*, 107(A12), SIA 15–1–SIA 15–16, doi:10.1029/2002JA009430.
- Picone, J. M., J. T. Emmert, and J. L. Lean (2005), Thermospheric densities derived from spacecraft orbits: Accurate processing of two-line element sets, *Journal of Geophysical Research: Space Physics*, 110(A3), doi:10.1029/2004JA010585.
- Pilinski, M. D. (2011), Dynamic Gas-Surface Interaction Modeling for Satellite Aerodynamic Computations, Ph.D. thesis, University of Colorado at Boulder.

- Pilinski, M. D., B. M. Argrow, and S. E. Palo (2013), Semiempirical Model for Satellite Energy-Accommodation Coefficients, *Journal of Spacecraft and Rockets*, 47(6), 951–956, doi:10.2514/1.49330.
- Pilinski, M. D., B. A. Bowman, S. E. Palo, J. M. Forbes, B. L. Davis, R. G. Moore, C. Koehler, and B. Sanders (2016), Comparative Analysis of Satellite Aerodynamics and Its Application to Space-Object Identification, *Advances in Space Research Journal*, 53(5), 1–11, doi:10.2514/1.A33482.
- Rees, M. H. (1989), *Physics and Chemistry of the Upper Atmosphere*, Cambridge Atmospheric and Space Science Series, Cambridge University Press, doi:10.1017/CBO9780511573118.
- Reigber, C., H. Lühr, and P. Schwintzer (2002), CHAMP mission status, *Advances in Space Research*, 30(2), 129–134, doi:10.1016/S0273-1177(02)00276-4.
- Reigber, C., H. Lühr, L. Grunwaldt, C. Förste, R. König, H. Massmann, and C. Falck (2006), *CHAMP Mission 5 Years in Orbit*, pp. 3–15, Springer Berlin Heidelberg, Berlin, Heidelberg, doi:10.1007/3-540-29522-4\_1.
- Ridley, A., Y. Deng, and G. Tóth (2006), The global ionosphere-thermosphere model, *Journal of Atmospheric and Solar-Terrestrial Physics*, 68, 839–864, doi:10.1016/j.jastp.2006.01.008.
- Saltsburg, H., J. Smith, and M. Rogers (1967), *Fundamentals of Gas-Surface Interactions*, 346–391, 406–414, 448–521 pp., Academic Press, ISBN: 978-1-4832-2901-0.
- Sarris, T., R. Elsayed, M. Palmroth, I. Dandouras, E. Armandillo, G. Kervalishvili, S. Buchert, D. Malaspina, A. Jaynes, N. Paschalidis, J. Sample, J. Halekas, S. Tourgaidis, V. Lappas, M. Clilverd, Q. Wu, I. Sandberg, A. Aikio, and P. Pirnaris (2019), Daedalus: A low-flying spacecraft for the exploration of the lower thermosphere - ionosphere, *Geoscientific Instrumentation, Methods and Data Systems Discussions*, pp. 1–59, doi: 10.5194/gi-2019-3.
- Schulz, H. (1999), CH-00-20/00.00 Launch Configuration, *Tech. rep.*, Daimler-Benz Aerospace.
- Sentman, L. (1961a), Free molecule flow theory and its application to the determination of aerodynamic forces, *Tech. Rep. TR LMSC-448514*, Lockheed Missile and Space Co., Sunnyvale, CA.
- Sentman, L. (1961b), Comparison of the Exact and Approximate Methods for Predicting Free Molecule Aerodynamic Coefficients, *American Rocket Society Journal*, 31(11), 1576–1579.
- Severino (2004a), G.O.C.E. Reference Axis, *Tech. rep.*, Alenia Spazio S.p.A. Stabilimento di Torino.
- Severino (2004b), GOCE/Launcher Mechanical I/F, *Tech. rep.*, Alenia Spazio S.p.A. Stabilimento di Torino.

- Siemes, C. (2018), Swarm satellite thermo-optical properties and external geometry, ESA-EOPG-MOM-MO-15, *Tech. rep.*, ESA.
- Siemes, C., J. de Teixeira da Encarnação, E. Doornbos, J. van den IJssel, J. Kraus, R. Perešty, L. Grunwaldt, G. Apelbaum, J. Flury, and P. E. Holmdahl Olsen (2016), Swarm accelerometer data processing from raw accelerations to thermospheric neutral densities, *Earth, Planets and Space*, 68(1), 92, doi:10.1186/s40623-016-0474-5.
- Sridharan, R., and A. F. Pensa (1998), U.S. Space Surveillance Network capabilities, in *Image Intensifiers and Applications; and Characteristics and Consequences of Space Debris and Near-Earth Objects*, vol. 3434, edited by C. B. Johnson, T. D. Maclay, and F. A. Allahdadi, pp. 88 – 100, International Society for Optics and Photonics, SPIE, doi: 10.1117/12.331225.
- Suetin, P., B. Porodnov, V. Chernjak, and S. Borisov (1973), Poiseuille flow at arbitrary Knudsen numbers and tangential momentum accommodation, *Journal of Fluid Mechanics*, 60, 581 – 592, doi:10.1017/S0022112073000352.
- Sutton, E. K. (2008), Effects of solar disturbances on the thermosphere densities and winds from CHAMP and GRACE satellite accelerometer data, Ph.D. thesis, University of Colorado at Boulder.
- Sutton, E. K. (2009), Normalized force coefficients for satellites with elongated shapes, *Journal of Spacecraft and Rockets*, 46(1), 112–116, doi:10.2514/1.40940.
- Szücs-Csillik, I. (2017), Analysis and prediction of tiangong-1 reentry, *Romanian Astronomical Journal*, 27, 241–251.
- Tavernier, G., H. Fagard, M. Feissel-Vernier, K. L. Bail, F. Lemoine, C. Noll, R. Noomen, J. C. Ries, L. Soudarin, J. J. Valette, and P. Willis (2006), The International DORIS Service: genesis and early achievements, *Journal of Geodesy*, 80(8), 403–417, doi: 10.1007/s00190-006-0082-4.
- Touboul, P., E. Willemenot, B. Foulon, and V. Josselin (1999), Accelerometers for CHAMP, GRACE and GOCE space missions: synergy and evolution, pp. 321–327, *bollettino di Geofisica Teorica ed Applicata*.
- van den IJssel, J. (2014), GPS-based precise orbit determination and accelerometry for low flying satellites, Ph.D. thesis, Delft University of Technology.
- van den IJssel, J., E. Doornbos, E. Iorfida, G. March, and O. Montenbruck (2020), Thermosphere densities derived from Swarm GPS observations, *Advances in Space Research*, 65(7), 1758–1771, doi: <https://doi.org/10.1016/j.asr.2020.01.004>.
- Visser, T., G. March, E. Doornbos, C. de Visser, and P. Visser (2019), Horizontal and vertical thermospheric cross-wind from GOCE linear and angular accelerations, *Advances in Space Research*, 63(10), 3139–3153, doi: 10.1016/j.asr.2019.01.030.

- Walker, A., P. M. Mehta, and J. Koller (2014), Drag coefficient model using the Cercignani–Lampis–Lord gas–surface interaction model, *Journal of Spacecraft and Rockets*, 51(5), 1544–1563, doi:10.2514/1.A32677.
- Weimer, D. R., E. K. Sutton, M. G. Mlynczak, and L. A. Hunt (2016), Intercalibration of neutral density measurements for mapping the thermosphere, *Journal of Geophysical Research: Space Physics*, 121(6), 5975–5990, doi:10.1002/2016JA022691.
- Weimer, D. R., M. G. Mlynczak, J. T. Emmert, E. Doornbos, E. K. Sutton, and H. L. A. (2018), Correlations Between the Thermosphere’s Semi-Annual Density Variations and Infrared Emissions Measured with the SABER Instrument, *Journal of Geophysical Research - Space Physics*, pp. 8850–8864, doi:10.1029/2018JA025668.
- Wermuth, M., O. Montenbruck, and T. van Helleputte (2010), GPS high precision orbit determination software tools (GHOST), in *4th International Conference on Astrodynamics Tools and Techniques*.
- Wilson, G. R., D. R. Weimer, J. O. Wise, and F. A. Marcos (2006), Response of the thermosphere to Joule heating and particle precipitation, *Journal of Geophysical Research*, 111(A10), doi:10.1029/2005JA011274.
- Xiong, C., H. Lühr, and B. G. Fejer (2015), Global features of the disturbance winds during storm time deduced from champ observations, *Journal of Geophysical Research: Space Physics*, 120(6), 5137–5150, doi:10.1002/2015JA021302.



## AWARDS AND SPONSORSHIPS

- 2014 Pegasus Award Certificate  
*The European Network of Excellence in Aerospace Engineering Education*
- 2014 ESA Sponsorship for the 6th European CubeSat Symposium  
*European Space Agency (ESA)*
- 2014 Fellowship of von Karman Institute for Fluid Dynamics  
*NATO-Science & Technology Organization*
- 2019 European Commission Grant for the Living Planet Symposium 2019  
*European Commission (EC)*
- 2019 High Altitude Observatory sponsorship for visiting scientist opportunity  
*National Research Center for Atmospheric Research (NCAR)*
- 2020 Outstanding Paper Award for Young Scientists (for the work of Chapter 2)  
*Committee On Space Research (COSPAR)*
- 2020 Outstanding Paper Award for Young Scientists (for the work of Chapter 3)  
*Committee On Space Research (COSPAR)*

# LIST OF JOURNAL PUBLICATIONS

1. *M. Palmroth, M. Grandin, T. Sarris, E. Doornbos, S. Tourgaidis, A. Aikio, S. Buchert, M. A. Clilverd, I. Dandouras, R. Heelis, A. Hoffmann, N. Ivchenko, G. Kervalishvili, D. J. Knudsen, A. Kotova, H.-L. Liu, D. M. Malaspina, G. March, A. Marchaudon, O. Marghitsu, T. Matsuo, W. J. Miloch, T. Moretto-Jørgensen, D. Mpaloukidis, N. Olsen, K. Papadakis, R. Pfaff, P. Pirnaris, C. Siemes, C. Stolle, J. Suni, J. van den IJssel, P. T. Verronen, P. Visser; and M. Yamauchi*, **Lower thermosphere – ionosphere (LTI) quantities: Current status of measuring techniques and models**, *Annales Geophysicae Discussions*, <https://doi.org/10.5194/angeo-2020-42>, Under review, 2020.
2. *G. Jiang, C. Xiong, C. Stolle, J. Xu, W. Yuan, J. J. Makela, B. J. Harding, R. B. Kerr, G. March, C. Siemes*, **Comparison of thermospheric winds measured by GOCE and ground-based FPIs located at low to middle latitudes**, *Journal of Geophysical Research: Space Physics*, Under review, 2020.
3. *G. March, T. Visser, J. van den IJssel, E. Iorfida, C. Siemes, P.N.A.M. Visser, F. Gasperini, M. Pilinski, E. Doornbos*, **Gas-surface interactions modelling influence on the CHAMP, GRACE, GOCE and Swarm aerodynamic and neutral density data sets with diffuse reflection and constant incomplete accommodation**, *Journal of Space Weather and Space Climate*, Under internal review.
4. *J. van den IJssel, E. Doornbos, E. Iorfida, G. March, C. Siemes and O. Montenbruck*, **Thermosphere densities derived from Swarm GPS observations**, *Advances in Space Research*, **65**(7), 1758–1771, <https://doi.org/10.1016/j.asr.2020.01.004>, 2020.
5. *G. March, T. Visser, E. Doornbos and P.N.A.M. Visser*, **CHAMP and GOCE thermospheric wind characterization with improved gas-surface interactions modelling**, *Advances in Space Research*, **64**(6), 1225–1242, <https://doi.org/10.1016/j.asr.2019.06.023>, 2019.
6. *T. Visser, G. March, E. Doornbos, C. De Visser and P.N.A.M. Visser*, **Characterization of Thermospheric Vertical Wind Activity at 225–295 km Altitude Using GOCE Data and Validation Against Explorer Missions**, *Journal of Geophysical Research*, **124**(6), 4852–4869, <https://doi.org/10.1029/2019JA026568>, 2019.
7. *T. Visser, G. March, E. Doornbos, C. De Visser and P.N.A.M. Visser*, **Horizontal and vertical thermospheric cross-wind from GOCE linear and angular accelerations**, *Advances in Space Research*, **63**(10), 3139–3153, <https://doi.org/10.1016/j.asr.2019.01.030>, 2019.
8. *G. March, E.N. Doornbos, P.N.A.M. Visser*, **High-fidelity geometry models for improving the consistency of CHAMP, GRACE, GOCE and Swarm thermospheric density data sets**, *Advances in Space Research* **63**(1), 213–238, <https://doi.org/10.1016/j.asr.2018.07.009>, 2019.
9. *D. Masutti, G. March, A. Ridley, J. Thoemel*, **Effect of the solar activity variation on the Global Ionosphere Thermosphere Model (GITM)**, *Annales Geophysicae*, **34**, 725–736, <https://doi.org/10.5194/angeo-34-725-2016>, 2016.



# SELECTED PRESENTATIONS

- *G. March, E. Doornbos, C. Siemes, P. Visser, J. van den IJssel and E. Iorfida*, **Update on aerodynamic and gas-surface interactions modelling for the Swarm L2 density product**, "9th Swarm Data Quality Workshop", Prague, Czech Republic, September 2019.
- *G. March, T. Visser, E. Doornbos, P. Visser, J. van den IJssel and E. Iorfida*, **Newly derived thermospheric products for CHAMP, GRACE, GOCE and Swarm**, "CEDAR 2019", Santa Fe, New Mexico, U.S.A., June 2019.
- *G. March*, **Thermosphere density and wind from satellite acceleration observations**, "NCAR-HAO Colloquium", Boulder, Colorado, U.S.A., June 2019.
- *G. March, E. Doornbos, T. Visser, J. van den IJssel, E. Iorfida, P. Visser and C. Siemes*, **Newly derived thermospheric densities and winds from satellite acceleration observations**, "Living Planet Symposium 2019", Milan, Italy, May 2019.
- *G. March, T. Visser, E. Doornbos, E. Iorfida, J. van den IJssel, P. Visser*, **Update on thermospheric density products from satellite observations**, "15th European Space Weather Week", Leuven, Belgium, November 2018.
- *G. March, E. Doornbos*, **Impact of gas-surface interactions modelling on acceleration-derived thermosphere data**, "8th Swarm Data Quality Workshop", ESRI, Frascati, Italy, October 2018.
- *G. March, E. Doornbos, P.N.A.M. Visser*, **CHAMP, GRACE, GOCE and Swarm density and wind characterization with improved gas-surface interactions modelling**, "42nd COSPAR Assembly 2018", Pasadena, California, U.S.A., July 2018.
- *G. March, T. Visser*, **Improving the consistency of aerodynamic models and thermospheric density and wind data**, "SPP1788 DynamicEarth Winter School", K uhlungsborn, Germany, January 2018.
- *G. March*, **Geometry and aerodynamic model improvement for Swarm thermospheric densities**, "7th Swarm Data Quality Workshop", Delft, The Netherlands, October 2017.
- *G. March, E. Doornbos, P.N.A.M. Visser*, **CHAMP, GRACE, GOCE and Swarm thermosphere density data with improved aerodynamic and geometry modelling**, "Fourth Swarm Science Meeting & Geodetic Missions Workshop", Banff, Canada, March 2017.